2002-04-26

Methodology for Correlating Experimental and Finite Element Modal Analyses on Valve Trains

Massimo Giorelli
Worcester Polytechnic Institute

METHODOLOGY FOR CORRELATING EXPERIMENTAL AND FINITE ELEMENT MODAL ANALYSES ON VALVE TRAINS

By

Massimo Giorelli

A Thesis

Submitted to the Faculty

of the

WORCESTER POLYTECHNIC INSTITUTE

In partial fulfillment of the requirements for the

Degree of Master of Science

in

Mechanical Engineering

by

_____

March 2002

APPROVED:

_____
Professor Robert L. Norton, Major Advisor

_____
Professor Joseph J. Rencis, Committee Member

_____
Professor Mikhail F. Dimentberg, Committee Member

_____
Professor John M. Sullivan Jr., Graduate Committee Representative

_____
Donald A. Jacques, Committee External Member, United Technologies Corp.

ABSTRACT

The widespread use of finite element models in assessing system dynamics for noise, vibration, and harshness (NVH) evaluation has led to recognition of the need for improved procedures for correlating models to experimental results. This study develops and applies a methodology to correlate an experimental modal analysis with a finite element modal analysis of valve trains in IC-engines. A pre-test analysis procedure is employed to guide the execution of tests used in the correlation process. This approach improves the efficiency of the test process, ensuring that the test article is neither under nor over-instrumented. The test-analysis model (TAM) that results from the pre-test simulation provides a means to compare the test and the model both during the experimental approach and during the model updating process. The validity of the correlation methodology is demonstrated through its application on the valve train of a single overhead cam (SOHC) engine.

ACKNOWLEDGEMENTS

Foremost, I would like to acknowledge the generous assistance and guidance of Donald Jacques, without whose insight this thesis would not have been possible. Additionally, I would like to thank my advisor, Professor Robert L. Norton, for his precious guidance and indulgence regarding my delays.

I would like to acknowledge DaimlerChrysler Corporation for supporting this research. Special thanks go to David Eovaldi for providing me valve train materials and information, and for generously agreeing to fit me into his busy schedule.

Finally, I would like to thank my parents, Anna and Roberto, for all their help since ever. Very special thanks go to Lara.

CONTENTS

LIST OF FIGURES

LIST OF TABLES

1. INTRODUCTION

The main intent of this project is to derive a methodology to correlate an experimental modal analysis with a Finite Element Method (FEM) modal analysis of valve trains in IC-engines. The methodology will describe a procedure to conduct an FEM modal analysis that reproduces the results of an experimental modal analysis on valve trains. The need for this correlation between the two modal analyses is fundamental to the validation of the numerical model. A numerical model (i.e. a FEM mesh with its boundary conditions, load cases, materials properties and type-of-solution settings) that possesses the same vibration characteristics of an actual mechanical system can, indeed, be considered a reliable model of such a system and is often called a *modal model.*

A validated numerical model of a mechanical system can be of immense utility in both prototype development and redesign processes. A *modal model* is a very efficient tool to address a variety of noise and vibration problems found in either the design phase, or the operation of a system. For instance, many noise and vibration problems are caused by resonance; resonance can cause mechanical amplification of normal operational forces, resulting in an unacceptable structural response. In such cases, a structural modification (in mass, stiffness or damping) must be suggested aimed at shifting the natural frequency that is triggering the undesired resonance. With a validated numerical model, alternative modifications can be timely and cost-efficiently evaluated using only a computer. The "what if?" approach can be made many times before the hardware modifications are implemented and finally tested.

The correlation methodology derived in this study is based on the experience and results of experimental and computer simulated modal analyses conducted on the valve train of a four-cylinder Chrysler engine. For simplicity, only the intake section of one cylinder of the engine is considered in the study.

2. OVERVIEW OF CORRELATION METHODOLOGY

The widespread use of finite element models in assessing system dynamics for noise, vibration, and harshness (NVH) evaluation has led to recognition of the need for improved procedures for correlating models to experimental results. Correlation is the process of quantifying the degree of similarity and dissimilarity between the two approaches. With the greater occurrence of finite element models preceding the first prototype hardware, it is now practical to employ pre-test analysis procedures to guide the execution of tests used in the correlation process. This improves the efficiency of the test process, ensuring that the test article is neither under nor over-instrumented. The test-analysis model (TAM) that results from the pre-test simulation provides a means to compare the test and the model both during the experimental approach and during the model updating process. The use of pre-test analysis methods for planning the test and aiding the correlation can significantly reduce the time required for model validation[1].

Three tasks can be defined for the validation process (refer to Figure 2.1):

1. *Pre-test simulation and TAM derivation*
2. *Modal survey*
3. *Model updating*

2.1. PRE-TEST SIMULATION AND TEST-ANALYSIS MODEL (TAM) DERIVATION

The first role of the pre-test simulation is to plan the artificial excitation test (modal test) in terms of selecting exciter and accelerometer locations. The number of

FIGURE 2.1. Model Validation Process

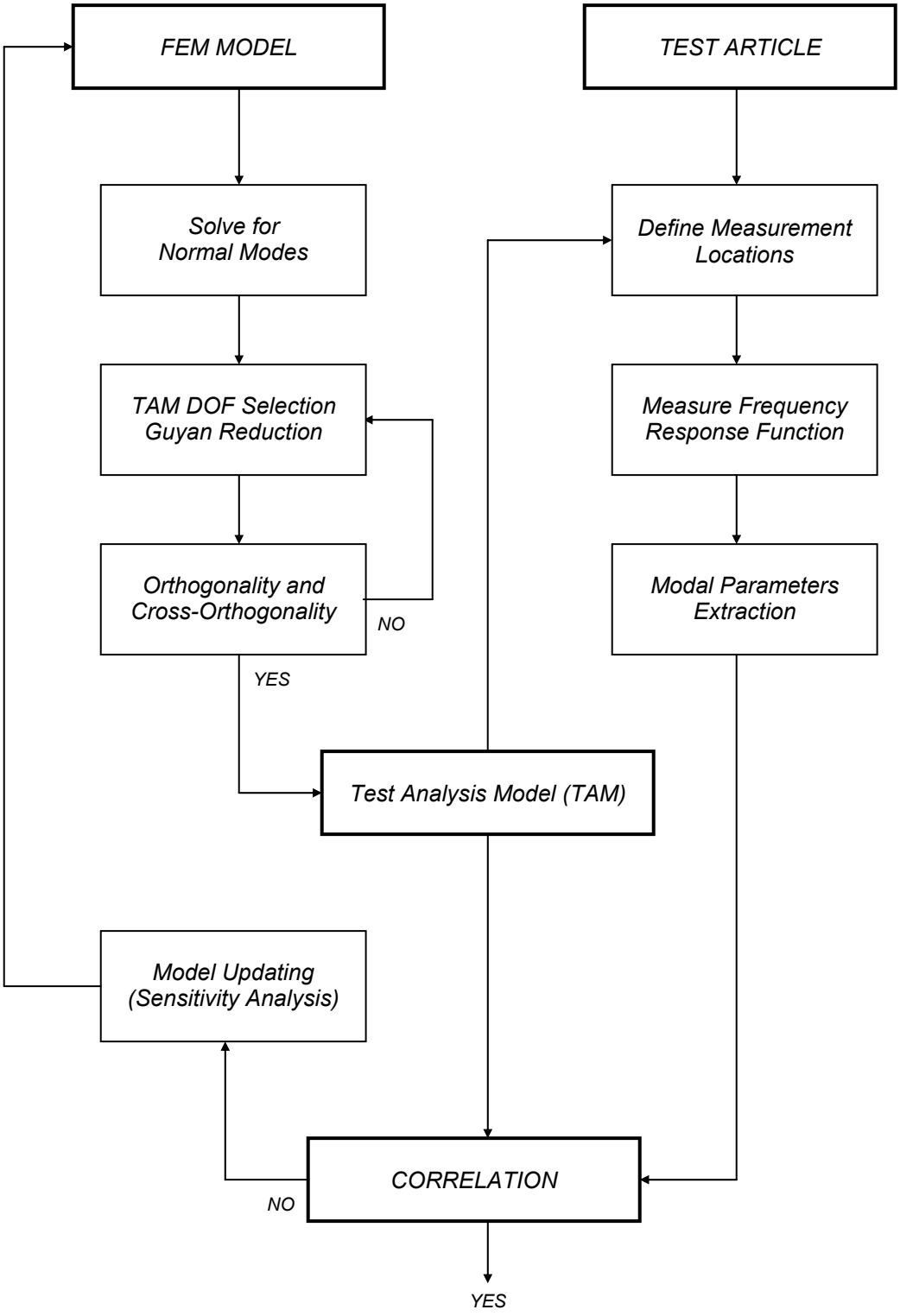

locations required depends largely on the number of target modes that exist in the frequency range of interest. In general, the more target modes there are, the more measurement locations will be needed. The modes that contribute most to the response that is being analyzed are selected as target modes. Automated methods have been developed to help in the accelerometer location selection process. These methods are not considered in this study except to note that they can often save a significant portion of the time required for the overall pre-test simulation. However, even with automated methods, accelerometer selection is still somewhat of a trial and error process[9].

An adequate accelerometer location distribution is one that gives an accurate TAM. Physically the TAM is a representation of the FEM model in the degrees of freedom (DOF) of the measured test locations. Mathematically, it is a matrix reduction for the FEM model mass and stiffness matrices from FEM model DOF size down to the test DOF size. Whereas an FEM model may have DOF numbering in the tens of thousands, the number of DOF of the reduced model usually numbers in dozens or less because of test measurement limitations. As it is expected with any model reduction, the reduced model is only a numerical approximation of the complete FEM model. For validation purposes it is important that this approximation be accurate. Its accuracy is a consequence of how well the test locations are selected.

Evaluation of the accuracy of the TAM is a crucial step. Possible sets of accelerometer locations, or test DOF, are evaluated by reducing the FEM model down to these DOF. The reduction is performed on both the mass and stiffness matrices, M_{FEM} and K_{FEM}, respectively. These matrices have the dimension of the FEM model. Mathematically, the reductions are computed as:

$$M_{TAM} = G^T M_{FEM} G$$

$$K_{TAM} = G^T K_{FEM} G$$

where M_{TAM} and K_{TAM} are the TAM mass and stiffness matrices and have the dimension of the test DOF. The matrix G is the transformation matrix. A number of different methods are available for computing this matrix; the method selected for this application is the *Guyan* reduction technique, which uses the constraint modes obtained from the static stiffness matrices.

Similarly to the FEM model, the reduced model, called the TAM, has natural frequencies and a mode shape matrix, Ψ_{TAM}. The accuracy of a TAM is evaluated based on how well the reduced modal properties approximate the FEM modal properties. For a *Guyan* reduction, the frequencies of the reduced model will always be higher than the FEM model[12]. In general, if the TAM frequency is within 10% of the FEM model frequency, the TAM is deemed adequate.

Mode shapes of the TAM and FEM models are compared by computing orthogonality, O, and cross-orthogonality, XO, matrices by the following matrices:

$$O = \Psi_{FEM}^T \; M_{TAM} \; \Psi_{FEM}$$

$$XO = \Psi_{FEM}^T \; M_{TAM} \; \Psi_{TAM}$$

In a perfect reduction, which of course cannot be obtained, the diagonal values of the orthogonality and cross-orthogonality matrices have the value of unity and the off-diagonal terms have the value of zero (assuming that the mode shapes have been *mass-normalized*). In practice, a TAM is usually deemed adequate if the ortho and cross-ortho matrices terms meet the following criteria[10]:

$$\textit{diagonal terms} > 0.90$$

$$\textit{off-diagonal terms} < 0.10$$

Although the ortho and cross-ortho matrices provide similar information about the TAM accuracy, they tend to indicate different things. The orthogonality matrix indicates the goodness of the mass distribution in the reduced model; the cross-orthogonality matrix indicates the accuracy of the reduced mode shapes.

2.2. MODAL SURVEY

As it was mentioned above, the purpose of pre-test analysis, and in particular the derivation of the TAM, is twofold. The accelerometer and exciter locations identified in the pre-test simulation are used to instrument the test article for modal test. After the test, the result of the pre-test analysis, the TAM, provides a means for comparing model and test data. It is recommended that initial comparisons between the test and FEM model be made during the testing phase. That way if problems occur, they can be identified quickly and adjustments to test plan can still be made if necessary.

The test and TAM shapes are compared by calculating a test/model cross-orthogonality matrix as:

$$XO = \Psi_{FEM}^{T} \; M_{TAM} \; \Psi_{TEST}$$

Initial comparison of test and model mode shapes should show at least a few of the shapes have good similarity. This is an indication that the FEM model and the TAM are reasonably accurate and gives confidence that the model can be correlated. Poor cross-orthogonality could indicate one or more things. First it may be a clue that some of the accelerometers are not working properly. In that case debugging methods can be used to identify the source of the bad data. Poor correlation may also indicate that fundamental

assumptions in the model such as the character of the boundary conditions are not correct. Alteration to the test plan may be required instead if the problem is identified among the test setup. Thus, during the testing, the TAM provides a quick "sanity" check at a time where it is still possible to alter the test setup.

2.3. MODEL UPDATING

In the model updating process, the test data is used as the target, and the FEM model parameters are updated to give better agreement between the model and the experimental results. Various approaches are available to help the analyst in making the correct changes to the model. These methods can be categorized as either modal based or response based. In both types of methods the analyst must select model design variables. The design variables are parameters of the model that are to be updated and should represent parts of the model for which there is less confidence.

Using design variables sensitivities, the updating methods indicate the amount of change to apply to the design variables that minimize the model error. With modal based methods, the test modal parameters, typically natural frequencies, are used as targets in the iterative updating process. Response based methods use the test frequency response functions (FRFs) as the correlation targets. The latter approach has the advantage that the determination of modal parameters from the test data is not needed (i.e. no need of performing modal curve-fit). However, in this study only modal based updating approaches are considered.

The TAM is used in both types of model updating methods. Its purpose is to compute, once more, orthogonality checks between the updated model and the

experimental results, using the same equation formulated in the previous section. This quantifies the final accuracy of the FEM mode shapes with respect of the experimental modes. In this experience, the objective is to obtain a model whose natural frequency values do not diverge by more than 10% from the corresponding values of the natural frequencies derived experimentally (at least over the frequency interval of interest). In addition, an orthogonality check between the results of the updated model and the experimental approach will have to meet the same criteria that was established for orthogonality checks between the pre-test complete model and TAM.

3. PRE-TEST SIMULATION AND TAM DERIVATION

3.1. SYSTEM DESCRIPTION

The valve train is one of the most complex and critical parts of the automotive engine. The valve lift characteristics not only radically contribute to engine efficiency and performance but also severely influence the engine emissions levels. Adversely, the valve train is a major contributor to engine vibrations and noise levels. Because of the crucial function of the valve train, a wide number of different design solutions have been and are being developed for this mechanism. In addition, the interactions between the multiple valve train components are often the object of separate and thorough studies in the mechanism design process. In modern automotive engines, the entire valve train is generally mounted over the cylinder engine block, in the cylinder head. This solution is denoted as *overhead camshaft* (OHC) type of valve train. When only one camshaft serves all the valves, the solution is called *single overhead camshaft* (SOHC) valve train. In this approach, the main components of the valve train mechanism are reduced to: the camshaft, rocker arms, valves and springs.

The correlation methodology for modal analyses that this study develops and validates is based on the application of such a procedure on the valve train of a two liter four-cylinder in line SOHC engine from Chrysler. The valve train of this engine has sixteen valves; in each cylinder, two valves are dedicated to the intake section and two to the exhaust section. Each intake valve is activated by its unique rocker arm. The exhaust valve pair, instead, is activated by one common rocker arm. For simplicity, only one valve of the intake section of one cylinder is considered in the application. However, the intake section considered is kept "seated" in its original environment. In other words, the

portion of the engine head in which the valve train is mounted is also included in the study. This decision is a consequence of the consideration that boundary conditions drastically affect the outcome of modal analyses. Therefore, in order to characterize the vibration modes and natural frequencies of a valve train, its supporting system cannot be overlooked.

Figure 3.1 depicts the test article prepared. An original four-cylinder head was cross-sectioned to obtain a single cylinder article that included the camshaft journals and bearings. The exhaust valve pair was removed along with its rocker arm. One intake valve, and corresponding rocker arm, were also removed. The remaining valve train mechanism was then reduced to a *linear* structure composed by non-moving parts, as

FIGURE 3.1. Test Article

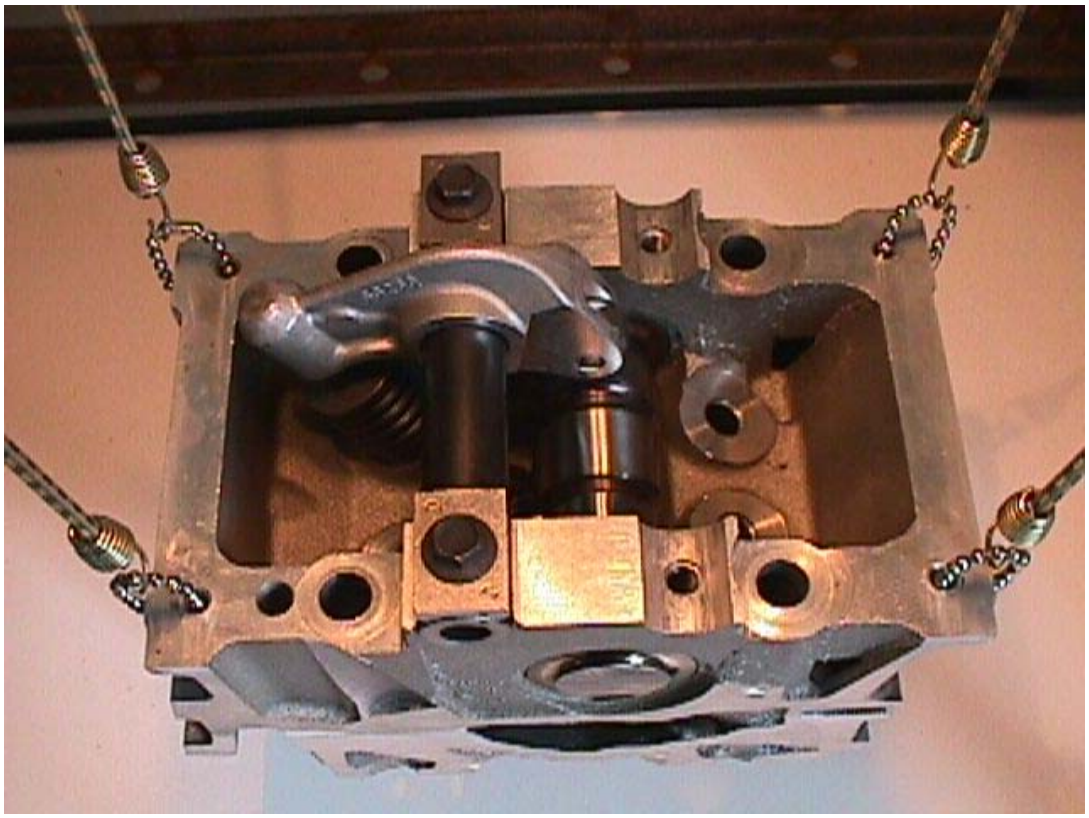

required in order to conduct a modal analysis. This was achieved by introducing a force that prevents the kinematic chain from altering its given configuration. The mechanism was fixed at the configuration in which the valve is said to be open, as illustrated by Figure 3.2 (the Figure also points all the valve train components included in the model). The only provider of the force is the spring, thus the applied force is an internal force. It is worth noting that this force not only fixes the mechanism at a particular configuration but also preloads clearances between the system components. Although the preloading provider is internal, it is crucial to understand, and account for, the modifications that it introduces in both the overall and spring structural characteristics. Nevertheless, considering that the test article is a mechanism that has been preloaded in order to reduce it to a *linear* structure, it is imperative to validate this conversion. These checks were performed, as illustrated in the next sections.

One important comment relative to this test article preparation concerns the lash-adjuster component (refer to Figure 3.2). The lash-adjuster is a *non-linear* spring that guarantees permanent contact between valve stem and rocker arm during normal engine operation. The lash adjuster, however, functions as a *non-linear* interface spring only when the proper oil pressure is provided within its cell. In the prepared test article there is no presence at all of oil; therefore the lash-adjuster does not act as a *non-linear* spring. The *non-linear* behavior of the lash-adjuster is not included then in the model.

Finally, the frequency interval of interest, over which it is desired a test article modal characterization, is set from a frequency of zero Hz up to frequencies of 5000 Hz. The feasibility of this statement also has to be verified.

FIGURE 3.2. Valve Train Configuration in Test Article (Courtesy of DaimlerChrysler Corp.)

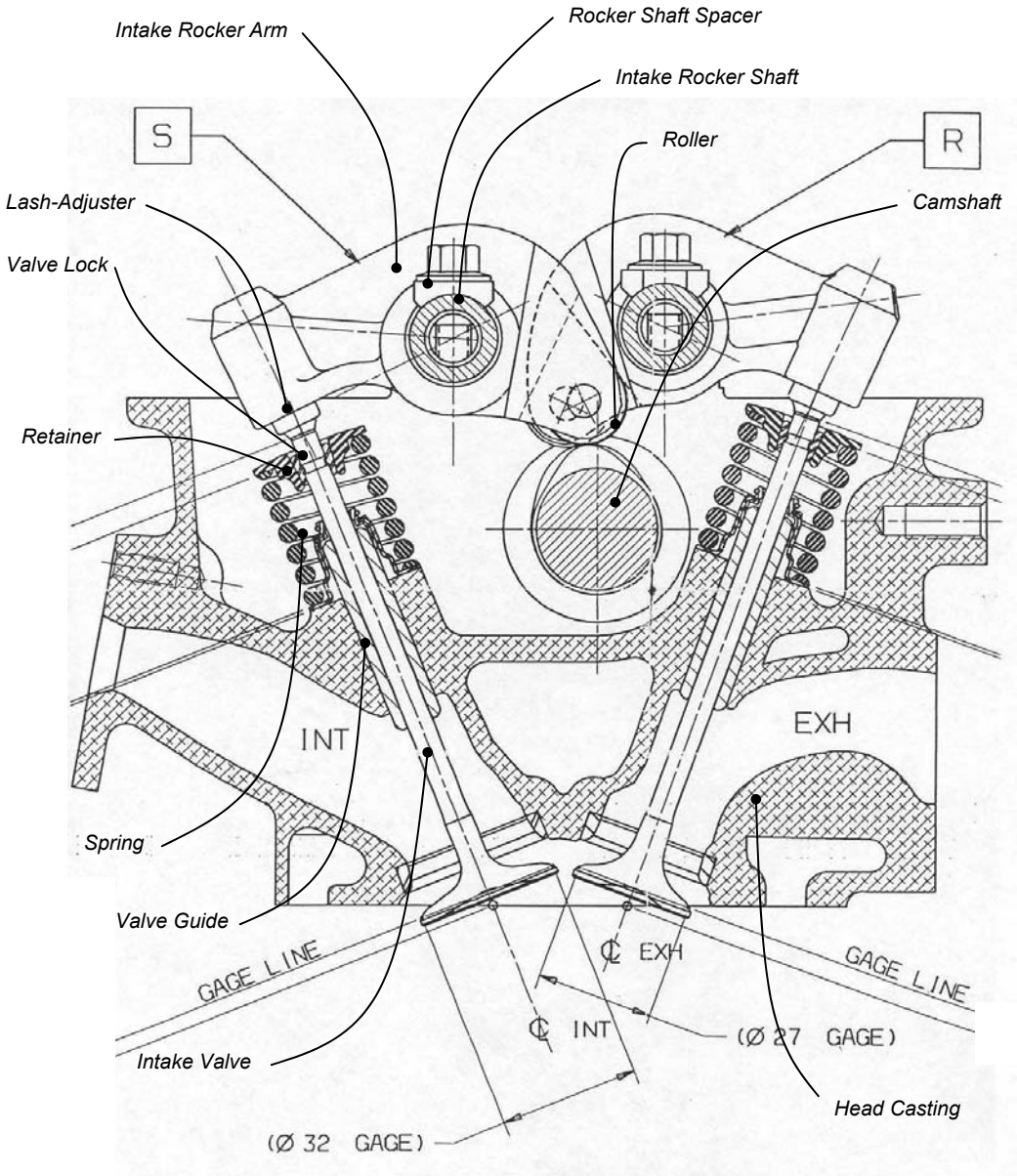

3.2. FEM MODEL PREPARATION

The finite element analysis software package selected for conducting the study is the robust and efficient NASTRAN from MSC. The model was prepared using the pre-post processor PATRAN, which is also a product of MSC that integrates well with the solver NASTRAN. The development of the model started from an existing complete model of the sole aluminum head casting of the engine introduced in the previous section. This model, which was obtained from DaimlerChrysler Corporation, had been developed to assess structural dynamics evaluations, as well, thus its overall mesh density was appropriate. The model, illustrated in Figure 3.3 as it was received, is composed primarily by solid elements (hexagonal and wedge elements). The rather complicated geometry of the intake and exhaust ducts (refer to Figure 3.2) is simplified using shell elements (quadrilateral and triangular elements). The area of the head casting above the ducts, in which the valve guides are mounted, is also modeled with shell elements with a fairly coarse pattern. Embedded shell elements are used in the model for transitioning from the shell mesh to the solid mesh; as solid elements do not have rotational DOF, moment transfer between shells and solids elements is obtained by extending the shell elements into the solid mesh.

The original head casting model was then cross-sectioned consistently with the cut performed on the actual engine head and described in the previous section. Three areas of this starting base model, illustrated in Figure 3.4, were remeshed in order to obtain a finer element density. The first area is the region of the camshaft journals. The second area is the region where the intake rocker shaft is fixed to the head casting. The

FIGURE 3.3. Original FEM Model of Head Casting

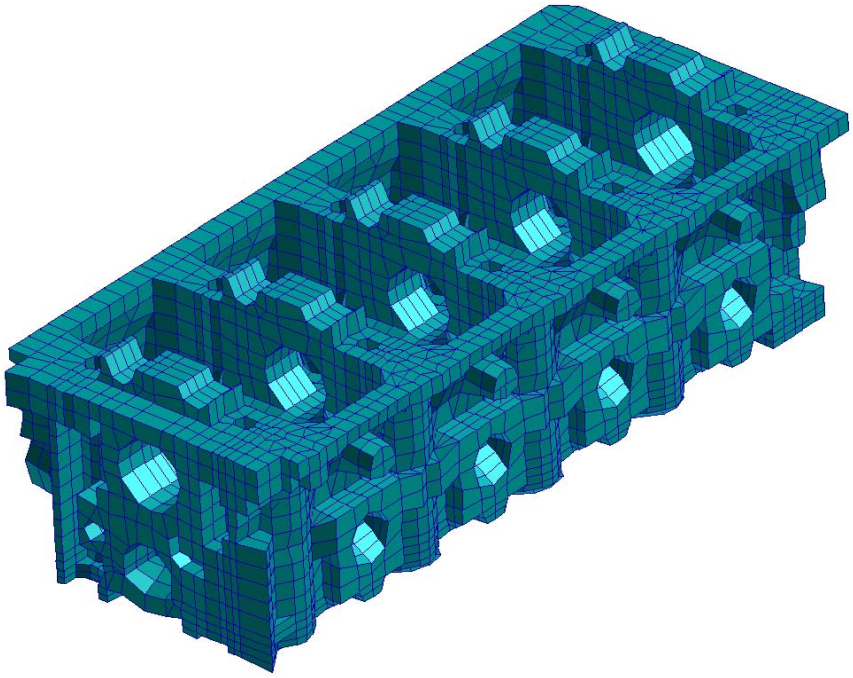

FIGURE 3.4. Starting One-Cylinder Head Casting Section

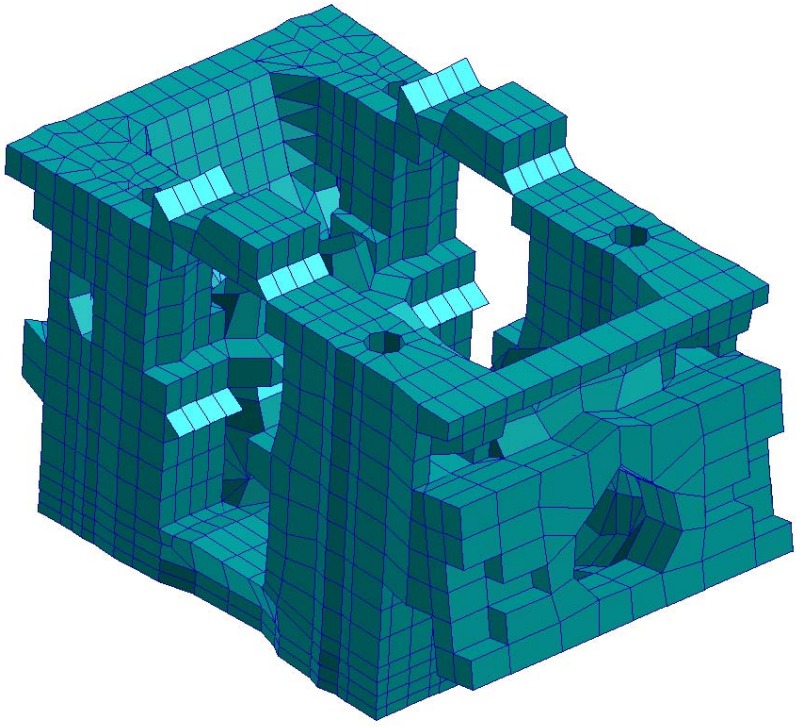

third remeshed area is the spot where the valve guides are mounted. A finer mesh was desirable for thesethree areas in order to be able to model detailed camshaft, rocker shaft, and valve, respectively. The results of this remesh operation are visible in Figures 3.5 A-B; these figures depict the complete model of the single-cylinder head casting cross-section considered in the study.

Once the head casting part was complete, the valve train components were added to the model. The camshaft (Figure 3.6), the rocker shaft (Figure 3.7) and the intake rocker arm (Figure 3.8) were modeled with solid elements (hexagonal and wedge elements). The geometries of the camshaft and rocker arm were imported in the pre-processor in order to use their curves and surfaces as guides in the modeling but no automatic volume mesher was employed. Subsequently, the remaining valve train components were introduced; the lash-adjuster, the roller and relative pin, and the retainer were also modeled with solid elements and are shown in Figures 3.9, 3.10, and 3.11, respectively. Figure 3.12 illustrates the valve and the valve guide. Whereas the valve head was modeled with solid elements, the valve stem was modeled with bar elements. Figures 3.13 A-B show the complete assembly of the valve train considered in the single-cylinder head casting.

The boundary conditions employed to assembly the valve train components in the model are considered design parameters for the model updating process and are discussed in the next section. The modeling of the spring is discussed in Section 3.2.2. Section 3.2.3 reviews some mathematical and general checks performed on the complete model including a mass comparison with the test article.

FIGURE 3.5.A. Modified One-Cylinder Head Casting Section

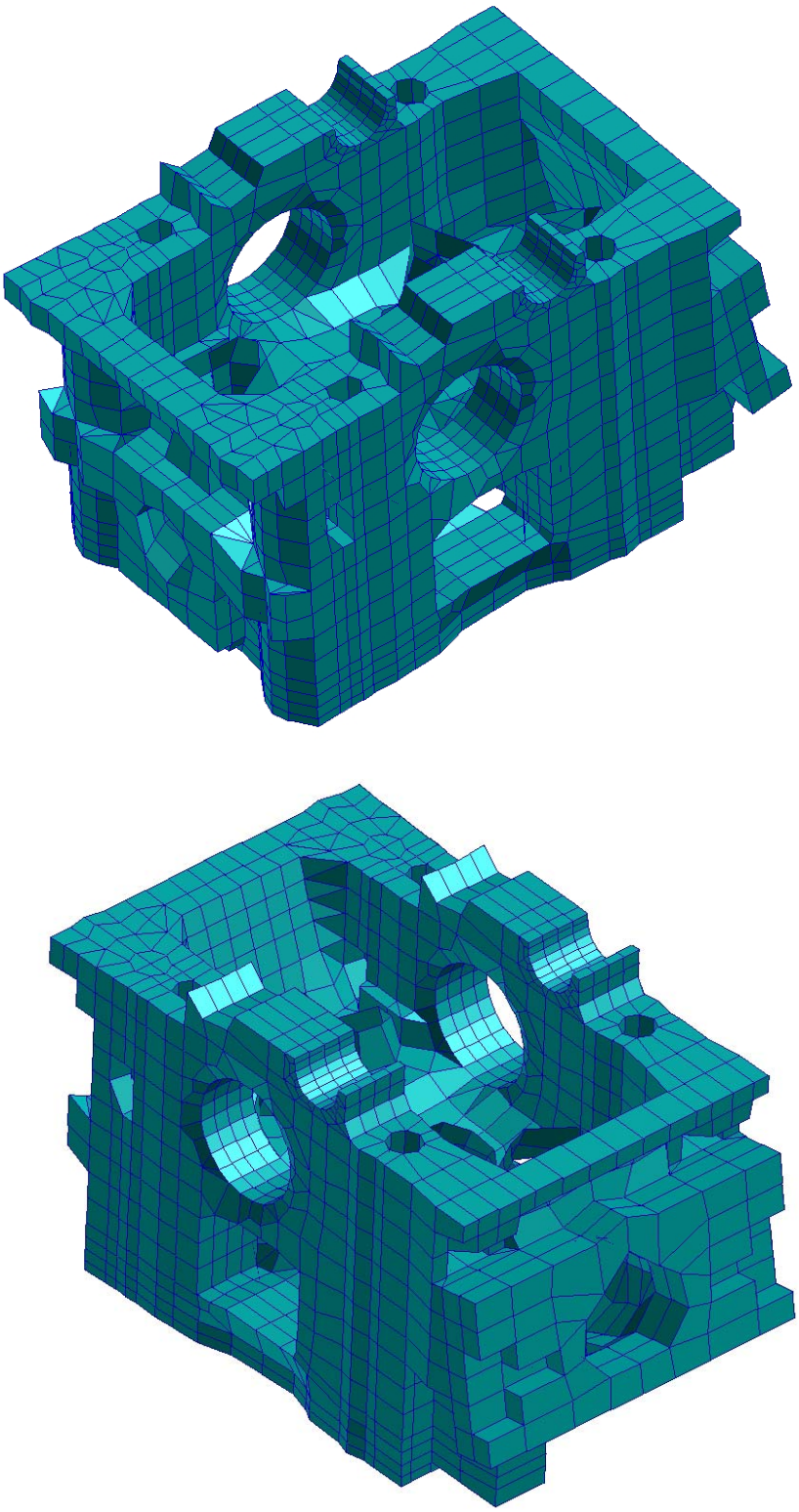

FIGURE 3.5.B. Modified One-Cylinder Head Casting Section

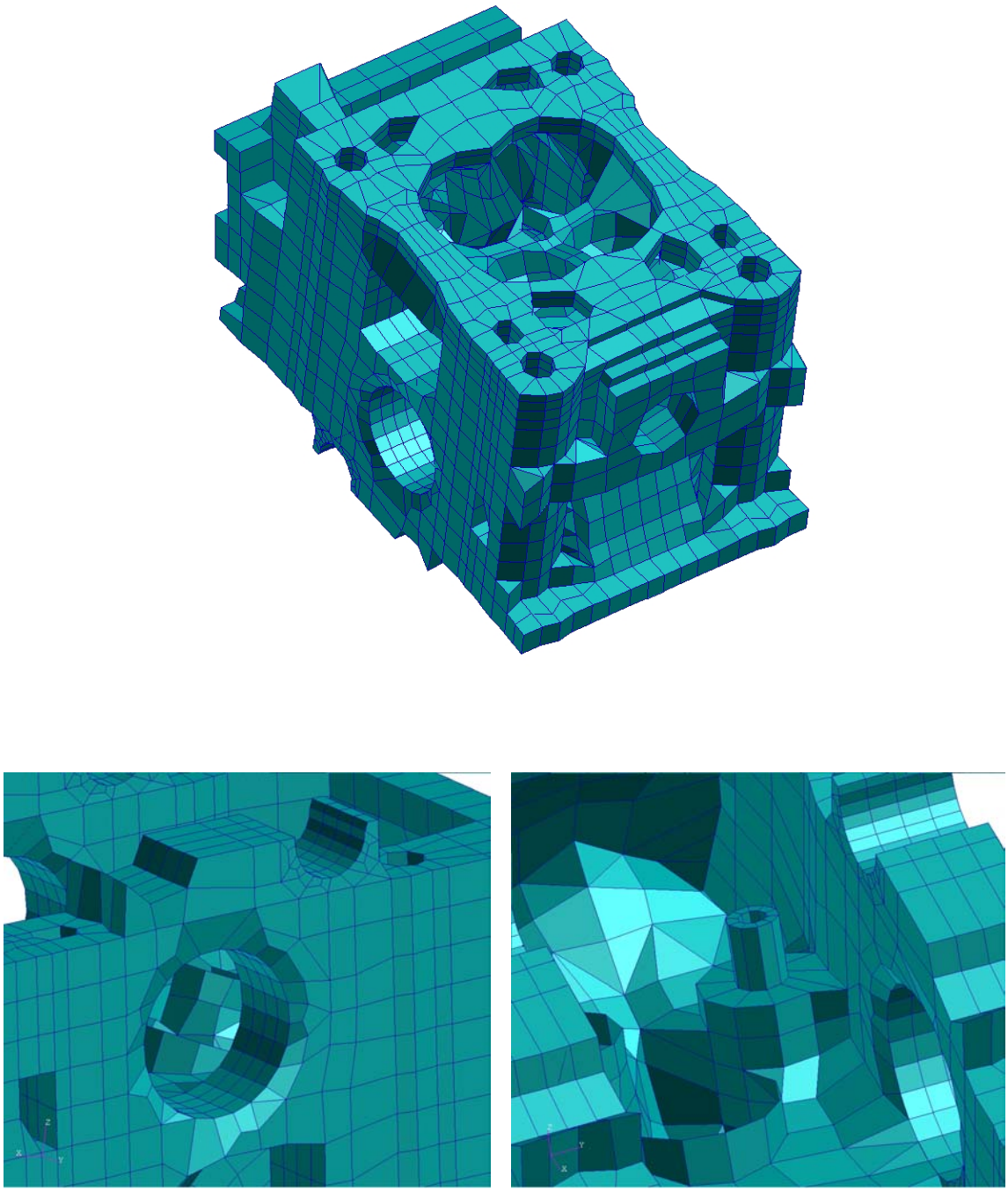

FIGURE 3.6. Camshaft

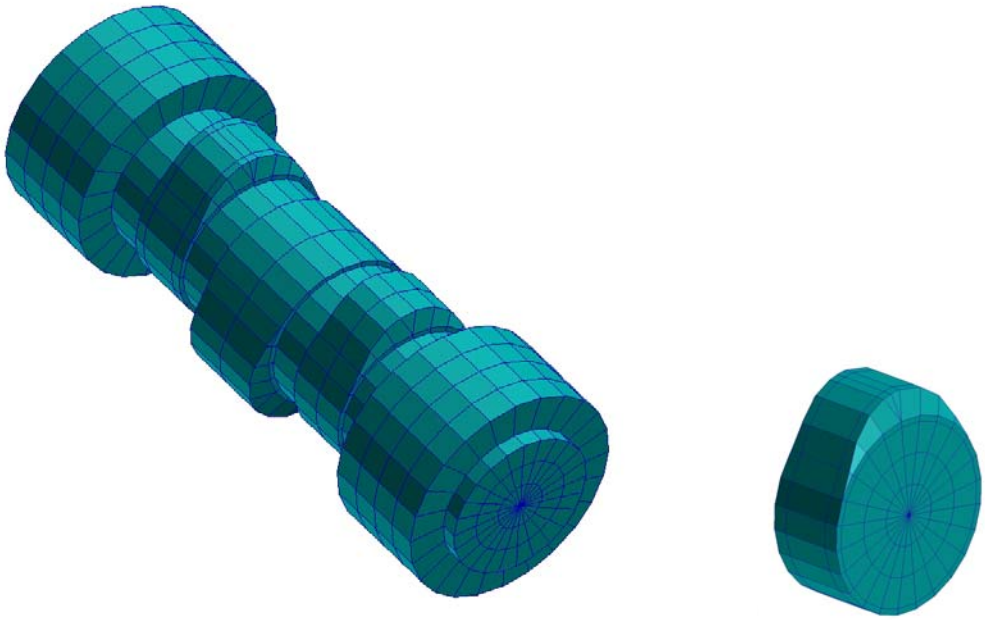

FIGURE 3.7. Rocker Shaft

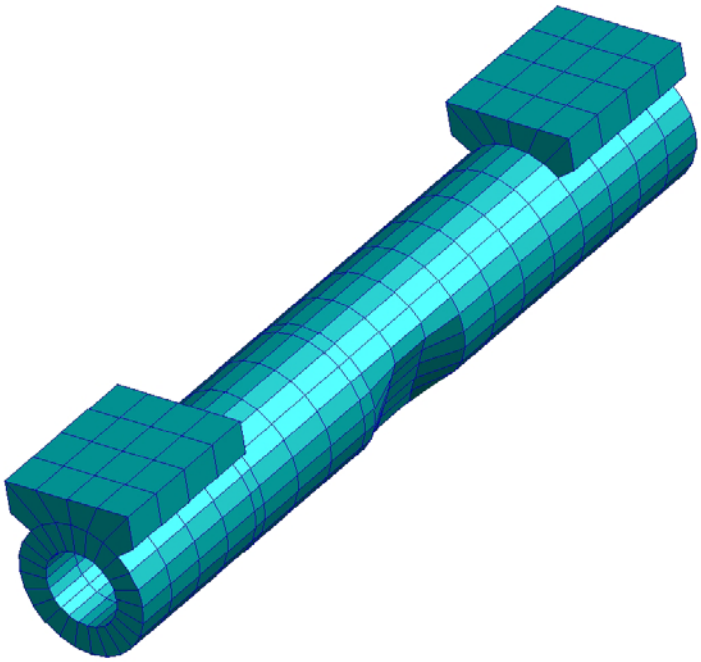

FIGURE 3.8. Rocker Arm

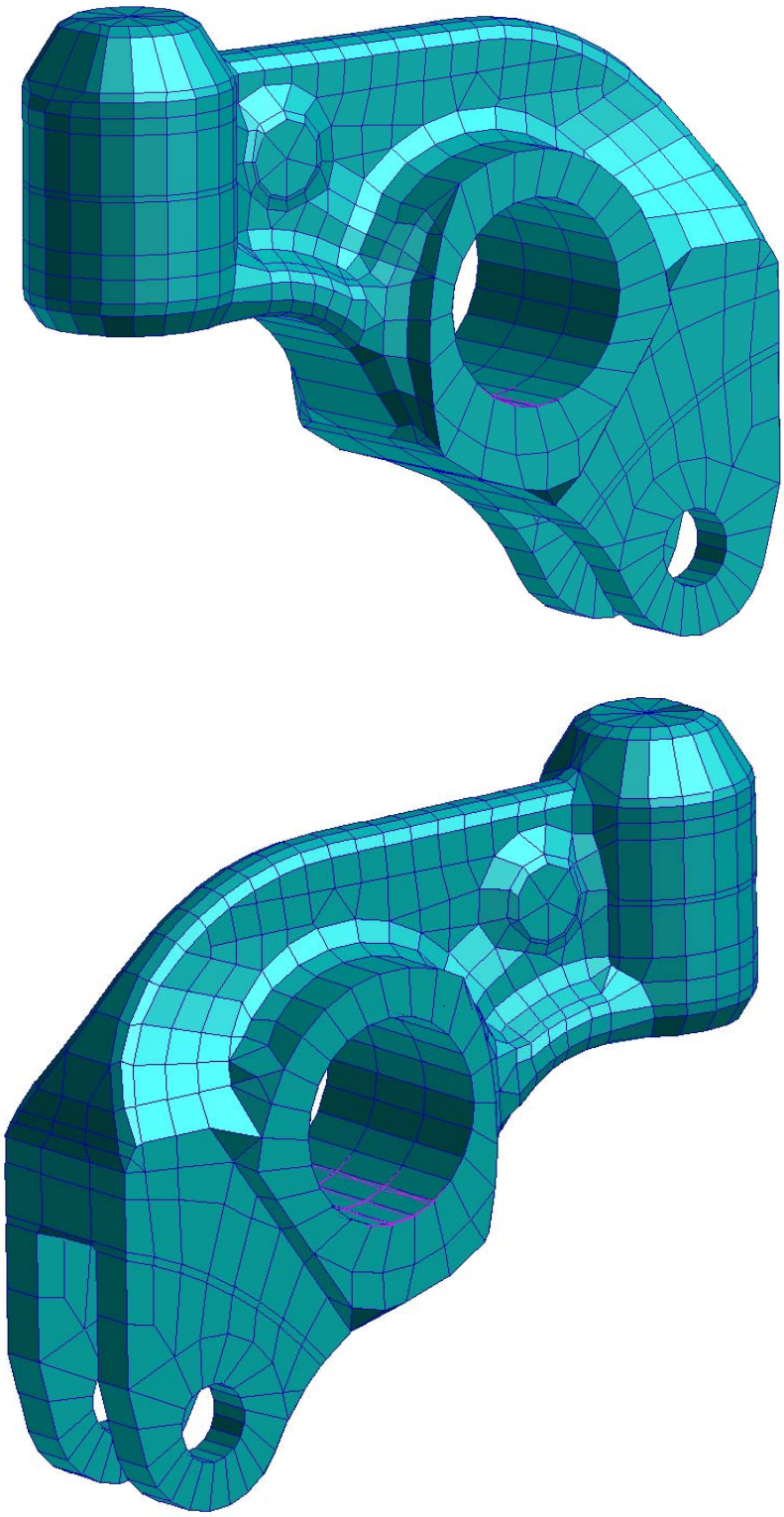

FIGURE 3.9. Lash Adjuster

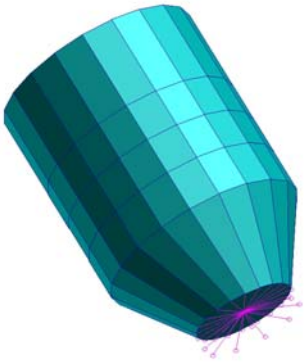

FIGURE 3.10. Roller and Pin

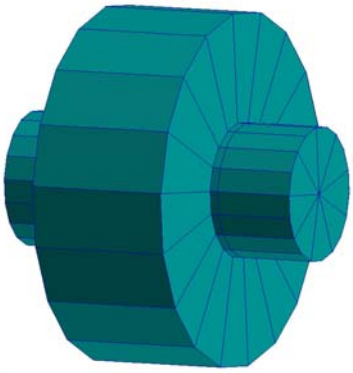

FIGURE 3.11. Retainer and Lock

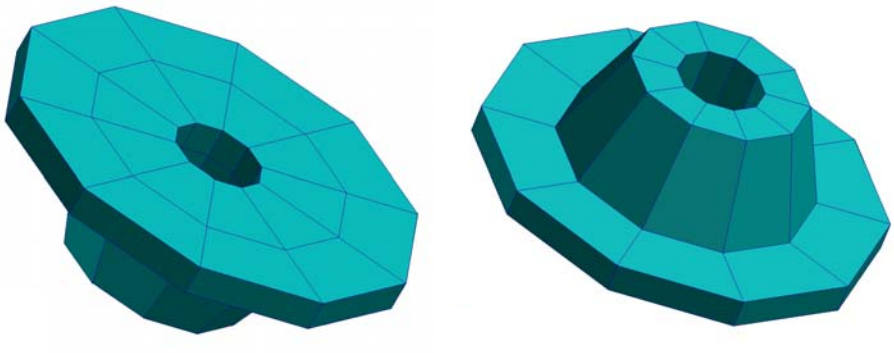

FIGURE 3.12. Valve and Valve Guide

FIGURE 3.13.A. Complete Assembly

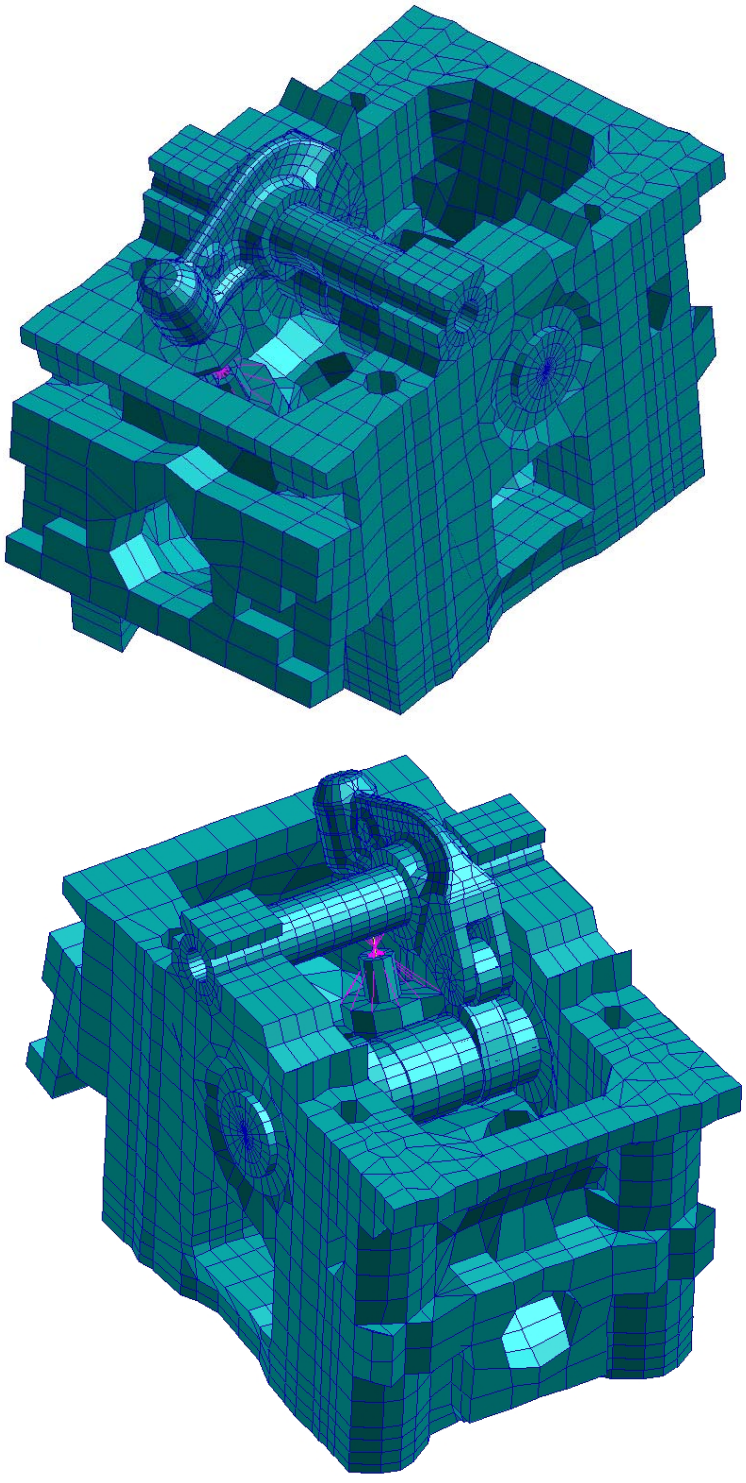

FIGURE 3.13.B. Complete Assembly

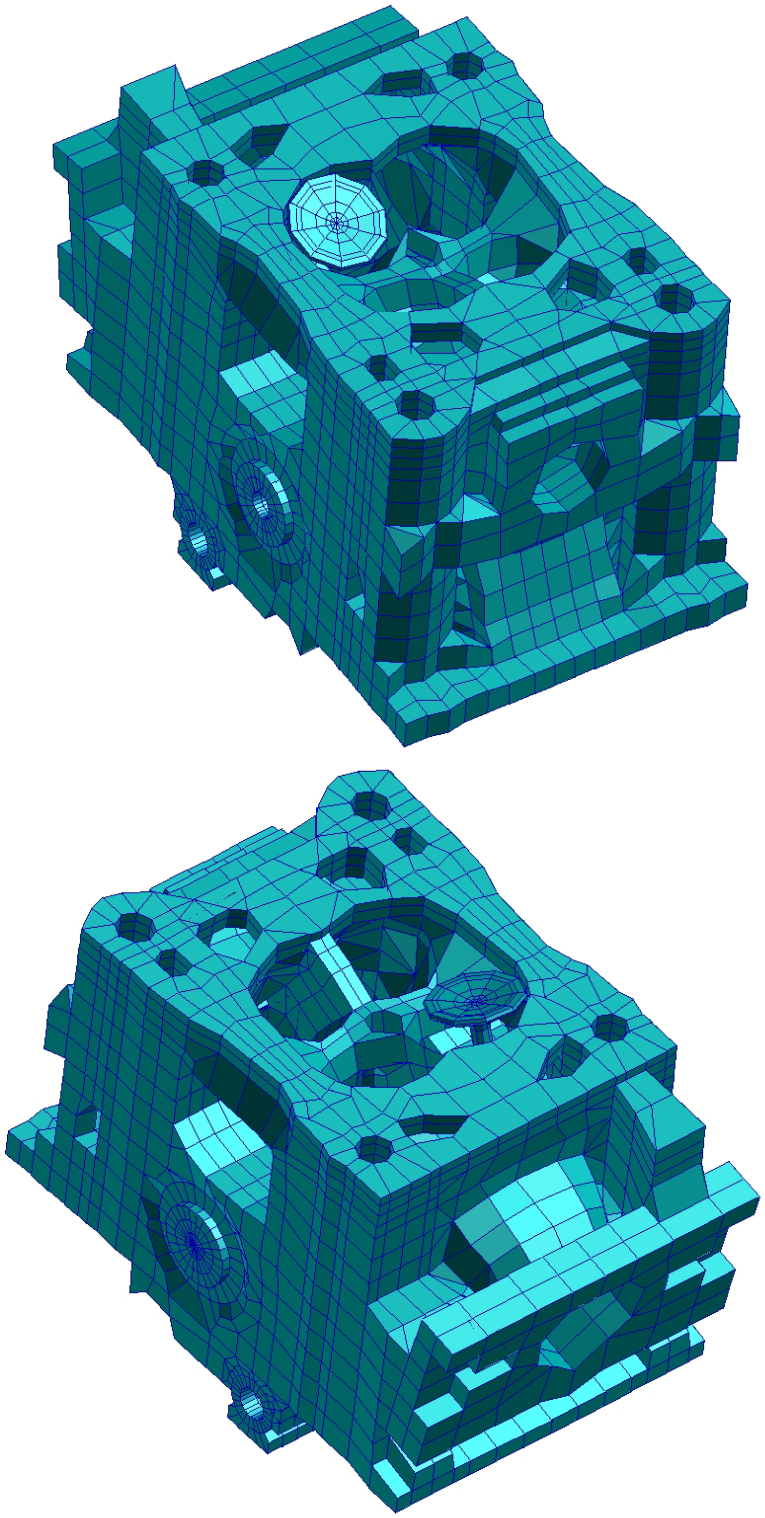

3.2.1. VALVE TRAIN BOUNDARY CONDITIONS

The boundary conditions employed to attach the valve train components together are a crucial factor in the impending numerical modal analysis, as the modal characterization of a structure is extremely sensitive to the applied constraints[10]. In this experience, valve train boundary conditions are considered the most important design parameter in the model updating process, as both material properties and geometry accuracy are deemed sufficiently adequate to obtain a valid test article modal characterization.

The spring force that fixes the valve train mechanism at the particular configuration illustrated in Figure 3.2 imposes distinctive patterns on the valve train component interfaces. The selected boundary conditions attempt to reproduce these patterns. In the test article, the compressed spring exerts a force, in the upward direction, on the rocker arm; the force is transmitted to the rocker arm through the lash-adjuster. The rocker arm, in turn, exerts a force in the downward direction on the camshaft. Thus, the interface clearance between camshaft bearings and head casting journals is preloaded and the major area of contact is located at the bottom of the interface. Similarly, the interface between the rocker arm and its shaft is also preloaded and their major area of contact is also located at the bottom of the interface. Therefore constraints between these parts were created at such areas of contact. The components were constrained together through the use of *rigid body elements* (RBE). RBEs are contact elements with independent DOFs at a node and dependent DOFs at an arbitrary number of nodes. The interface between the rocker arm roller and the cam is a line; the nodes on the roller and cam element edges that share such a line were merged. Similarly, the rocker shaft was

attached to the head casting model by merging the nodes at the corresponding interface, as the screws that are involved in this coupling provide a very stiff pairing. The screws were not explicitly modeled but the spacers were (refer to Figure 3.7); rocker shaft spacers account for the mass of the screws and are fastened to the shaft by the use of merged nodes, as well.

The boundary conditions relative to the valve are schematized in Figure 3.14. The lash-adjuster was modeled as a solid; it was bonded with the rocker arm by merging the nodes at their interface. The lash adjuster is connected to the valve through RBEs. The retainer and valve lock were modeled as a single solid; the upper part of the valve stem is embedded in such a solid by node merging, as well. The spring was modeled by inserting six spring elements, one per DOF (X, Y, Z, RX, RY, RZ), between two coincident nodes, which were physically located at the centroid of the equivalent spring. The two coincident nodes were then connected to the retainer and head casting through RBEs. The spring model is discussed in details in the next section. The valve guide was fully modeled as a solid (refer to Figure 3.12) and it was fixed to the head casting through the node merging technique. As it was mentioned in the previous section, the valve stem was primarily modeled with bar elements. The main reason for this selection and for the selection of modeling the complete valve guide derives from the constraints imposed on the valve. The valve stem bar elements were allowed to slide into the valve guide; torsion of the valve stem was also allowed. This condition was achieved through the use of RBEs; the fact of having bar elements inside the valve guide significantly simplified the RBE definitions. RBEs were also employed, within the valve model, for transitioning from the bar mesh of the valve stem to the solid mesh of the valve head and retainer. As

solid elements do not have rotational DOF, moment transfer between bar and solid elements is obtained through the use of RBEs; in the solid mesh, the nodes adjacent to the node at which the bar element is attached are constrained to follow the interconnect node motion. Figure 3.15 depicts the model of the sole valve train components.

FIGURE 3.14. Valve Model Scheme

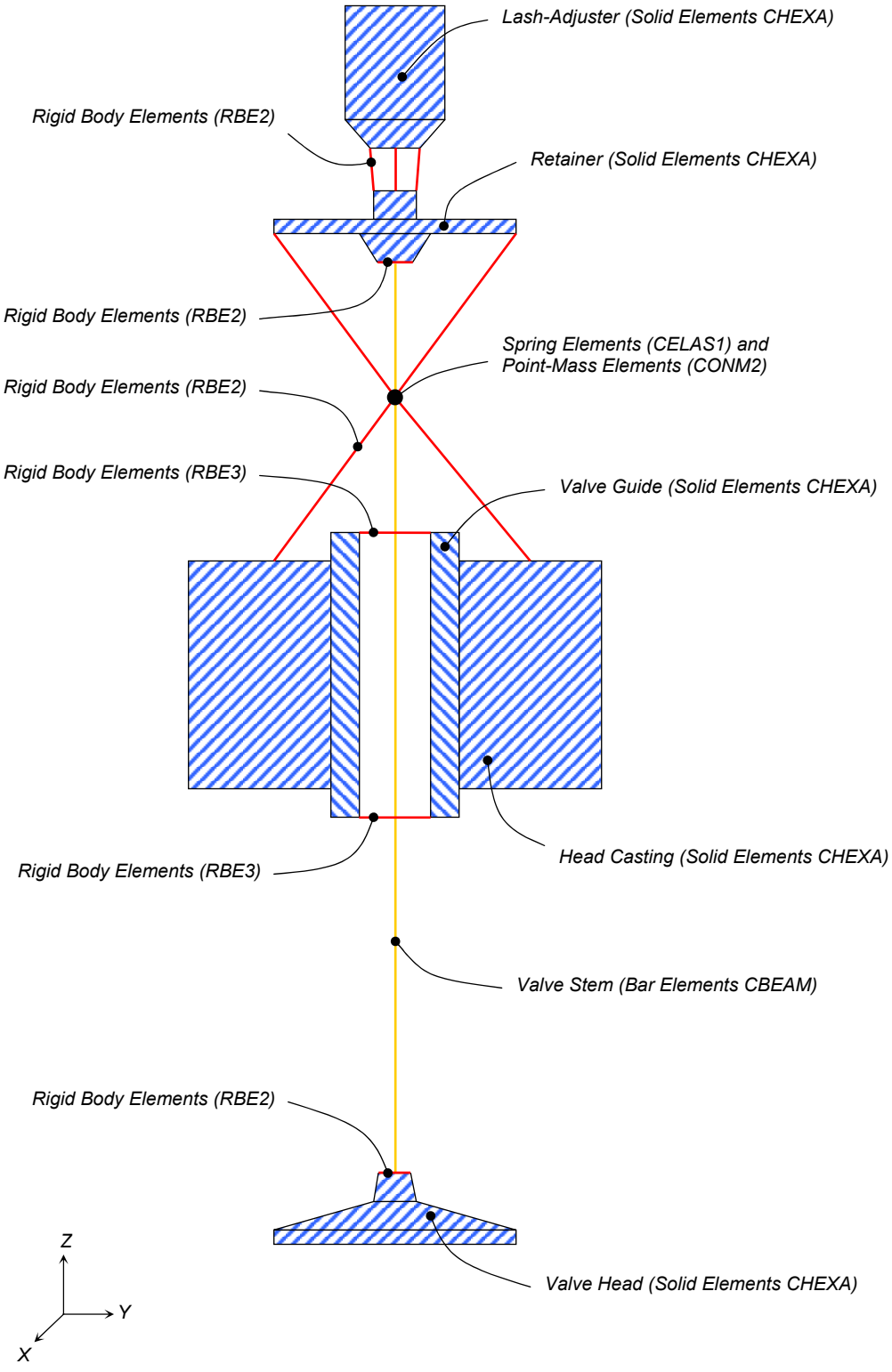

FIGURE 3.15. Valve Train Model

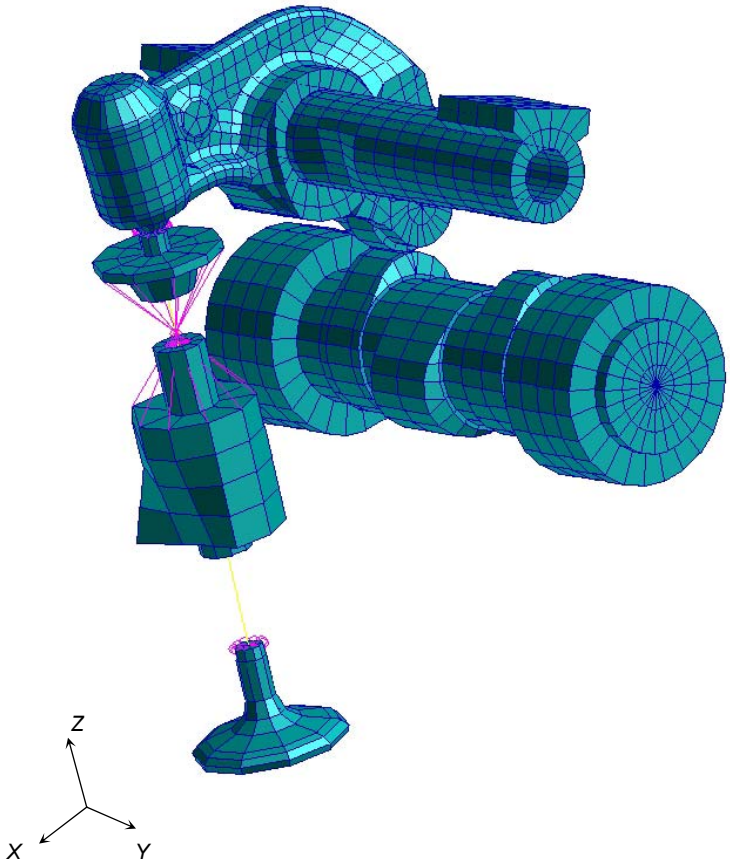

3.2.2. SPRING MODEL

As illustrated in Section 3.1, the valve train mechanism has been reduced to a structure composed of non-moving parts. This was achieved by introducing a force that prevents the kinematic chain from altering its given configuration. The only provider of the force is the spring, thus the applied force is an internal force. Recall that the force not only fixes the mechanism at a particular configuration but also serve to preload clearances between the system components. Although the preloading provider is internal, it is crucial to understand, and account for, the modifications that it introduces in both the overall and spring structural characteristics.

In order to analyze the spring behavior under the conditions set in the test article setup, a separate spring model was prepared. This test-vehicle model, shown in Figure 3.16, comprehends the full geometry of the spring in its free state. After having prepared a solid model of the part, the entire volume was then meshed with tetrahedral elements using an automatic mesher. Two different numerical modal analyses were performed with this mesh. The first was a *normal modes* solution (refer to Section 3.3) considering the spring in its free state and free of any boundary conditions. The second was a *normal modes with differential stiffness* solution considering the spring fixed at one end and compressed by a force at the other. The magnitude of the force compressed the spring to its actual length in the test article (i.e. it compressed the spring to the length it has when the valve is open). Obtaining a *normal modes with differential stiffness* solution means to account, in the stiffness matrix of the system, for the added stiffness that an initial load introduces in the structure. The eigenvalue extraction process required for the calculation of modal parameters becomes a non-linear problem, as this differential stiffness matrix is

able to account for the changes in potential energy associated with the ongoing element deformations. In other words, a differential stiffness matrix depends on element geometry, displacement field, and state of stress; it is independent from the elastic properties of the element's material. Table 3.1 illustrates and compares the results of these two solutions. As expected, the compressed spring shows an increased stiffness in every direction, thus its natural frequencies are shifted to higher values.

FIGURE 3.16. Spring Test-Vehicle Model

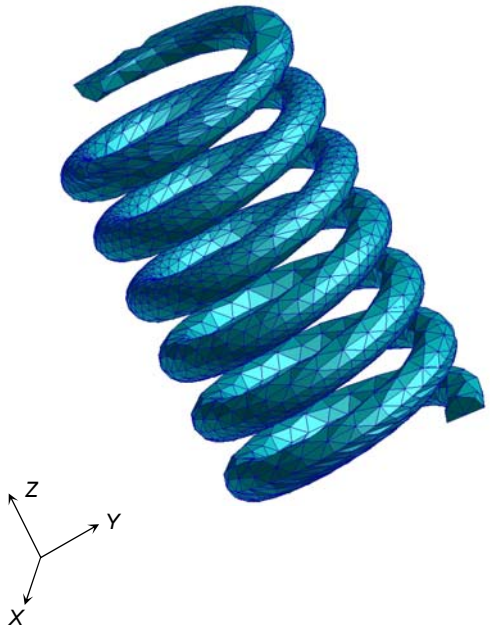

TABLE 3.1. Free and Compressed Spring Natural Frequencies Comparison

FREE AND COMPRESSED SPRING NATURAL FREQUENCIES COMPARISON						
Mode No.	***FEM Mode No.***	***Free Spring Frequency (Hz)***	***Compressed Spring Frequency (Hz)***	***Difference (Hz & %)***		***Mode Description***
1	*7*	***579***	***686***	*107*	*18.5%*	***1st Compression Z***
2	*8*	***648***	***859***	*211*	*32.6%*	***1st Lateral Bending X***
3	*9*	***649***	***861***	*212*	*32.7%*	***1st Lateral Bending Y***
4	*10*	***1148***	***1385***	*237*	*20.6%*	***2nd Compression Z***
5	*11*	***1210***	***1491***	*281*	*23.2%*	***Coil Local Mode***
6	*12*	***1220***	***1574***	*354*	*29.0%*	***2nd Lateral Bending X***
7	*13*	***1223***	***1580***	*357*	*29.2%*	***2nd Lateral Bending Y***
8	*14*	***1696***	***2231***	*535*	*31.5%*	***3rd Compression Z***
9	*15*	***1751***	***2280***	*529*	*30.2%*	***Coil Local Mode***

In order to validate the test-vehicle model reliability, the natural frequency of the first compression mode for the free spring was analytically calculated. The first natural frequency, in Hertz, of a free-free helical compression spring is given by[17]

$$f_n = \frac{2}{\pi N_a}\frac{d}{D^2}\sqrt{\frac{Gg}{32\gamma}}$$

where d – wire diameter

D – mean coil diameter

N_a – number of active coils

G – shear modulus

g – gravitational constant

γ – weight density

$$f_n = \frac{2}{\pi(5.02)} \frac{(4.32\times10^{-3}\,\text{m})}{(23.12\times10^{-3}\,\text{m})^2} \sqrt{\frac{(80.8\times10^{9}\,\text{Pa})(9.81\text{m/s}^2)}{32(76518\text{N/m}^3)}} = 583\text{Hz}$$

The difference between the numerical solution and the analytical solution is less than 1%. Figure 3.17 illustrates the spring modes.

In modeling the spring to be included in the FEM assembly, two factors were particularly considered. One was the proven modified structural characteristic of the spring and the other was desired simplicity of the spring model solution. The spring model schematic is described in Figure 3.18. As presented in the previous section, six spring elements, one per DOF (X, Y, Z, RX, RY, RZ), were placed between two coincident nodes. The nodes were physically located at the centroid of the equivalent spring (refer also to Figure 3.14). The mass of the spring was included by placing a concentrated mass, with magnitude equal to half of the total spring mass, on each of the two nodes. These two point-mass elements that represent the spring mass include, as well, the spring inertia as an element property. The inertias, with respect of the spring centroid, were calculated using the test-vehicle model, which is a full representation of the spring. The two coincident nodes were then connected to the retainer and head casting meshes through RBEs. Table 3.2 lists the estimated spring model stiffness values that account for the modified spring characteristics; these stiffness constants are considered model parameters to be updated in the model correction phase. Figure 3.19 illustrates the spring model as it looks in the complete model.

FIGURE 3.17. Spring Modes

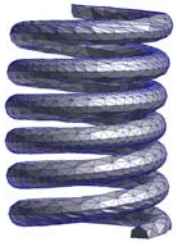

Mode 1: 1st Compression Z

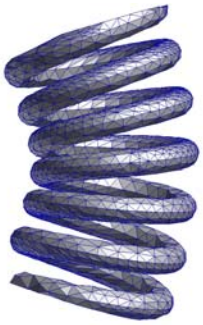

Mode 2: 1st Lateral Bending X

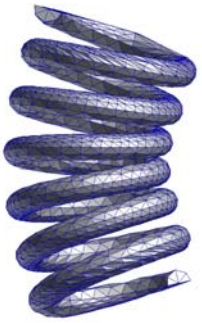

Mode 3: 1st Lateral Bending Y

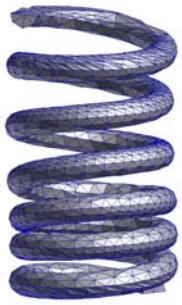

Mode 4: 2nd Compression Z

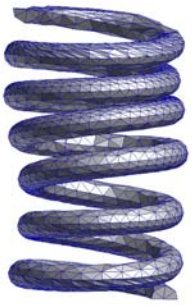

Mode 5: Coil Local Mode

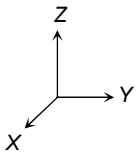

FIGURE 3.18. Spring Model Scheme

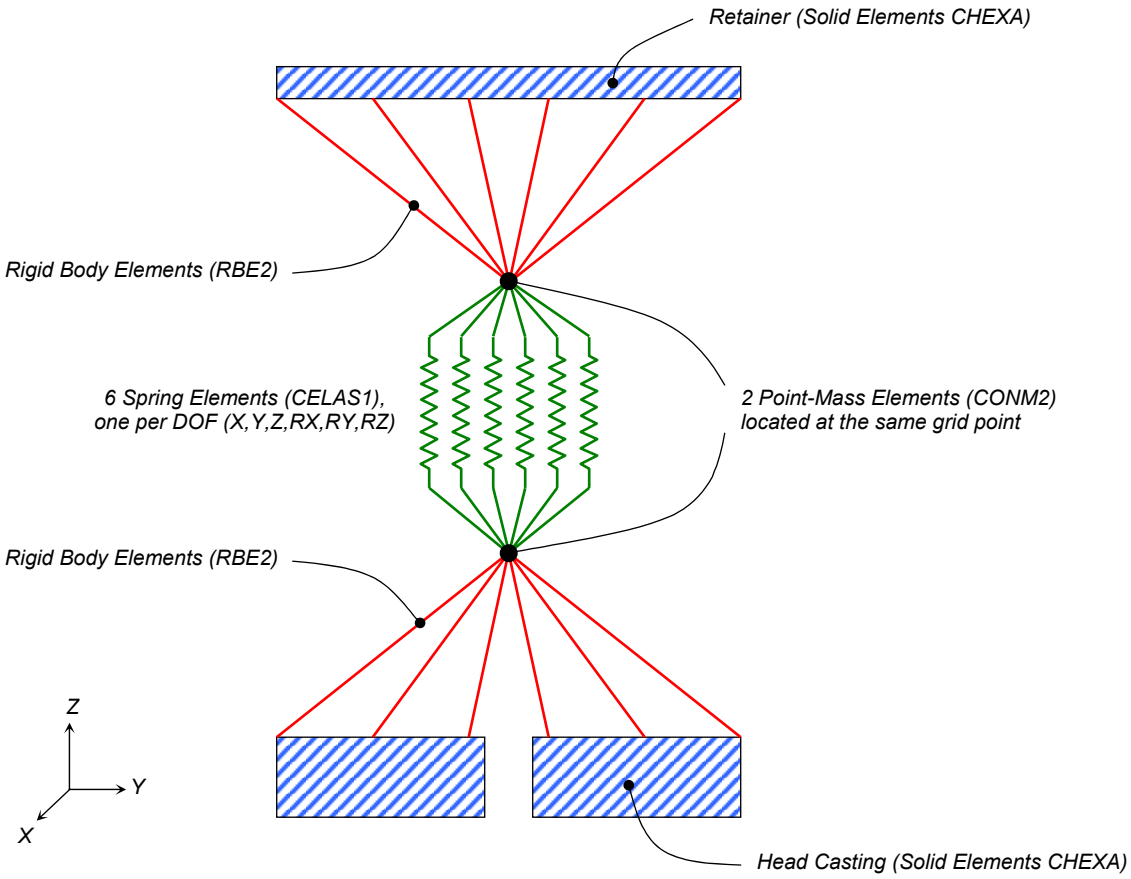

TABLE 3.2. Spring Model Stiffness Values

SPRING MODEL STIFFNESS VALUES	
DOF	***Stiffness Constant (N/m)***
Compression Z (Nominal Value = 57441 N/m)	*66650*
Lateral Bending X	*76650*
Lateral Bending Y	*76650*
Rotation RX	*66650 x 10^3*
Rotation RY	*66650 x 10^3*
Rotation RZ	*66650 x 10^3*

FIGURE 3.19. Spring Model

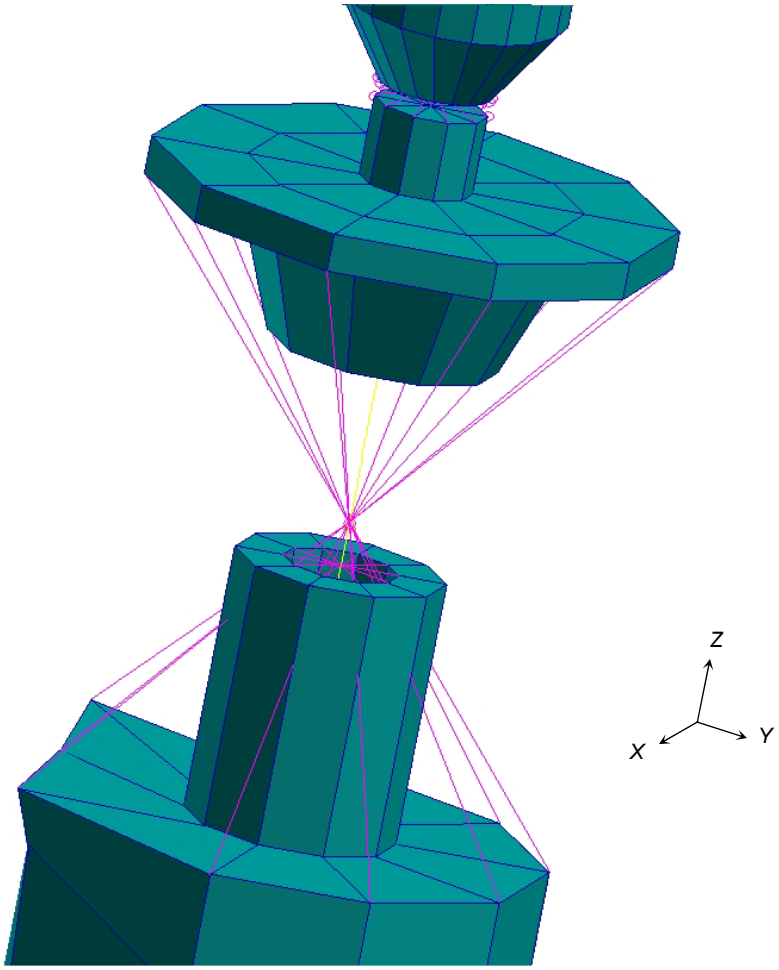

3.2.3. MODEL CHECKS

After the FEM model was developed, a number of validity checks were performed on the model prior to conducting the desired analysis. One mathematical check that it is good practice to perform on a FEM model prior to using results from it is the *unit gravity loading* validity check. This static analysis verifies that the model will provide proper displacements and reactions forces under gravity loading. The outcome of this validity check, in which the model must be grounded at some DOF, should show no large displacements for any node; in addition, reaction forces and moments should occur only at grounded locations. Another mathematical check that was performed on the model concerns rigid body modes; this validity check, however, is presented in the next section

In addition at the two mathematical checks just mentioned, a number of "common sense" accuracy checks were performed. These checks, which speak for themselves, are listed below since the purpose of this experience includes providing a methodology for developing a FEM model:

- *Units*
- *Mass comparison*
- *Material and element properties*
- *Input and output coordinate systems*
- *Rigid body elements*

Table 3.3 reports the mass comparison between the complete model and the test article. Table 3.4 lists the model element and node count, and the subsequent model total number of DOF.

TABLE 3.3. Test Article and FEM Model Weight Comparison

TEST ARTICLE AND FEM MODEL WEIGHT COMPARISON				
Component	***Test Article (g)***	***FEM Model (g)***	***Difference (g & %)***	
Head Casting	*3478.7*	*3574.00*	*95.3*	*2.74%*
Camshaft	*904.4*	*877.70*	*-26.7*	*-2.95%*
Intake Rockershaft	*191.8*	*196.80*	*5*	*2.61%*
Intake Rocker Arm Spacers	*34.6*	*40.50*	*5.9*	*17.05%*
Intake Valve	*48.2*	*46.72*	*-1.48*	*-3.07%*
Retainer and Lock	*14.6*	*15.96*	*1.36*	*9.32%*
Guide	*20.9*	*22.67*	*1.77*	*8.47%*
Spring	*50.3*	*48.00*	*-2.3*	*-4.57%*
Lash-adjuster	*14.9*	*13.07*	*-1.83*	*-12.28%*
Intake Roller & Axle	*21.7*	*22.86*	*1.16*	*5.35%*
Intake Rocker Arm (Casting Only)	*87.0*	*86.56*	*-0.44*	*-0.51%*
Complete Head Assembly	***4910.0***	***4946.00***	***36***	***0.73%***
Intake Rocker Arm Assembly	*122.4*	*120.10*	*-2.3*	*-1.88%*

TABLE 3.4. FEM Model Element, Node, and DOF Count

FEM MODEL ELEMENT, NODE, AND DOF COUNT				
Component	***Element Type***	***Number of Elements***		***Number of Nodes***
		Per Type	***Total***	
Head Casting	*Hexagonal Solid (CHEXA)*	*2308*	*3349*	*4495*
	Wedge Solid (CPENTA)	*419*		
	Quadrilateral Shell (CQUAD4)	*395*		
	Triangular Shell (CTRIA3)	*227*		
Intake Valve	*Hexagonal Solid (CHEXA)*	*50*	*128*	*206*
	Wedge Solid (CPENTA)	*60*		
	Beam (CBEAM)	*18*		
Camshaft	*Hexagonal Solid (CHEXA)*	*1412*	*1748*	*2165*
	Wedge Solid (CPENTA)	*336*		
Spring	*Spring (CELAS1)*	*6*	*8*	*2*
	Point-Mass (CONM2)	*2*		
Intake Rocker Arm (Casting Only)	*Hexagonal Solid (CHEXA)*	*682*	*810*	*1506*
	Wedge Solid (CPENTA)	*128*		
Intake Roller & Axle	*Hexagonal Solid (CHEXA)*	*63*	*63*	*150*
Retainer and Lock	*Hexagonal Solid (CHEXA)*	*30*	*30*	*50*
Lash-adjuster	*Hexagonal Solid (CHEXA)*	*50*	*50*	*137*
Intake Rockershaft with Spacers	*Hexagonal Solid (CHEXA)*	*528*	*528*	*1078*
Valve Guide	*Hexagonal Solid (CHEXA)*	*60*	*60*	*147*
Total			***6774***	***9303***
Total Degrees of Freedom (DOF)				***55818***

3.3. NORMAL MODES SOLUTION

The finite element method (FEM) techniques currently available to solve the real eigenvalue problem, which in turn provides the modal parameters of a FEM model, are well established and are not an object of analysis or evaluation in this study[7]. The modal parameters of a structure comprise natural frequencies and corresponding normal mode shapes. The natural frequencies are the frequencies at which a structure will tend to vibrate if subjected to a disturbance. The numerical computation of normal modal parameters is often denoted as *normal modes* analysis in FEM terminology. Thus, a *normal modes* solution computes the natural frequencies and normal mode shapes of a structure's model.

Normal modes analysis forms the foundation for a thorough understanding of the dynamic characteristics of a structure. For instance, the derived mode shapes may serve for a subsequent forced response analysis. The natural frequencies can be used to assess effects of design changes on the structural characteristics of a system. Alternatively, the natural frequencies may guide the selection of the proper time or frequency step in transient and frequency response analyses, respectively. Lastly, the normal modal parameters serve in assessing the degree of correlation between experimental modal data and numerical results.

In *normal modes* analysis there is no applied load and the structure has no damping properties. The equation of motion is of the form:

$$[M]\{\ddot{U}\}+[K]\{U\}=0$$

where $[M]$ – mass matrix

$[K]$ – stiffness matrix

The above equation can be reduced to an eigenvalue problem, in which the eigenvectors corresponds to modal vectors, or mode shapes, and their relative eigenvalues are proportional to natural, or characteristic, frequencies. The form of the eigenvalue problem is[16]:

$$[K - \lambda_i M]\{\theta_i\} = 0$$

where λ – eigenvalue

θ – eigenvector, or modal vector

The eigenvalues are related to the natural frequencies as follows:

$$f_i = \frac{\sqrt{\lambda_i}}{2\pi}$$

Each mode shape computed is similar to a static displaced shape in which each node can sustain displacements and rotations. However, there is one important difference between the mode shapes and the static displacements: the scaling. In static analysis the displacements are the true physical dislocations due to the applied loads. Since there is no applied load in *normal modes* analysis, the mode shape components can all be scaled by an arbitrary factor. For instance, a possible scaling method is to set equal to unity the maximum node displacement in any mode. This scaling process is known as *normalization* and the resulting modal vectors are said to represent *normal modes.* Clearly, being *normalization* arbitrary, it does not affect the mode shape, as all the components of the normalized vector are changed in the same proportion. A convenient *normalization,* in the view of a correlation with experimental modal data (i.e. orthogonality check matrix operations), is to choose the magnitude of the modal vectors so as to reduce the mass matrix [*M*] to the identity matrix. This will automatically reduce

the stiffness matrix [*K*] to the diagonal matrix of natural frequencies squared. This process is known as *mass-normalization*.

In *normal modes* analysis, element state of stress and reaction forces are computed in the same manner as for static analysis, with each mode shape treated the same as a set of static displacements. Due to the scaling of each mode, the resulting element stresses and forces are on a "per-mode" basis and cannot directly compared from one mode to another.

NASTRAN software provides a number of different eigenvalue extraction techniques, as no single eigenvalue extraction method is perfect for all models[7]. The method selected is the *Lanczos* technique; this sparse matrix solver is, for most applications, the fastest and most accurate eigenvalue extractor available in NASTRAN. Table 3.5 reports the natural frequencies and corresponding normal mode shape descriptions of a *normal modes Lanczos* solution for the developed FEM model over the frequency interval of interest. It is worth noting that this solution is obtained leaving the model unconstrained with respect of the "ground"; the model is free of any external boundary conditions. This free-state condition is a consequence of considerations regarding the supporting system selected for the test article in the experimental approach that are extensively discussed in Section 4.3. In this unrestrained condition, the structure exhibits rigid body modes, which are determined purely by its mass and inertia properties and in which there is no bending or torsion at all. Theoretically, any structure under this condition will disclose six rigid body modes and each of these has a natural frequency of zero Hz. Using numerical methods, the computed rigid body mode frequencies will not have exact zero values; however, they will exhibit values very close to zero. A *normal*

modes solution free of boundary conditions is indeed another validity check that verifies that the model will act as a rigid body when it is unconstrained; it also verifies that the stiffness matrix does not contain any grounding effects, such as illegally specified RBEs. The fifteen mode shapes derived with this solution are illustrated in Figures 3.20 A-D; the expected rigid body modes were properly computed but are not shown in the figures. The mode shapes derived in this preliminary solution will serve as target modes in the experimental approach.

TABLE 3.5. Pre-Test Target Modes

PRE-TEST TARGET MODES			
Mode No.	***FEM Mode No.***	***FEM Frequency (Hz)***	***Mode Description***
1	*7*	***469***	***Valve - 1st Bending X***
2	*8*	***470***	***Valve - 1st Bending Y***
3	*9*	***682***	***Spring - 1st Compression Z***
4	*10*	***844***	***Spring - 1st Bending X***
5	*11*	***846***	***Spring - 1st Bending Y***
6	*12*	***1631***	***Valve - 1st Torsion Z***
7	*13*	***2102***	***Rocker Arm - 1st Torsion***
8	*14*	***2243***	***Rocker Arm - 1st Bending Lateral***
9	*15*	***2319***	***Head Casting - 1st Torsion X***
10	*16*	***3207***	***Head Casting - 1st Torsion Y***
11	*17*	***3412***	***Rocker Shaft - 1st Bending Z***
12	*18*	***3492***	***Head Casting - 1st Bending X***
13	*19*	***4507***	***Valve - 2nd Bending X***
14	*20*	***4522***	***Valve - 2nd Bending Y***
15	*21*	***4584***	***Head Casting - 1st Bending Z***

FIGURE 3.20.A. Pre-Test Target Modes

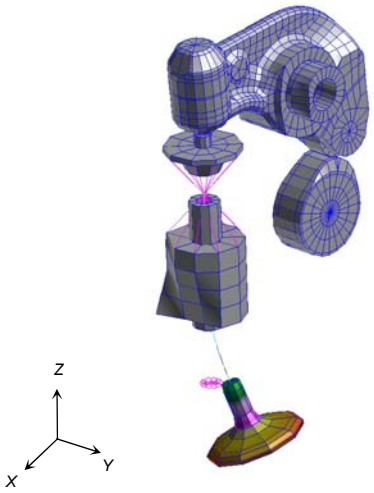

Mode 1 - Valve 1st Bending X

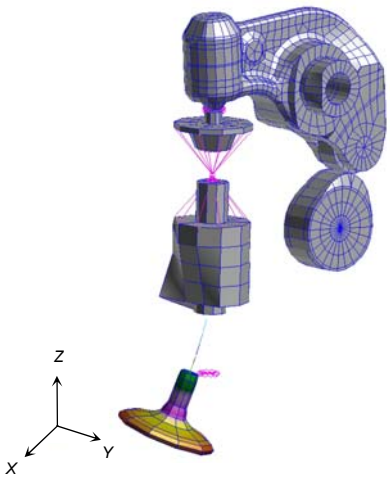

Mode 2 - Valve 1st Bending Y

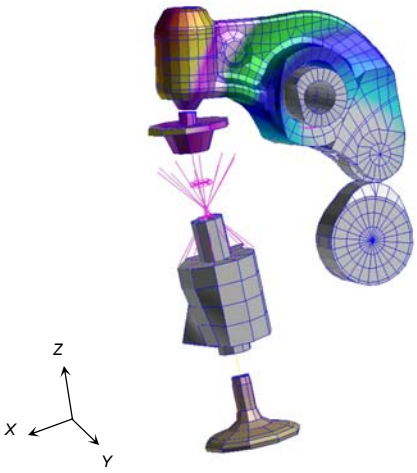

Mode 3 - Spring 1st Compression Z

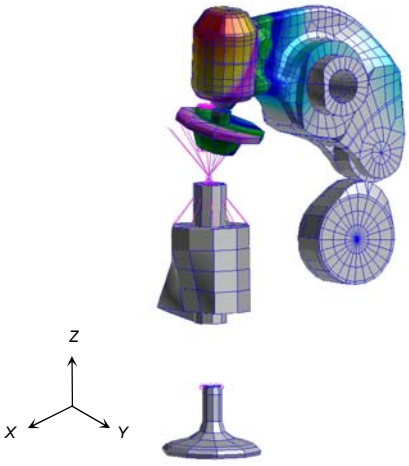

Mode 4 - Spring 1st Bending X

FIGURE 3.20.B. Pre-Test Target Modes

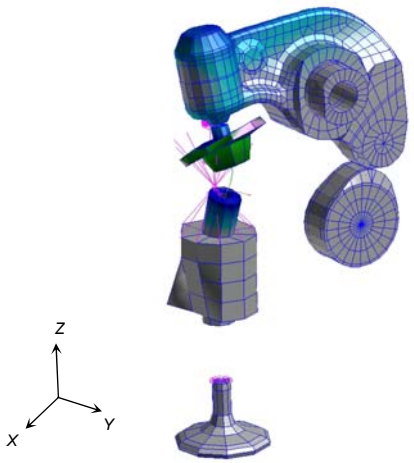

Mode 5 - Spring 1st Bending Y

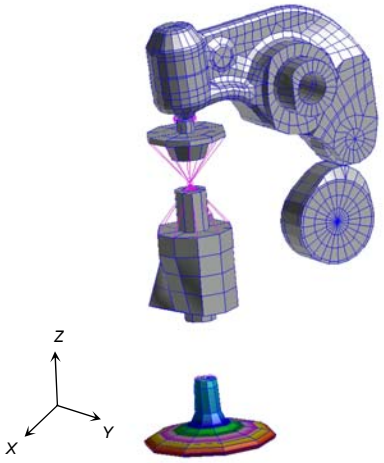

Mode 6 - Valve 1st Torsion Z

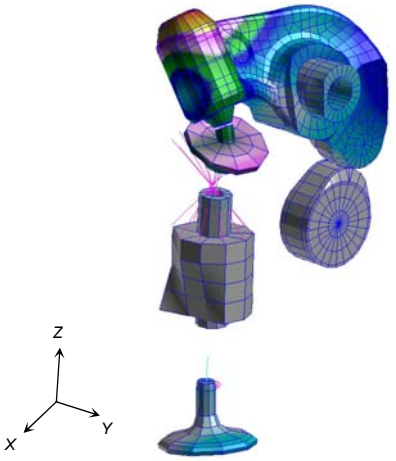

Mode 7 – Rocker Arm 1st Torsion Y

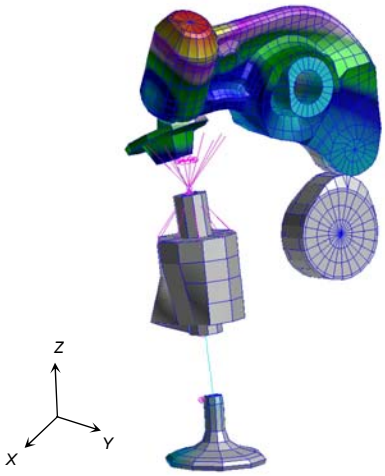

Mode 8 – Rocker Arm 1st Bending Lateral

FIGURE 3.20.C. Pre-Test Target Modes

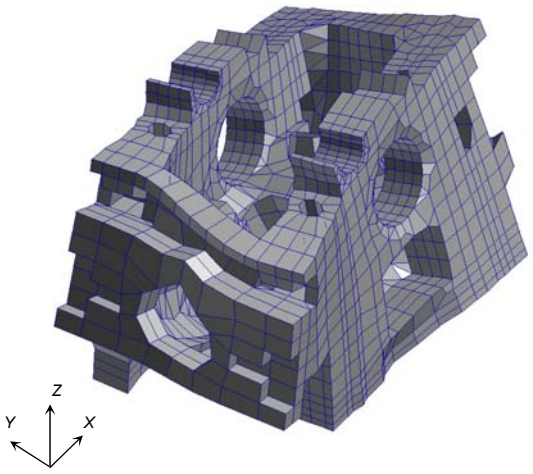

Mode 9 – Head Casting 1st Torsion X

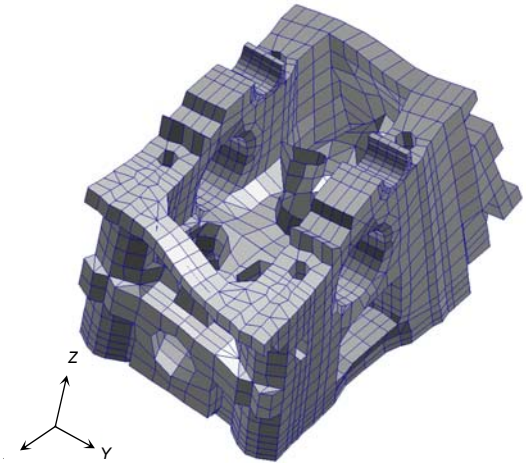

Mode 10 – Head Casting 1st Torsion Y

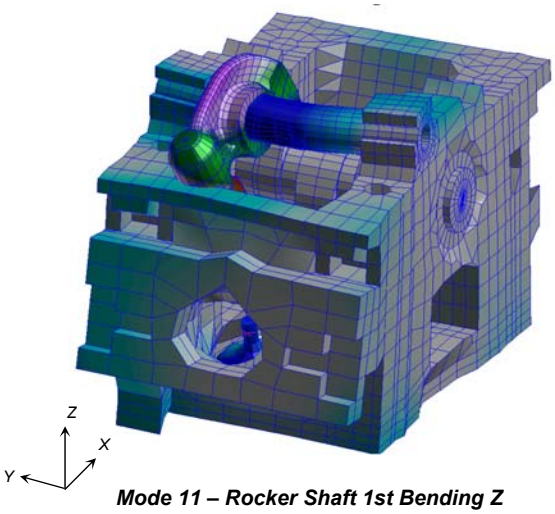

Mode 11 – Rocker Shaft 1st Bending Z

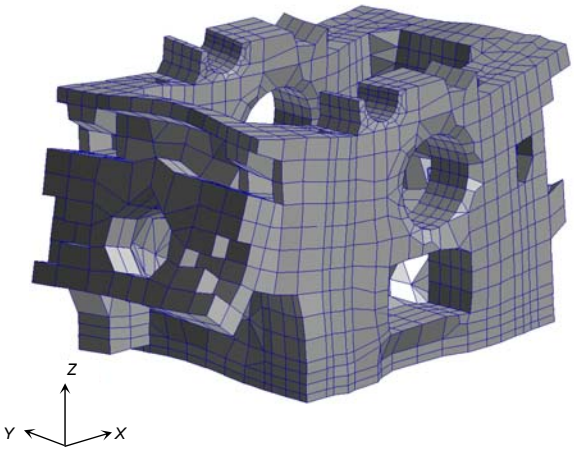

Mode 12 – Head Casting 1st Bending X

FIGURE 3.20.D. Pre-Test Target Modes

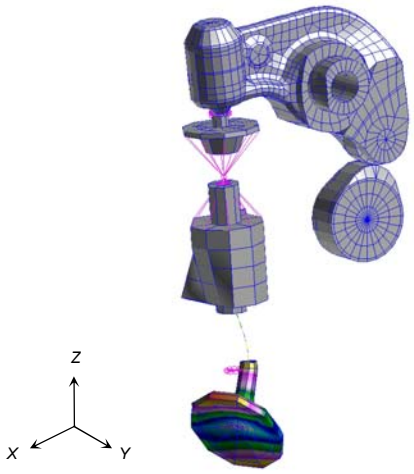

Mode 13 - Valve 2nd Bending X

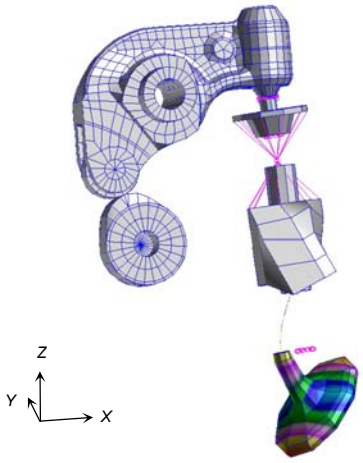

Mode 14 – Valve 2nd Bending Y

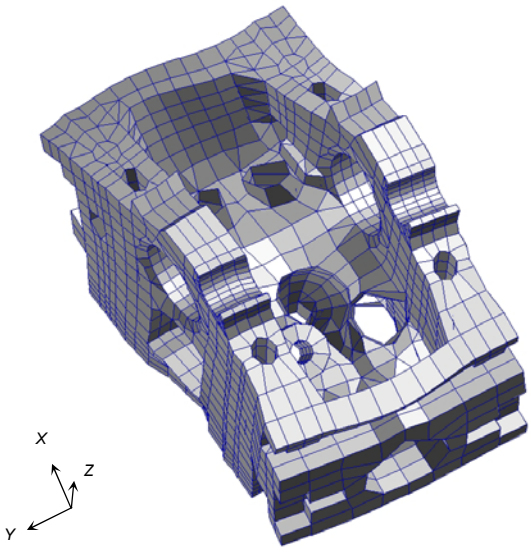

Mode 15 – Head Casting 1st Bending Z

3.4. TEST-ANALYSIS MODEL (TAM) DERIVATION

The basic objective of the forthcoming modal survey is to verify that the developed finite element model of the system is sufficiently accurate to predict the structure's modal behavior. The modal survey will measure the natural frequencies, damping, and mode shapes of the structure for use in model verification. The developed FEM model comprehends many more degrees of freedom than the test configuration will have accelerometers, due to obvious practical measurement limitations. Whereas the developed FEM model has DOF numbering in the thousands, the measured responses will possibly number in the dozens. In order to compare the model with the test results directly, a reduced representation, or test-analysis model (TAM), must be generated. The degrees of freedom of the TAM will correspond one for one with accelerometers in the modal survey test configuration. Therefore, while physically the TAM is a representation of the FEM model in the degrees of freedom of the measured test locations, mathematically, it is a matrix reduction for the FEM model mass and stiffness matrices from FEM model DOF size down to the test DOF size

The development of a TAM serves several major functions. The selection of TAM degrees of freedom optimizes the test response measurements and excitation locations. The reduced mass matrix enables a quantitative comparison of the accuracy of the FEM model during post-test correlation activities in the form of orthogonality and cross-orthogonality checks. All of these tasks require an accurate reduction of the FEM mass and stiffness matrices down to the TAM DOF, otherwise the TAM will not be able to perform efficiently its functions.

3.4.1. GUYAN REDUCTION

Several methods exist for reducing the mass and the stiffness matrices of a finite element model to a test-analysis model (TAM) whose degrees of freedom correspond to modal survey accelerometer location. These reduction methods differ in both the accuracy and robustness. Reduction accuracy is a measure of the TAM ability to reproduce the modal frequencies and mode shapes predicted by the complete finite element model. Reduction robustness, instead, is a measure of the TAM ability to produce valid orthogonality checks of test modes that prove that the finite element model contains inaccuracies. Robustness is of particular importance because showing orthogonal test modes is a commonly used requirement to determine the success of a modal survey correlation[12].

Matrix reduction procedures for FEM models are based on transformation methods of the form:

$$B = T^T A T$$

where A – original matrix

B – new matrix

T – transformation matrix

As it is expected with any analytical reduction, the reduced entities are only analytical/numerical approximations of the original entities. The matrix reduction methods that involve deriving test-analysis models must satisfy much greater demands than matrix transformations performed for other purposes. The major challenge is the matrix size large difference between the complete FEM model and the TAM. The TAM reduction produced must be able to accurately approximate the motion ability of the FEM

model DOF using a limited set of DOF. Since the ratio of the complete FEM model DOF and TAM DOF is very large, the method of producing the desired approximation must be precisely built for the goal of obtaining a test-analysis model.

The interpolation shapes used to "guess" the motion of the omitted DOF are the key to the accuracy and robustness of the matrix reduction methods commonly applied to derive TAM reductions. The type of information used to generate the interpolation functions will determine the accuracy of the TAM. In addition, the number of vectors used in the interpolation will affect the robustness of the TAM to handle model error[12].

The simplest procedure for producing a TAM uses a *Guyan* reduction method and this is the technique that is employed in this study, considering the fact that *Guyan* technology is one of the reduction methods that NASTRAN software is capable of performing. The *Guyan* reduction method is based on solving a static problem of the form[12]:

$$\begin{Bmatrix} F_o \\ F_a \end{Bmatrix} = \begin{bmatrix} K_{oo} & K_{oa} \\ K_{ao} & K_{aa} \end{bmatrix} \begin{Bmatrix} U_o \\ U_a \end{Bmatrix}$$

where o – omitted (non-instrumented) DOF

a – analysis (instrumented) DOF

Assuming that there are no loads on the omitted DOF, the upper partition of the above static problem can be solved:

$$U_o = -K_{oo}^{-1} K_{oa} U_a$$

The transformation matrix from the FEM model DOF to the TAM DOF is then:

$$\begin{Bmatrix} U_o \\ \hline U_a \end{Bmatrix} = \begin{bmatrix} -K_{oo}^{-1} K_{oa} \\ \hline I \end{bmatrix} U_a$$

or

$$G_{Static} = \frac{-K_{oo}^{-1} K_{oa}}{I}$$

The reduced stiffness and mass matrices can now be formed using the original FEM model matrices and the transformation matrix G*:*

$$M_{TAM} = G^T M_{FEM} G$$

$$K_{TAM} = G^T K_{FEM} G$$

where M_{TAM} – TAM mass matrix

K_{TAM} – TAM stiffness matrix

The *Guyan* reduction method makes the assumption that there are no forces on the omitted DOF. This is not a very accurate assumption considering the modal behavior of most structures[12]. In other words, the *Guyan,* or static, reduction provides a reduced model that shows close frequency and mode shape correlation with the full FEM model only when all the DOF that have significant inertia effects are considered. For some systems the number of DOF in this set greatly exceeds the number of experimental responses available in a realistic situation, not only due to hardware limitations but also time constraints. New reduction methods have been developed in order to more precisely include mass effects in the construction of the transformation matrix. If the simplified *Guyan* technique leads to unsatisfactory reductions, then other approaches need to be attempted.

3.4.2. ACCELEROMETER DISTRIBUTION

As stated earlier, the first role of the pre-test simulation is to identify the optimal accelerometer and exciter locations for the impending modal test. The number of locations required depends largely on the number of target modes that exist in the frequency range of interest. In general, the more target modes there are, the more measurement locations will be needed[1]. The modes that contribute most to the response that is being analyzed are selected as target modes. Therefore, in this context to optimize the accelerometer locations means to ensure that the test article is neither over nor under instrumented for obtaining the desired mode characterization.

Although a number of automated methods have been developed to help in the accelerometer location selection process, the selection still is to some extent a trial and error process[10]. As mentioned earlier, these iterative methods for deriving and evaluating reduced models were not considered in this correlation methodology. It is noted that although these algorithms can reduce the time required for the accelerometer selection process, generally, in order to be implemented they need a candidate DOF set, which confirm the trial and error nature of this selection.

Once the target modes have been identified, an adequate accelerometer location distribution is one that gives an accurate TAM with respect of such target modes. Figures 3.21 A-B show the result of the accelerometer distribution selection considering the target modes derived in the pre-test simulation, illustrated in the previous section, and listed in Table 3.5. Each arrow in the figure corresponds to a DOF included in the TAM, or to a DOF whose response is desired in the experimental approach. The total number

of TAM DOF selected is forty, distributed over sixteen nodes. The accuracy of this reduction, or measurement location set, is discussed in the next section.

FIGURE 3.21.A. TAM Degrees of Freedom – Accelerometer Distribution

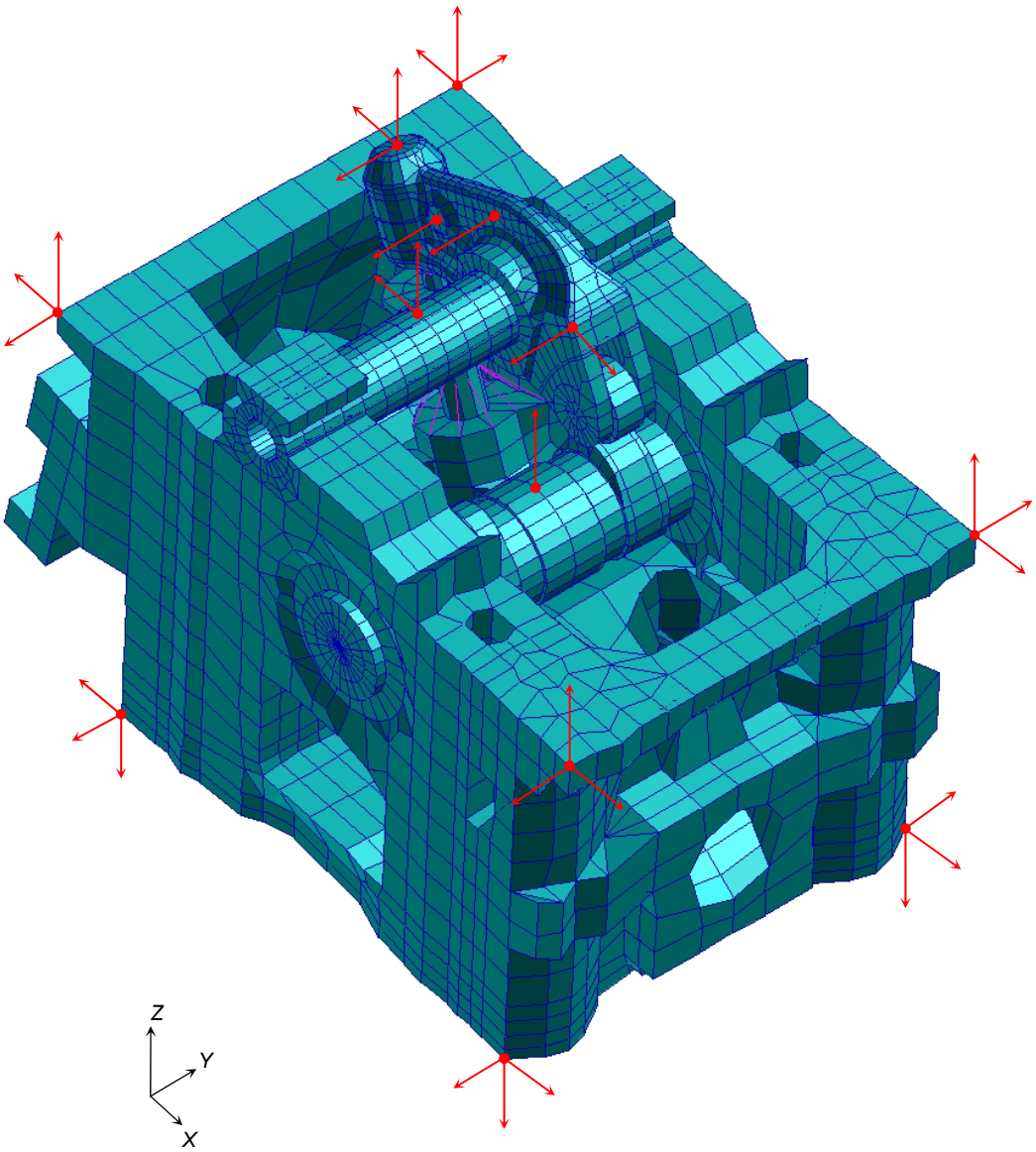

FIGURE 3.21.B. TAM Degrees of Freedom – Accelerometer Distribution

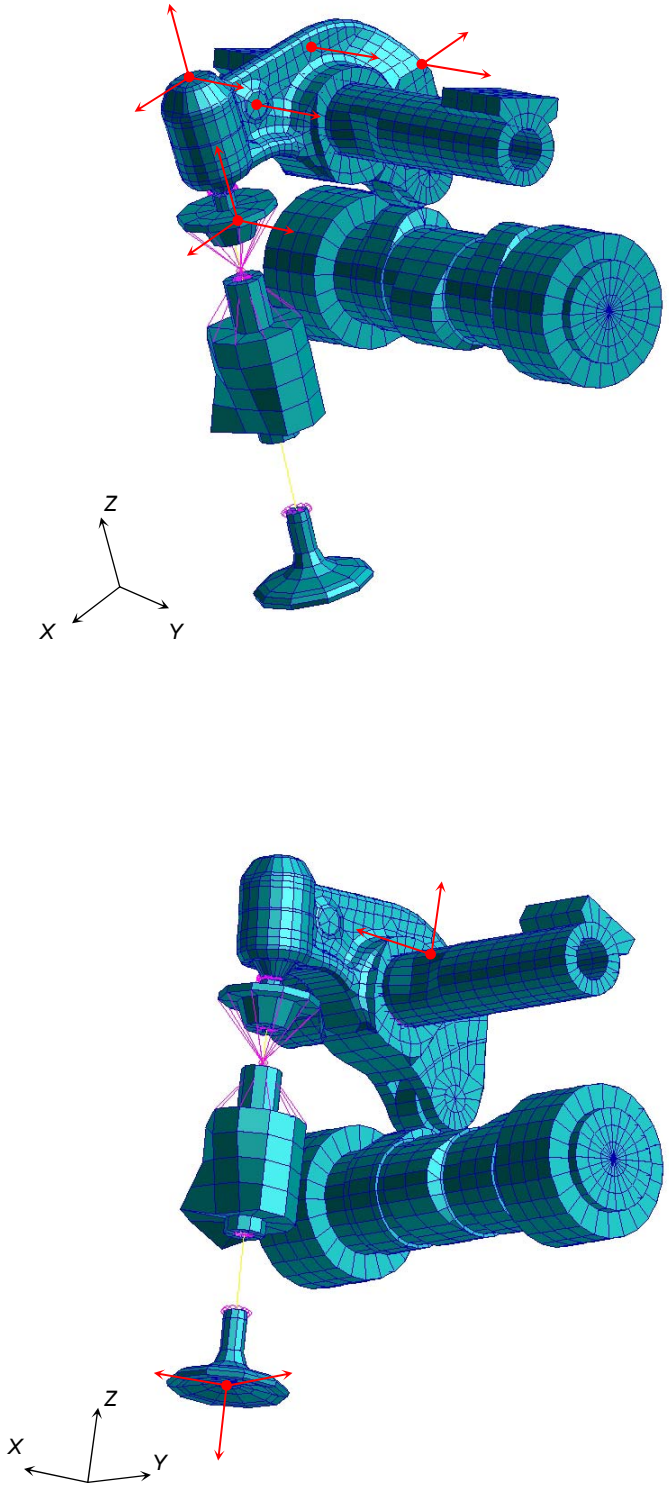

3.4.3. ACCURACY OF TAM

Evaluation of the accuracy of the TAM is a crucial step, as potential sets of accelerometer locations, or test DOF, are evaluated at this point. It is recalled that the FEM model reduction is performed on both the mass and stiffness matrices, M_{FEM} and K_{FEM}, respectively. Likewise the FEM model, the reduced model, or TAM, has its own modal parameters; thus it has characteristic natural frequencies and a characteristic mode shape matrix, Ψ_{TAM}. The accuracy of a TAM is evaluated based on how well the reduced modal properties approximate those of the original FEM model. For a *Guyan* reduction, the natural frequencies of the reduced model will generally be higher in value than those of the complete FEM model[12]. This apparent increment in stiffness is a direct consequence of the fact that the reduction omits a large number of DOF. In general, if the TAM frequency is within 10% of the FEM model frequency, the TAM is deemed adequate.

Mode shapes of the TAM and FEM models are compared by computing orthogonality, O, and cross-orthogonality, XO, matrices by the following matrices:

$$O = \Psi_{FEM}^{T} \; M_{TAM} \; \Psi_{FEM}$$

$$XO = \Psi_{FEM}^{T} \; M_{TAM} \; \Psi_{TAM}$$

In a perfect reduction, which of course cannot be obtained, the diagonal values of the orthogonality and cross-orthogonality matrices have the value of unity and the off-diagonal terms have the value of zero (assuming that the mode shapes have been *mass-normalized*). As stated earlier, in practice, a TAM is usually deemed adequate if the ortho and cross-ortho matrices terms meet the following criteria[10]:

$$\textit{diagonal terms} > 0.90$$

$$\textit{off-diagonal terms} < 0.10$$

It is recalled that although the ortho and cross-ortho matrices provide similar information about the TAM accuracy, they tend to indicate different things. The orthogonality matrix indicates the goodness of the mass distribution in the reduced model; the cross-orthogonality matrix indicates the accuracy of the reduced mode shapes.

Table 3.6 reports a comparison between the natural frequencies of the target modes, derived using the complete FEM model, and the natural frequencies of the TAM modes. The TAM natural frequencies were obtained by performing a *normal modes* solution on a *Guyan* reduction that included the forty DOF showed in the previous section. From this numerical analysis, it can be asserted that the selected TAM DOF set is adequate to positively approximate the modal parameters computed using the complete FEM model. No natural frequency difference exceeds the 10% value over the frequency interval of interest. The increment in stiffness trend is also observed as expected, as in the TAM all the structure's modes shifted upward their corresponding natural frequencies. NASTRAN software not only is capable of computing a *Guyan* reduction and solving it for the *normal modes* but it is also capable of calculating the orthogonality check described above. However, this task is achieved with a separate solution and by properly preparing a script that specifies the desired matrix operation. Figure 3.22 reports the diagonal and off-diagonal term values of the orthogonality check; they meet the desired criteria.

TABLE 3.6. Target Modes and TAM Frequencies Comparison

TARGET MODES AND TAM FREQUENCIES COMPARISON							
Mode No.	**FEM Mode No.**	**FEM Frequency (Hz)**	**TAM Mode No.**	**TAM Frequency (Hz)**	**Difference (Hz & %)**		**Mode Description**
1	7	**469**	7	**470**	1	0.2%	**Valve - 1st Bending X**
2	8	**470**	8	**471**	1	0.2%	**Valve - 1st Bending Y**
3	9	**682**	9	**684**	2	0.3%	**Spring - 1st Compression Z**
4	10	**844**	10	**850**	6	0.7%	**Spring - 1st Bending X**
5	11	**846**	11	**852**	6	0.7%	**Spring - 1st Bending Y**
6	12	**1631**	12	**1647**	16	1.0%	**Valve - 1st Torsion Z**
7	13	**2102**	13	**2211**	109	5.2%	**Rocker Arm - 1st Torsion**
8	14	**2243**	14	**2348**	105	4.7%	**Rocker Arm - 1st Bending Lateral**
9	15	**2319**	15	**2464**	145	6.3%	**Head Casting - 1st Torsion X**
10	16	**3207**	16	**3422**	215	6.7%	**Head Casting - 1st Torsion Y**
11	17	**3412**	17	**3634**	222	6.5%	**Rocker Shaft - 1st Bending Z**
12	18	**3492**	18	**3735**	243	7.0%	**Head Casting - 1st Bending X**
13	19	**4507**	19	**4810**	303	6.7%	**Valve - 2nd Bending X**
14	20	**4522**	20	**4826**	304	6.7%	**Valve - 2nd Bending Y**
15	21	**4584**	21	**4915**	331	7.2%	**Head Casting - 1st Bending Z**

FIGURE 3.22. Orthogonality Check between Target Modes and TAM Modes

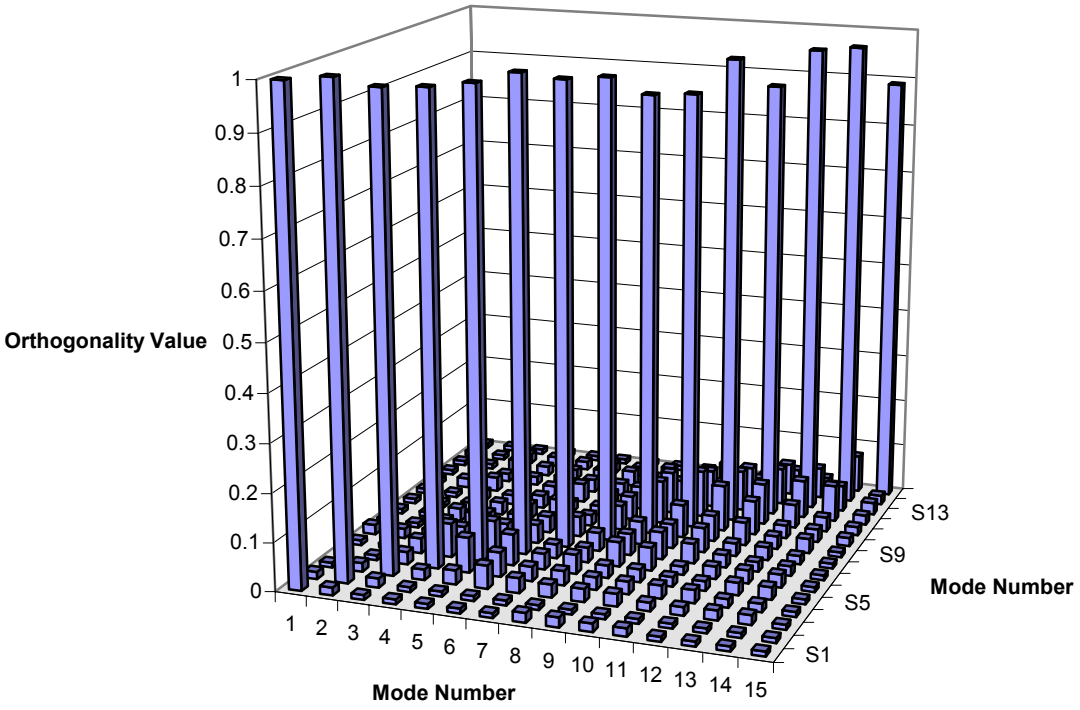

4. MODAL SURVEY

4.1. EXPERIMENTAL MODAL ANALYSIS OVERVIEW

Experimental modal analysis is the process of experimentally determining the modal parameters (natural frequencies, damping factors, and modal vectors) of a linear, time-invariant system. A common reason for performing an experimental modal analysis is to verify the results of an analytical/numerical approach, such as finite element method.

The process of determining modal parameters from experimental data involves several phases. The accuracy of the results of an experimental modal analysis depends not only upon understanding of the basis for each phase, but also on the establishment of specific goals for the test situation. One possible delineation of these phases is:

1. *Test article setup*
2. *Modal data acquisition*
3. *Modal parameter estimation*
4. *Modal data presentation*

During the *test article setup* phase, decisions regarding the test system configuration are made. A key test configuration factor is the type of support fixture (boundary conditions) chosen to constraint the structure to be tested. Boundary conditions are particularly important because they affect the overall structural characteristics of the test article. Sub-structuring a large and/or complex test article is a decision that must be evaluated during the *test article setup*. Simplifying the structure often improves dramatically the efficiency and quality of the test. The excitation type and method of applying it are, as well, test definition factors that are arranged during the

first phase of a modal survey.

The *modal data acquisition* phase involves the acquisition of data required to serve as input to the modal parameter estimation phase. Therefore, much care must be taken to ensure that the data match the requirements of the theory, as well as the requirements of the numerical algorithm involved in the modal parameter estimation. The theoretical requirements involve concerns such as system linearity and time invariance of system parameters. The numerical algorithms are particularly concerned with the bias errors in the data, as well as overall dynamic range considerations.

The *modal parameter estimation* phase is concerned with the practical problem of estimating the modal parameters, which are based upon a choice of a mathematical model, from the measured data. Problems that occur at this phase most often arise from violations of assumptions used to justify previous phases. Serious theoretical problems such as non-linearity cause serious problems in the estimation of modal parameters and may be reason to invalidate completely the experimental modal analysis approach. Serious practical problems, such as bias errors resulting from the digital signal processing, cause similar problems but are a function of data acquisition techniques that can be altered to minimize such errors. The *modal parameter estimation* phase is that point in the experimental modal analysis process where the errors of all previous work accumulate[11].

Modal data presentation represents the final phase of the process; it provides a physical interpretation of the modal parameters. It may simply be the numerical tabulation of the frequency, damping, and modal vectors, along with the associated geometry of the measured degrees-of-freedom. More often, modal data presentation is

concerned with the plotting and animation of such information. This involves the additional information required to construct a three-dimensional representation of the test article.

4.2. MODAL ANALYSIS THEORY

A single degree-of-freedom (DOF) system, presented and evaluated in the time and frequency domains, serves as the basis for many of the models that are used in modal parameter estimation. The multiple DOF linear case can be viewed simply as a linear superposition of single DOF systems[14]. The general mathematical representation of a single DOF system, represented schematically in Figure 4.1, is given by

$$m\ddot{x} + c\dot{x} + kx = f(t) \tag{1}$$

where *m, c* and *k* are the mass, damping and stiffness constants, respectively, and *f(t)* is function that represents the excitation applied to the system.

FIGURE 4.1. Single Degree of Freedom (SDOF) System

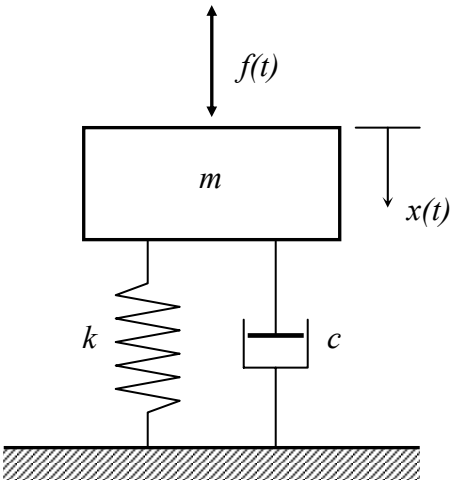

By setting *f(t)* equal to zero, the homogeneous form of the equation can be solved. The general solution of Equation (1) then is

$$x(t) = Ae^{p_1 t} + Be^{p_2 t}$$

where A and B are constants and the values of p_1 and p_2, for an under damped system are given by

$$p_r = \sigma_r + j\omega_r$$

where σ_r is the damping factor in radians per time-unit and ω_r is the damped natural frequency in radians per time-unit. For most real structures, unless active damping systems are present, the fraction of critical damping is rarely greater than 10%. For such underdamped systems, the two roots, p_1 and p_2, are always complex conjugates and are referred to as the *poles* of the system. Also, the two coefficients, A and B, are complex conjugates of one another.

Equation (1) is the time-domain representation of the system in Figure 4.1. An equivalent equation of motion may be determined for the frequency domain. This representation has the advantage of converting a differential equation to an algebraic equation. This is accomplished by taking the Fourier transform (basic Fourier analysis is presented in Appendix A) of Equation (1). Thus, it becomes

$$\left[-m\omega^2 + jc\omega + k\right]X(\omega) = F(\omega) \tag{2}$$

Letting

$$B(\omega) = -m\omega^2 + jc\omega + k$$

then Equation (2) becomes

$$B(\omega)X(\omega) = F(\omega) \tag{3}$$

Equation (3) is an equivalent representation of Equation (1) in the Fourier domain. The

system response $X(\omega)$ is directly related to the system forcing function $F(\omega)$ through the quantity $B(\omega)$. If the system forcing function $F(\omega)$ and its response $X(\omega)$ are known, $B(\omega)$ can be calculated by

$$B(\omega) = \frac{F(\omega)}{X(\omega)}$$

Rearranging this equation as follows

$$X(\omega) = \frac{F(\omega)}{B(\omega)} \tag{4}$$

and defining $H(\omega) = 1 / B(\omega)$, Equation (4) becomes

$$X(\omega) = H(\omega)F(\omega)$$

The quantity $H(\omega)$ is known as the frequency response function (FRF) of the system. A frequency response function relates the Fourier transform of the system input to the Fourier transform of the system response. Thus, the frequency response function is defined as

$$H(\omega) = \frac{X(\omega)}{F(\omega)}$$

Using Equation (2), the frequency response function can be written as

$$H(\omega) = \frac{\frac{1}{m}}{-\omega^2 + j\frac{c}{m}\omega + \frac{k}{m}}$$

The characteristic values of this equation are known as the complex roots of the characteristic equation or the *complex poles* of the system[11]. The frequency response function $H(\omega)$ can now be rewritten as a function of the complex poles

$$H(\omega) = \frac{\frac{1}{m}}{(j\omega - p_1)(j\omega - p_2)}$$

where $p_1 = \sigma_1 + j\omega_1$ is the complex pole and p_2 its complex conjugate. Since the frequency response function is a complex-valued function of a real-valued independent variable ω, the frequency response function is represented by a pair of curves (real and imaginary parts) as shown in Figure 4.2.

FIGURE 4.2. Frequency Response Function Real and Imaginary Parts

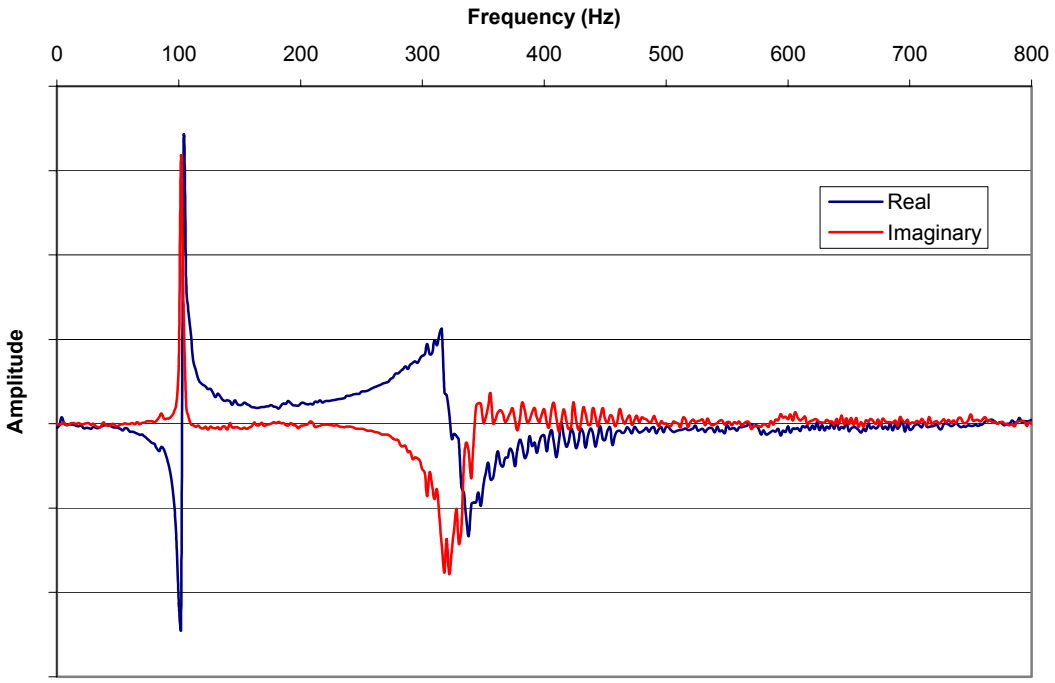

4.2.1. FREQUENCY RESPONSE FUNCTION METHOD

The frequency response function (FRF) method of experimental modal analysis is the most commonly used approach to the estimation of modal parameters. In this method, frequency response functions are measured throughout the structure using excitation at single or multiple points. This excitation may be narrowband or broadband as well as being random or deterministic. The frequency response functions are then used as input to a modal parameter estimation process. Often, and as it is the case in this study, a curve-fitting procedure is used to extract the modal parameters in the parameter estimation procedure. The curve-fitting extracts the location of system poles from the measured frequency response functions. A weighted orthogonality check may be made of the modal vectors in order to evaluate the relationship of the estimates to some analytical or numerical model[8].

The frequency response function, which has been mathematically defined in Section 4.2 as the quotient between the input and output Fourier transforms, can be represented by the diagram in Figure 4.3. It is evident that in modal testing the input excitation and output response need to be measured simultaneously. As frequency response functions are being acquired and stored for subsequent modal parameter estimation, an adequate set of measurement must be collected in order to arrive at an exhaustive set of modal parameters. To this purpose, the employment of pre-test analysis procedures, such as the development of a test-analysis model (TAM), to guide the execution of the test will significantly improve the efficiency of the test process. It is recalled that the TAM that results from the pre-test simulation also provides a means to

FIGURE 4.3. Frequency Response Function Diagram

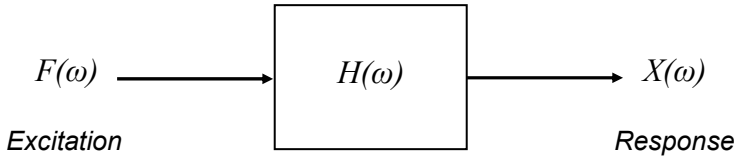

compare the test and the model both during the experimental approach and during the model updating process.

Frequency response function technology involves obtaining and evaluating multiple independent modal vector estimates from multiple rows or columns of the frequency response function matrix. A complete, although redundant, set of frequency response measurements would form a square matrix of size *n,* where the rows correspond to response points and the columns to excitation points, as follows

$$M_{FRF} = \begin{bmatrix} H_{11} & H_{12} & \cdots & H_{1n} \\ H_{21} & H_{22} & & \\ \vdots & & \ddots & \\ H_{n1} & & & H_{nn} \end{bmatrix}$$

However, it can be analytically proved that any particular row or column contains sufficient information to compute the complete set of natural frequencies, damping factors, and mode shapes[11]. In other words, if the excitation is restricted at one point and the response is measured at all the points, including the excitation point, then only one column of the response matrix is being constructed and the modal parameter extraction is still possible. This procedure is commonly known as *single-point excitation* technique.

On the other hand, if an accelerometer is fixed to one point and the structure is excited at all points, including the accelerometer location, then only one row of the response matrix is being collected and the modal parameter extraction is equally possible.

The measurement where response point and direction coincide with the excitation point and direction is often called a *driving point measurement.* The input location is denoted also as the *reference*. *Driving point measurements* form the diagonal of the frequency response matrix introduced above. *Driving point measurements* exhibit unique characteristics that are not only useful for checking measurement quality, but necessary for accomplishing a comprehensive modal analysis, which includes not only frequencies, damping factors and scaled mode shapes, but also modal mass and stiffness. It is not necessary to include *driving point measurements* in the modal parameter estimation algorithms in order to obtain only frequencies, damping factors and unscaled mode shapes. However, a set of scaled mode shapes and consequently modal mass and stiffness cannot be extracted from a set of measurements that does not contain *driving point measurements*. This concept must absolutely be recalled during test planning since subsequent orthogonality checks that involve modal mass and stiffness matrices are desired, in the view of a correlation with a numerical approach.

This study implemented the *single-point excitation* technique. The input force was restricted to one location while the response was collected at forty different degrees of freedom throughout the structure. The input location and excitation method selected are discussed in Section 4.5. The forty response measurement locations were dictated by the TAM degrees of freedom derived in the pre-test simulation (refer to Section 3.4.2). This measurement location set included the *reference*, thus, one *driving point*

measurement was also acquired. Due to hardware limitations (i.e. the availability of only one accelerometer with the desired characteristics), the frequency response functions were acquired one at a time. This approach has the convenience of limiting the instrumentation imposition on the structure, but it can significantly decrease the test efficiency from a time point of view.

The frequency response matrix of a linear system has an additional important property. When the system is assumed to behave linearly, the frequency response matrix is always symmetric due to *Maxwell's Reciprocity Theorem*[16]. Simply stated, a measurement with the excitation at point *i* and the response at point *j* is equal to the measurement with the excitation at point *j* and the response at point *i*. For example, referring to the matrix above, $H_{12} = H_{21}$. This property is helpful in proving the linearity assumption. By comparing two reciprocal measurements at various pairs of points and observing any differences between them, the degree of linearity of the system can be estimated. Section 4.6.1 describes the reciprocity measurements taken to prove the linearity of the test article, while Section 4.4 reviews some considerations about the linearity assumption.

4.2.2. THE FAST FOURIER TRANSFORM

The acquisition of frequency response functions for the formulation of a modal model involves the use of a frequency spectrum analyzer, or Dynamic Signal Analyzer (DSA). A spectrum analyzer is a signal processor that allows recording a signal in both the time and frequency domains. Modern Dynamic Signal Analyzers are digital signal processors that transform the data from the time domain to the frequency domain by use

of a very efficient algorithm, the Fast Fourier Transform (FFT) algorithm[3]. The FFT algorithm is the basis for the formulation of any frequency-domain function in modern acquisition systems. The basic theory of Fourier analysis is presented in Appendix A.

In terms of an integral Fourier transform, a function must exist for all time in a continuous sense in order to be evaluated, or "transformed". For the realistic measurement situation, data are available in a discrete sense over a limited time period. The FFT, therefore, is based upon a set of assumptions concerning this discrete sequence of values. The assumptions can be reduced to one of two situations that must be met by every signal processed by the FFT algorithm:

1. *The transient signal must be captured completely within the time record*
2. *The signal must be composed only of harmonics of the time record (i.e. it must be exactly periodic in the time record)*

If one of these two assumptions is not met by any discrete history processed by the FFT algorithm, then the resulting spectrum will contain bias errors accordingly.

The accurate measurement of frequency response functions depends significantly upon the errors involved with the digital signal processing. In order to take full advantage of experimental data in the correlation of experimental procedures with numerical approaches, the errors in measurement, generally designated as noise, must be reduced to acceptable levels. Various types of errors are discussed in Section 4.7, including bias errors associated with the improper implementation of the FFT algorithm.

4.3. SUPPORTING THE STRUCTURE

One important preliminary decision in modal testing concerns whether the structure is to be tested in a "free" condition or "grounded". This is a key step in the process as the constraint state affects the overall structural characteristics. The applied constraints, or boundary conditions, are even more important when test correlation to an analytical or numerical model is desired. Analytically, and thus numerically, boundary conditions can be specified in a completely free, as illustrated in Section 3.3, or completely constrained sense. However, in testing practice it is not possible to fully achieve neither of these two conditions.

The free condition means that the structure is not attached to ground at any of its coordinates and is, in effect, freely suspended in space. In this condition, the structure will exhibit rigid body modes, which are determined merely by its mass and inertia properties and in which there is no bending or torsion at all. Theoretically, any structure will disclose six rigid body modes and each of these has a natural frequency of zero Hz. The grounded condition, on the other hand, attempts to fix a number of selected points on the structure to ground. While this conditions is extremely easy to apply in a theoretical analysis, by simply forcing to zero the displacement of the appropriate coordinates, it is much more difficult to implement in the test environment. The reason for this is that it is very difficult to provide a sufficiently rigid base or fixturing mechanism on which to attach the test article. In other words, it is difficult to approximate the grounded condition without taking the extraordinary precautions that make this condition impractical to implement in a variety of applications.

Whereas the grounded condition is difficult to approximate, it is generally

feasible to provide the test article with a suspension system that closely approximates the free condition. This can be achieved by suspending the structure from very soft elastic cords or by placing it on a very soft cushion. In the presence of this type of supports, the structure rigid body modes will no longer have zero natural frequencies but their frequency values will be very low relative to those of the first bending modes. It was thus decided to test the structure objective of this modal testing and described in Section 3.1 in a free condition. The test article was suspended via four very soft elastic cords, as shown in Figure 4.4. It was, however, necessary to validate this free state approximation as the suspension system could still interfere in the modes of vibration of the structure. Section 4.6.3 describes how this validation was achieved. It is now recalled that the pre-test simulation performed to obtain the target modes and develop the TAM must also reproduce the test article supporting system selected. Thus, the decision concerning the supporting system in the experimental approach is really a decision that must be taken in the pre-test simulation phase.

FIGURE 4.4. Test Article Boundary Conditions

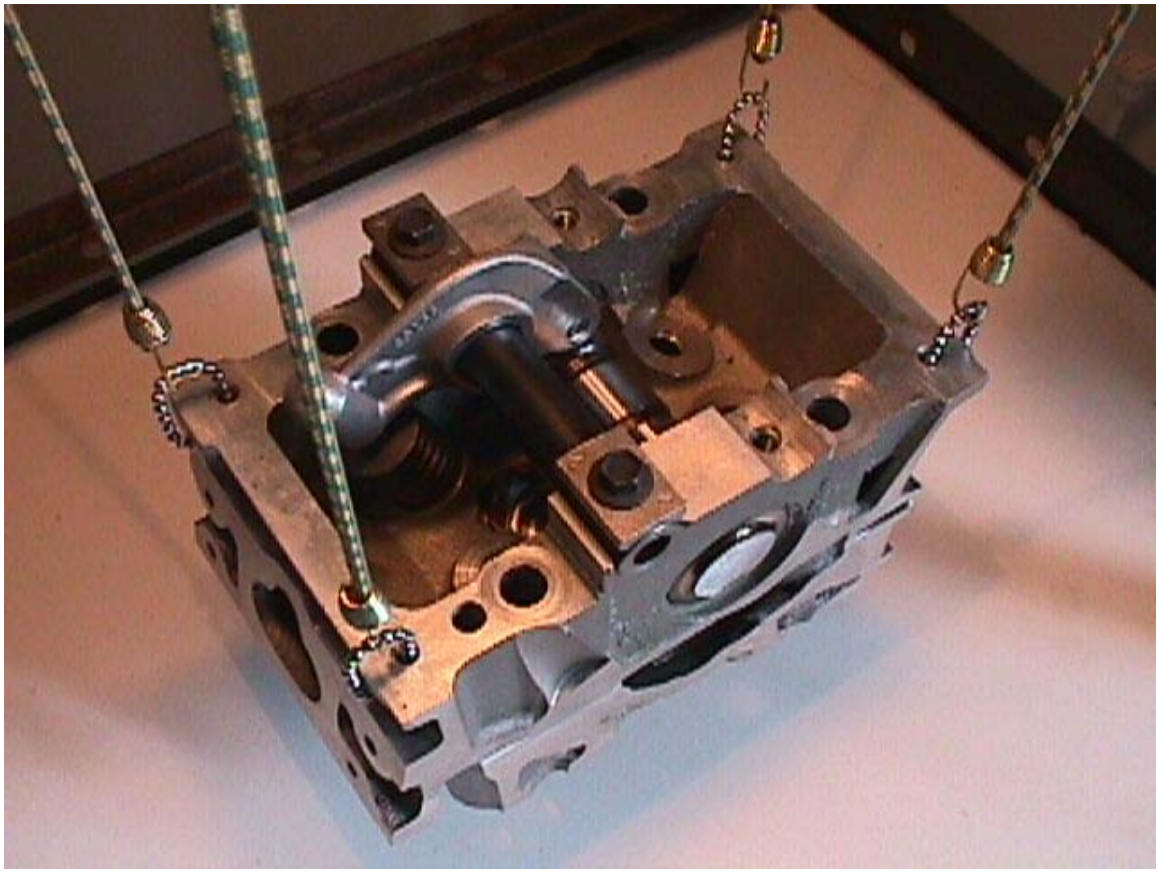

4.4. SYSTEM ASSUMPTIONS

In performing an experimental modal analysis, three basic assumptions are made concerning any structure. The structure is assumed to be:

1. *Linear*
2. *Time-invariant*
3. *Observable*

Assuming a structure to be *linear* means that the response of the structure to any combination of forces, simultaneously applied, is the sum of the individual responses to each of the forces acting alone. This is a very good assumption for a wide variety of structures. When a structure is *linear*, its modal parameters can often be characterized by exciting the system through one or more controlled forces that have form and location convenient for measurement and parameter estimation rather than being similar to the forces that are actually applied to the structure in its normal environment.

The linearity assumption has three implications for the frequency response functions (FRF). One is that the measured FRF is not dependent on the type of excitation waveform used to excite the structure. Secondly, a measured FRF is independent of the excitation level, as well. The last implication of linearity on FRF is concerned with *reciprocity*. As stated in Section 4.2.1, in a *linear* mechanical system the frequency response matrix is symmetric. This implies that the FRF measured between any two DOF is independent of which of them is used for excitation or response.

When a structure is assumed to be *time-invariant*, the modal parameters that are to be determined are constants. A system that is not *time-invariant* has components whose mass, stiffness, or damping depend on factors that may vary with time. For

instance, if some components are temperature dependent, the temperature of the component is viewed as a time-varying signal, and the entire system may have time-varying modal characteristics. Therefore, the modal parameters that would be determined by any measurement and estimation process would depend on the time (as temperature may vary with time) at which the measurements were made. If the structure that is being tested changes with time, then measurements made at the end of the test period determine a different set of modal parameters than measurements made at the beginning of the test period. Thus, the measurements made at the two different times will be inconsistent, violating the assumption of time invariance.

Assuming a structure to be *observable* means that the input-output measurements that are made contain enough information to generate an adequate behavioral model of the structure. Structures that have components whose certain DOF are not considered in the measurements are not completely *observable*. Sometimes, a sufficient number of measurements can be made so that the system is *observable* under the form chosen for the model, and sometimes no realistic number of measurements will be sufficient until the model is changed. This assumption is particularly relevant to the fact that the data normally describe an incomplete modal behavior of the structure. This occurs in at least three different ways. First, the experimental data are normally limited to a minimum and maximum frequency, as well as to a limited frequency resolution. Secondly, sometimes no information is available relative to a particular DOF because of the physical limitation of locating a transducer in that area. The third case concerns local rotations. Local rotation is a DOF that is often overlooked and that radically contributes to the characterization of certain modes. It is worth noting that even when the three main

directions (X, Y, and Z) relative to a certain point are being captured, the three local rotations (RX, RY, and RZ) for the same point might be completely missed.

Another assumption that might be formulated concerns repeated roots. The experimental setup and parameter estimation algorithm chosen may not allow the determination of repeated roots based upon a limited ability to gather and process data, respectively. Repeated roots refer to the situation where one complex root or eigenvalue occurs more than once in the characteristic equation. Each root with the same value has an independent modal vector or eigenvector. This situation, which is critical in developing a truly complete modal model, can only be detected by the use of multiple inputs or *references*. However, sometimes the occurrence of repeated roots is easily theoretically predictable and it can be assumed even if it is not being measured and included in the modal parameter estimation process.

4.5. EXCITING THE STRUCTURE

A key step in the measuring process involves selecting an excitation function along with the excitation application system that best suites the test requirements. The excitation function is the mathematical description of the signal used for the input. The excitation system is the physical mechanism or device employed to provide such a signal. The type of input function desired and the type of excitation system are interrelated. The choice of the excitation function usually dictates the choice of the excitation system. Excitation functions can be categorized into four general types: steady-state, random, periodic, and transient. In the modal testing literature, there are several studies that go into great detail examining the applications of a variety of excitations functions. As

predictable, the choice of the excitation function depends on several factors. The characteristics of the structure and general measurement considerations are among the most important aspects to consider in selecting the function. The characterization of the system is primarily concerned with the linearity of the system; as long as the system is linear, all inputs should grant the same response values. General measurement considerations include frequency range of interest, minimization of bias and variance errors, simplicity of excitation system setup, and measurement time.

The type of excitation function selected for this study is the transient impact type. Section 4.5.1 illustrates the properties of this input function, as well as the method used to applied this type of signal. A periodic function was also considered but deemed not easily applicable on the test article, as described in Section 4.5.2.

Once the excitation function and system have been selected, the excitation assumptions need to be formulated. The primary assumption concerning the excitation of a linear structure is that the excitation is *observable.* In the case of impulsive excitation, such as the case of transient impact excitation, the power spectrum of the excitation signal is also assumed sufficiently smooth over the frequency interval of interest. This concept is better addressed in the next section. Nevertheless, this assumption regarding the excitation frequency spectrum should always be confirmed in the pre-test experiments (refer to Section 4.6.2).

4.5.1. IMPACT TESTING

The use of an impact device is a common method of excitation in modal survey. Although impact testing is a relatively simple technique to implement, it may be difficult

to obtain consistent results throughout the measurement process[11]. The convenience of this technique is attractive because it requires very little hardware and simplifies the test setup; depending on the number of desired measurements, it can also provide shorter measurement times. The method of applying the impulse involves the use of a manually operated hammer. Integral with the impact hammer tip, there is a force transducer, which detects the magnitude of the force felt by the impact device; this force is assumed to be equal and opposite to that experienced by the structure.

When the hammer tip impacts the structure, the test article experiences a force pulse that is substantially shaped as a half-sine function. The frequency content of such a force pulse is essentially flat up to a certain frequency and then diminishes rapidly. Clearly, a pulse of this type is effective at exciting only test article vibrations that occur in the frequency range that corresponds to the flat portion of the pulse frequency spectrum. It is thus imperative to determine, from the pulse frequency spectrum, the frequency limit at which the flat trend surrenders to an exponential decay. This frequency limit will indicate the maximum frequency that is meaningful to monitor and record in the measurement. In Section 4.6.2, the frequency spectrum of a pulse generated by the hammer employed is examined; results are then related to the testing frequency range of interest.

Since the input force is an impulse, the amplitude level of the energy applied to the structure is a function of the mass and velocity of the hammer. In other words, the magnitude of the impact is determined by both the mass of the hammer head and the velocity with which it is moving at the time of impact. This translates into the consideration that in order to adjust the input force level, the operator can vary both the

impact velocity and the mass of the hammer head. One of the difficulties of implementing impact testing using a hammer is ensuring that each impact is essentially the same as the previous one. This concern is not much related to the magnitude of the pulse force, as this is accommodated by the frequency response function property of independence from the excitation level; the concern originates from the potential difference in impact location and orientation relative to the normal of the structure surface. Another potential problem in impact testing is associated with noise, which can be present in both the force and response signals. Noise considerations are addressed in Section 4.7.

Since the force pulse is usually very short relative to the length of the time record, the portion of the input signal after the pulse is noise and can be eliminated without affecting the pulse itself. This is accomplished with the introduction of a window, called the *force window,* that truncates the input signal when the pulse energy has expired, so that noise present after the applied impact is not interpreted as part of the excitation function. The small amount of oscillation that occurs at the end of the pulse is part of the pulse and should not be truncated. A typical value for the width of the *force window* is one seventh of the length of the time record. This formula was used to calculate the width of the *force window* employed in the impact testing implemented.

The frequency content of the energy applied to the structure is a function of the stiffness of the contacting surfaces and, to a lesser extent, the mass of the hammer. The stiffness of the contacting surfaces affects the shape of the force pulse, which in turn determines the frequency content. Obviously, it is not feasible to vary the stiffness of the test article surface, therefore the frequency content is controlled by varying the stiffness

of the hammer tip. The harder the tip, the shorter the pulse duration and thus the higher the frequency content. The hammer tip employed was made of aluminum. Its efficiency in exciting the structure throughout the frequency range of interest was proved in the pre-test experiments, as illustrated in Section 4.6.2.

As stated in the section that introduced the frequency response function method of modal analysis, this study implemented the *single-point excitation* technique. The input pulse force was restricted to one location while the response was collected at forty different locations, including the input location itself, or *reference*. The input location selected is illustrated in Figure 4.5. The camshaft was selected as input location due to its property of main contributor to valve train motion. The camshaft can be thought as being located at one extreme of the valve train kinematic chain. Camshaft excitation proved to propagate well the pulse energy throughout the mechanism and the surrounding valve train supporting fixtures as the clean frequency response function measurements indicated. The exact point of impact was located at the center of the exhaust cam.

FIGURE 4.5. Excitation Location or Reference

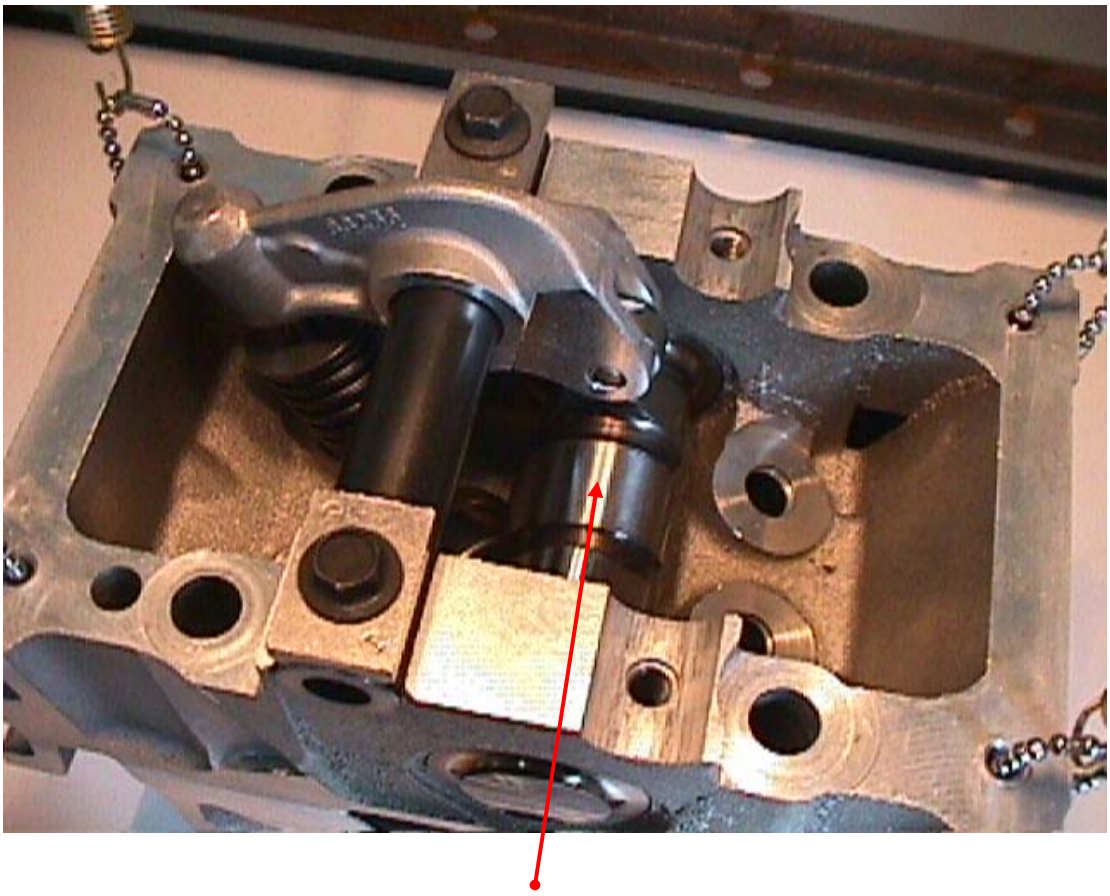

4.5.2 INADEQUACY OF SHAKER

Another method of implementing the *single-point excitation* technique is through the use of a shaker. A common type of shaker used in modal testing is the electromagnetic shaker. In electromagnetic shakers, the supplied input signal is converted to an alternating magnetic field in which is placed a magnetic coil; an input force is generated as the driving part of the device is attached to both this coil and the structure. Shakers are an attractive system of excitation because they are capable of providing a wide variety of excitation functions, both periodic and random. However,

there are several potential problem areas that need to be considered when implementing a shaker system of excitation[11].

The main concern arises from the fact that, when implementing any shaker system, it is necessary to connect the driving platform of the shaker to the structure, inserting at some point in the connection a force transducer, which will capture the input applied. To begin with, if the force transducer cell is mounted directly on the structure, the possibility of altering the test article structural characteristics must be carefully assessed. Nevertheless, the most important precaution that must be taken in executing this connection derives from a stipulation in the definition of the *single-point excitation* method. In the *single-point excitation* method, the frequency response function calculation assumes a single input function, therefore the shaker must transmit only one component of force in line with the force transducer. Although it may seem that the exciter is capable of applying a force in one direction only, as a shaker is essentially a unidirectional device, there exists a practical problem on most structures whose vibration is generally complex and multidirectional. The problem is that, when pushed in one direction, the structure responds not only in that same direction but also in others, including the three rotation directions. Such a behavior is perfectly in order and expected but it can create a secondary form of excitation if the shaker is incorrectly attached to the structure. The driving part of the shaker is usually very mobile along the driving axis but it is rather stiff in the other directions. Thus, if the structure wants to respond in a direction different than the direction in line with the driving axis, then the stiffness of the exciter will generate resisting forces or moments that are exerted on the structure in the form of a secondary excitation. The response transducer will capture the total response,

which is caused not only by the intended and known driving force but also by the secondary and unknown forces. Therefore, the frequency response function estimated using the response transducer signal and the force transducer signal will be erroneous.

In order to minimize the problem of introducing undesired forces, the shaker can be connected to the structure through a slender rod, usually called a stinger, that allows the test article to move freely in the other directions. In other words, the stinger must be stiff in the driving direction and, at the same time, relatively flexible in the other five directions. In effect, it must act like a truss member, carrying only axial loads but no moments or shear loads. In addition, the stinger cannot be too long, otherwise it can introduce the effects of its own resonances into the measurement, and these can be very difficult to extricate from the genuine data.

As originally it was desired to employ a periodic function as the excitation function, an attempt was made to prepare a shaker setup. From the very beginning, it was decided not to mount the force transducer cell directly on the structure in order to avoid altering the test article structural characteristics. The considerations made in the previous section regarding the validity of the camshaft as input location, apply in the case of using a shaker as excitation source, as well. However, it was rapidly evident that it was very difficult to create a stinger with the characteristics described above. One fairly efficient stinger solution involved the use of a thin steel wire. In this case the goal was to prepare a shaker configuration in which the wire was initially in slight tension so that the driving motion would provide the excitation by releasing/reapplying this tension. Nevertheless, the major source of troubles in any attempted stinger solution was the bond of the stinger with the exhaust cam, which is not a flat surface. The connection was attempted through

gluing the slender stingers at the cam with epoxy; the results were not satisfying as the link was inevitably fragile. Using this setup and a periodic chirp as the input function, the frequency response functions measured were consistently contaminated with excessive noise. It must be acknowledged that another factor possibly contributed to the inconsistency of the data; the limited power of the electromagnetic shaker available was an object of uncertainty. The capability for this shaker of sufficiently spreading the excitation energy throughout the structure was never proved. The idea of implementing a shaker to provide a periodic excitation function was then abandoned.

It is worth mentioning that the method of supporting the shaker itself is another factor that can affect the force imparted to the structure. The main body of the shaker must be isolated from the structure to prevent any reaction forces from being transmitted from the base of the shaker into the structure. This can be accomplished by suspending the shaker through very soft elastic cords, similarly to the technique selected to suspend the test article and described in Section 4.3. Figure 4.6 depicts the attempted shaker setup, in which the exciter device was also suspended.

FIGURE 4.6. Test Article and Shaker

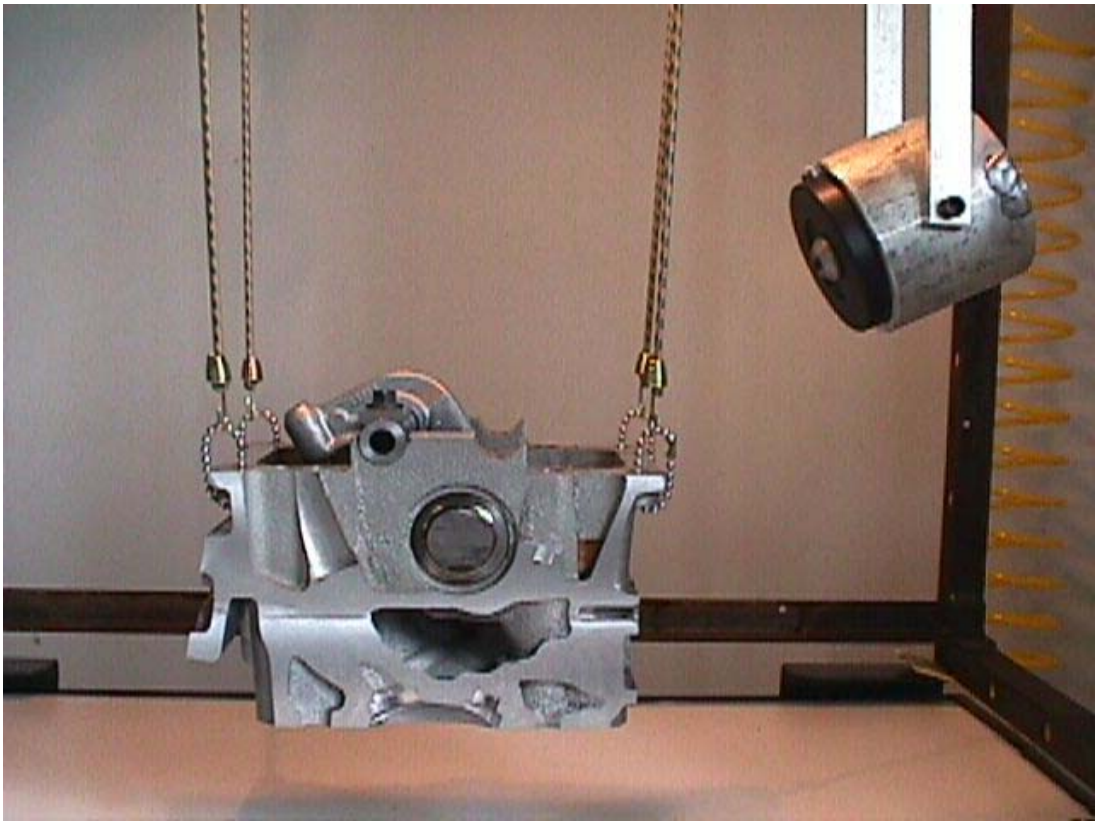

4.6. PRE-TEST EXPERIMENTS

4.6.1. RECIPROCITY MEASUREMENTS

As stated in Section 4.4, when performing an experimental modal analysis, the system must be assumed to behave linearly so that the response is always proportional to the excitation. It was also noted that this assumption implies the *reciprocity* property for certain measured FRF. Thus, one way to check that the system is *linear* is to prove the *reciprocity* of the FRF calculated at some DOF. When the assumption of *reciprocity* is formulated, then the response at any point in the structure coincides with the response obtained by switching the excitation input location with the response measurement location. *Reciprocity* is normally assumed but is generally not enforced by the modal parameter estimation algorithms.

Most common types of non-linearities result from clearances between components in the system. Their effect may result not only in poor FRF repeatability, but also in greater apparent damping and a mistaken estimate of static stiffness. Non-linearities may also hide in joints whose damping is a function of the relative displacement of the joint motion.

Considering that the test article described in Section 3.1 is a mechanism that has been pre-loaded in order to reduce it to a *linear* structure, it was imperative to validate this conversion. The system linearity was then confirmed through a FRF *reciprocity* check. The two DOF chosen for the check were selected upon their location on the extremes of the valve train mechanism. As illustrated by Figure 4.7 through the FEM model, one DOF is the *reference* and the other is located at the valve head, with direction parallel to valve axis. The reciprocal FRF measured are shown in Figure 4.8.

FIGURE 4.7. Locations Selected for Reciprocity Check

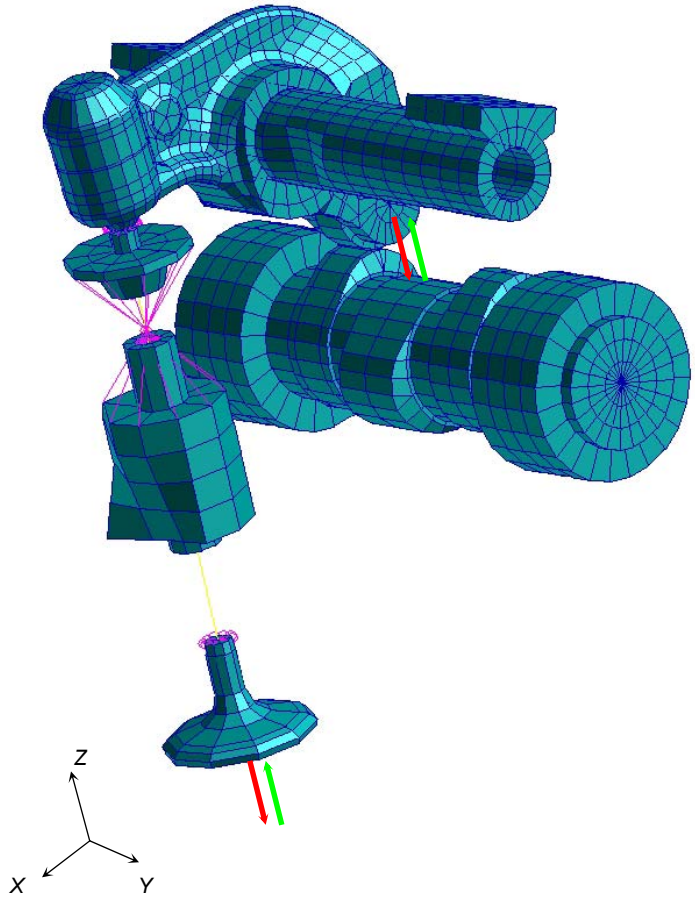

FIGURE 4.8. Reciprocal Frequency Response Functions

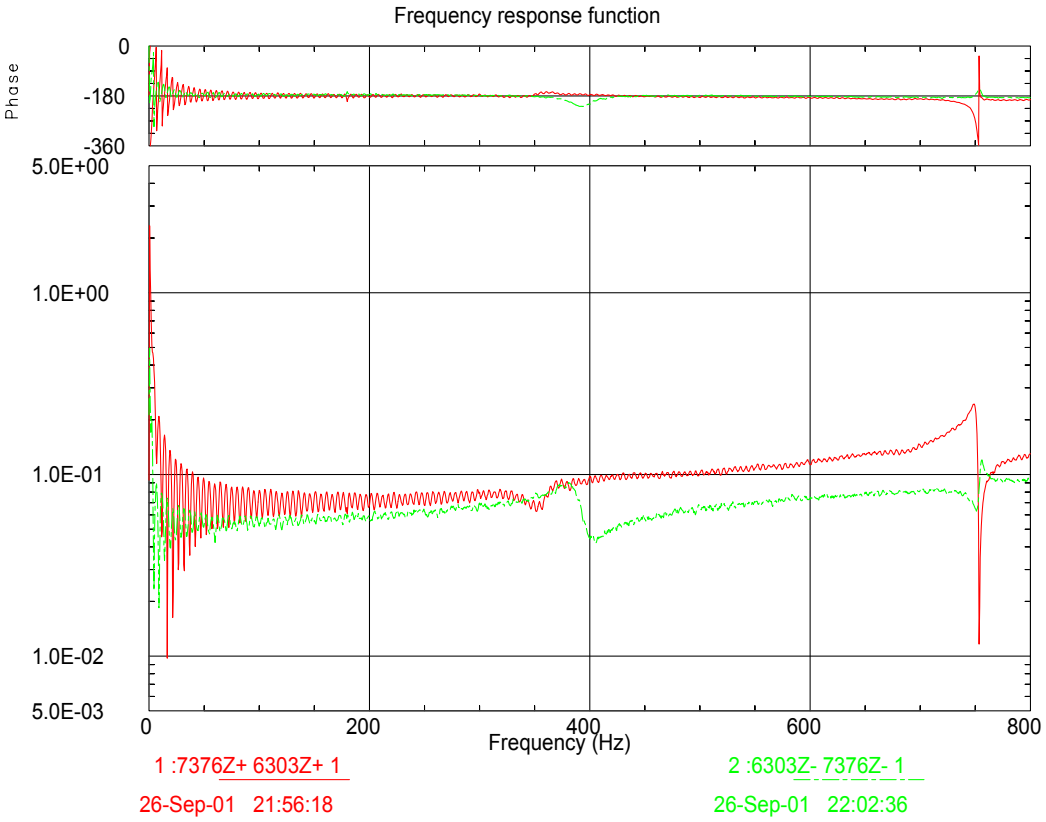

4.6.2. POWER SPECTRUM OF EXCITATION

In the section relative to the excitation function, it was mentioned that in the case of impulsive excitation, such as the case of transient impact excitation, the power spectrum of the excitation signal is required to be sufficiently smooth over the frequency interval of interest. The typical frequency content of a force pulse was also described as being essentially flat up to a certain frequency and then decaying rapidly. It was also stated as imperative to determine, from the pulse frequency spectrum, the frequency limit at which the flat trend surrenders to an exponential decay, in order to establish the maximum frequency effectively excited on the test article.

The frequency power spectrum of a pulse generated by impacting the head of the hammer employed, with the aluminum tip mounted, at the input location selected is shown in Figure 4.9. The rule of thumb is to declare extinguished the flat portion of the force spectrum when the amplitude has decayed by more than 20 dB. From Figure 4.9, it can be noted that the amplitude of the force spectrum stays between –70 dB and –90 dB, an interval of 20 dB, up to the frequency of 4800 Hz; beyond this frequency the amplitude decays more rapidly. Thus the frequency limit of the force spectrum flat trend is set at 4800 Hz. Once more, this limit indicates that this pulse might not effectively excite test article vibrations that occur at frequencies above the 4800 Hz. The frequency interval of interest of this study was then definitively confined from zero to 4800 Hz. This interval is consistent with the goal stated in the Section 3.1.

FIGURE 4.9. Useful Frequency Range of Pulse Spectrum

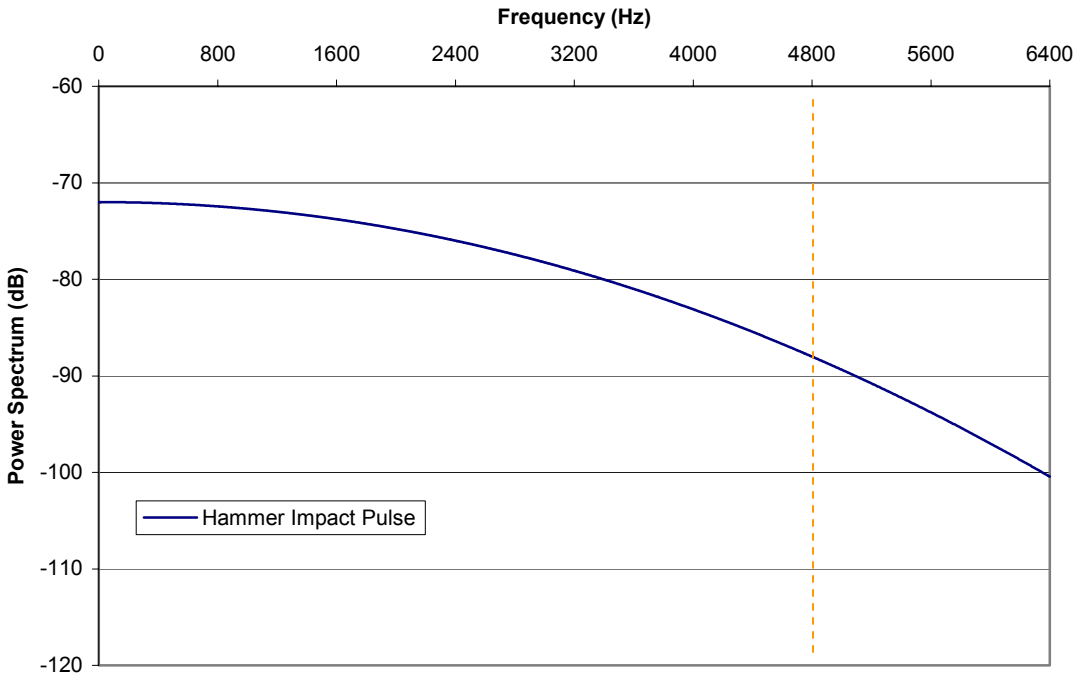

4.6.3. RIGID BODY MODES

In Section 4.3, the outcome regarding the test article supporting system selection was illustrated and justified; the free condition was preferred over the grounded condition. As in practice it is not feasible to provide a truly free support, it is necessary to evaluate the "softness" of the structure suspension system employed in order to confirm its negligible effect on the test article structural characteristics. It was stated that a very soft system of suspension will limit the structure rigid body modes to occur at very low frequencies relative to those of the first bending modes. "Very low" in this context means that the highest rigid body mode frequency must be less than 15% of that for the lowest bending mode. Figure 4.10 shows the frequency response function in which the natural frequency of the first bending mode was detected. This measured response

indicates that this bending mode occurs at approximately 360 Hz. Figure 4.10 also reveals that the frequency response function peaks corresponding to rigid body modes occur before the 20 Hz. Therefore, it can be stated that the soft elastic cords selected do not interfere with the overall test article structural characteristics.

FIGURE 4.10. Rigid Body Modes in the Frequency Response Function

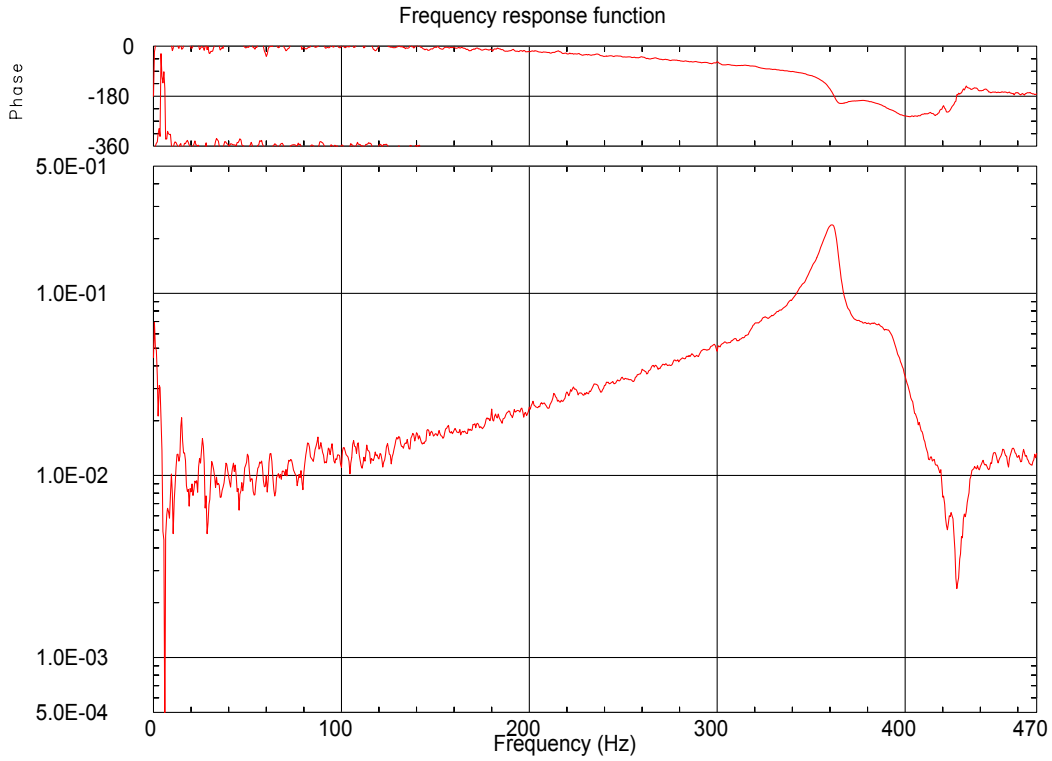

4.6.4. BROADBAND MEASUREMENTS

Even modern Dynamic Signal Analyzers (DSA) based on Fast Fourier Transform (FFT) analysis often have limitations of inadequate frequency resolution. This is especially true if multiple resonances occur at natural frequencies that are very close to

each other. This problem arises because of the constraints imposed by the limited number of discrete points available, the maximum frequency range to be covered and/or the length of time sample necessary to gather the data. To improve frequency resolution, the time length of the data record must be increased until the desired Fourier series frequency is achieved. Since most FFT analyzers calculate a fixed number of Fourier series frequencies, the only means by which higher resolution can be attained is to calculate that number of closely spaced set of Fourier series frequencies in the interval of interest only. In other words, the common solution to the need for finer frequency resolution is to "zoom in" on the frequency range of interest and to concentrate all the spectral lines into a narrow band. When using zoom to measure FRF in a narrow frequency range, it is important to ensure that there is as little vibration energy as possible outside the frequency range of interest.

The first step in determining if zooming is needed is to collect broadband FRF measurements that cover the entire frequency range of interest. Subsequently, and depending on the natural frequency density observed, zoomed FRF measurements are collected accordingly. As justified in the previous section, in this study the frequency range of interest spans from zero to 4800 Hz. Broadband measurements of the entire span revealed that a higher frequency resolution was desirable particularly in the 700 – 3200 Hz frequency range. It was decided then to divide the frequency range of interest into six narrower spans of 800 Hz each in order to capture all the target modes with sufficient resolution. The number of spectral lines for the measurements collected in each 800-Hz span was 1600.

4.7. MODAL DATA ACQUISITION

In the presented experimental modal analysis approach, the quality of the frequency response function estimates is a crucial factor for the final outcome[11]. Even when the system has been proven to behave linearly, the excitation applied and supporting system selected are appropriate, and measurement errors are avoided, still some noise will be present in the measurement process. Noise is a general designation describing the difference between the true value and the estimated value of the response. A more exact designation is to view noise as the total error comprised of two terms, variance and bias. Each of these classifications is merely a convenient grouping of many individual errors that cause a specific kind of inaccuracy in the frequency response function estimate.

The variance portion of the error essentially is Gaussian distributed and can be reduced by any form of synchronization in the measurement process[11]. In the presence of variance or random errors, the averaged response value, in the limit, approaches the expected response value. The bias or distortion portion of the error causes the expected value of the estimated function to be different from the true value. In the presence of bias errors, the averaged response value, in the limit, does not approach the expected response value. Many bias errors can be removed or reduced in magnitude because their form and/or source are predictable.

Several approaches are available to reduce the error involved in frequency response function measurements in Fast Fourier Transform analyzers. The approaches used in this study are presented in the next sections together with considerations made in selecting the transducers employed. Table 4.1 lists the values of the impact testing

parameters used in each frequency span tested. Some of the parameters listed have been already introduced in the previous sections; the remaining parameters are described in the next sections.

TABLE 4.1. Modal Data Acquisition Parameters in Impact Testing

MODAL DATA ACQUISITION PARAMETERS IN IMPACT TESTING						
Parameter Description	***Frequency Span (Hz)***					
	0 - 800	***800 - 1600***	***1600 - 2400***	***2400 -3200***	***3200 - 4000***	***4000 - 4800***
DOF Measured (TAM DOF)	*40*	*40*	*40*	*40*	*40*	*40*
Frequency Span Length (Hz)	*800*	*800*	*800*	*800*	*800*	*800*
Time Record Length (sec)	*1.95*	*1.95*	*1.95*	*1.95*	*1.95*	*1.95*
Lines of Resolution	*1600*	*1600*	*1600*	*1600*	*1600*	*1600*
Trigger Delay (sec)	*-0.195*	*-0.195*	*-0.195*	*-0.195*	*-0.195*	*-0.195*
Window Function Type	*Exponential*	*Exponential*	*Exponential*	*Exponential*	*Exponential*	*Exponential*
Force Window Width (sec)	*0.279*	*0.279*	*0.279*	*0.279*	*0.279*	*0.279*
Exponential Decay Constant (sec)	*0.488*	*0.488*	*0.488*	*0.488*	*0.488*	*0.488*
Average Type	*RMS*	*RMS*	*RMS*	*RMS*	*RMS*	*RMS*
Number of Averages per FRF	*10*	*10*	*10*	*10*	*10*	*10*
Total Hammer Impacts	*400*	*400*	*400*	*400*	*400*	*400*
Coherence Functions Checked	*40*	*40*	*40*	*40*	*40*	*40*
Accelerometer Sensitivity (pC/g)	*1.4*	*1.4*	*1.4*	*1.4*	*1.4*	*1.4*
Hammer Force Transducer Sensitivity (mV/lbf)	*100*	*100*	*100*	*100*	*100*	*100*

4.7.1. TRANSDUCER CONSIDERATIONS

Once the excitation system has been selected, the transducers for sensing force and motion need to be selected. The transducers considerations are often an overlooked aspect of the experimental modal analysis[11]. Although there are various types of

transducers, the piezoelectric type is the most widely used in modal testing. Piezoelectric transducers are electromechanical sensors that generate an electrical output when subjected to vibration; in general, they have wide frequency and dynamic operational ranges and good linearity.

The properties to consider in selecting force transducers and accelerometers include both the type and the performance characteristics. Among the operating specifications to consider there are sensitivity, amplitude response (or frequency range of operation), resonant frequency, and shock limit. Sensitivity is measured in terms of voltage/force in force transducers (typically, with units of mV/lbf or mV/N), and it is measured in terms of voltage/acceleration (mV/g) in accelerometers. In accelerometers that require signal amplification (*charge* accelerometers) the sensitivity is measured in terms of charge/acceleration (pC/g). The frequency range of the test should fall within the linear range and below the resonant peak of the transducer frequency response. The maximum vibration level expected during the test should not exceed one third of the transducer shock limit. In general, the optimum accelerometer has high sensitivity, wide frequency range and small mass. However, it must be noted that high sensitivity usually dictates a larger mass and size, and a lower resonant frequency.

It is important to understand that the addition of even a small transducer to the system to be tested imposes an additional and undesired mass on the structure. The inertia forces and moments associated with the motion of the accelerometer along with the structure may sensibly modify the structural characteristics of the original system. In order to minimize these effects, care should be taken in selecting the smallest transducer that will provide the necessary signal. While it is impossible to completely eliminate

accelerometer mass loading effects (unless a non–contacting transducer is employed, such as an acoustical or optical sensor), it is possible to account for their contribution to modal behavior in a correlated FEM model. This can be accomplished by simply adding to the model mass-point elements with relative inertia information at accelerometer locations.

This accelerometer mass correction was not performed on the FEM model developed in this study because the mass of the accelerometer employed was considered negligible. The accelerometer used is, indeed, one of the lightest uni-axial *charge* piezoelectric transducers currently available on the market. It weighs 0.5 grams, which is approximately 0.01% of the test article weight. Its full characteristics are listed in Appendix B together with its calibration data. Appendix B also reports properties for the force transducer mounted on the impact hammer used.

The accelerometer was fixed at all locations through a very thin layer of bees wax, which is one of the few mounting techniques applicable to this accelerometer given its reduced dimensions. The correct transducer mounting technique is also important, considering that each technique has its own characteristic frequency response and, thus, its own characteristic resonance frequency. The bees wax mounting technique reveals its limits at frequencies that are well above the frequency range of interest of this study (0 – 4800 Hz); typically, resonances caused by this mounting method occur at frequencies above 15 kHz[11].

4.7.2. LEAKAGE AND WINDOWING

There is a property of the Fast Fourier Transform (FFT) that affects the energy

distribution in the frequency spectrum. It is the result of the physical limitation of measuring a finite length time record along with the periodicity assumption required of the time record by the FFT. This does not constitute a problem when the signal is exactly periodic in the time record or when a transient signal is captured completely within the time record. However, in the case of random excitation or in the transient case when the entire response is not captured, a phenomenon called *leakage* occurs. The *leakage* bias error has the effect of "leaking" energy into adjacent frequency lines of the spectrum, thus distorting it. The undesired effect is to underestimate the signal amplitude and overestimate the damping factor.

The most practical solution for reducing the effects of *leakage* with a non-periodic signal is to artificially force the signal to zero at the beginning and end of the time record to make it appear periodic. This is accomplished by multiplying the time record by a mathematical curve, known as a *window* function, before processing the FFT. To this purpose, there are a number of different *window* functions available. In the transient vibration applications where much of the important information is concentrated in the initial part of the time record, such as the case of impact testing, the *window* must have an exponential profile which forces the signal to decay to zero at the end of the time record.

Imposing a prescribed profile on the time signal prior to performing the Fourier transform, or *windowing*, does not eliminate leakage completely and, most important, still distorts the measurement as a result of eliminating some data. When performing a modal survey, the physical meaning of this distortion is that the modes derived from windowed frequency response functions will appear more damped than what they are in reality, as a

result of the FRF decay imposition. However, if the exact form of the applied exponential *window* function is known, it is possible to correct the damping estimated in the subsequent modal parameter extraction process. Section 4.7.5 presents the exponential *window* function employed and describes in details how the damping correction was performed for each mode derived.

Now that the *leakage* bias error has been presented, it is worth noting that the increase of frequency resolution through zooming, discussed in Section 4.6.4, also contributes in reducing this type of error. When frequency resolution is increased by dividing the frequency range of interest into narrower frequency spans, the leakage error is automatically lessened due to the use of longer measurement time records in each span.

4.7.3. AVERAGING AND REPEATABILITY

Signal averaging can significantly reduce errors of variance and is probably the most general technique in the reduction of errors in frequency response function measurement. By averaging several frequency-domain records together, statistical reliability can be increased and spurious random noise can be removed or reduced from the signals. Each of the 240 frequency response functions measured was obtained averaging ten response estimates. The type of average used was the root-mean-square (RMS) average. RMS average is calculated by squaring all the values, adding the squares together, dividing by the number of measurements (ten, in this case), and taking the square root of the results.

One obvious and essential post-test experiment for any modal test is to check the repeatability of certain measurements. Remeasuring a limited number of frequency

response functions from time to time ensures that neither the structure nor the measurement system have experienced significant changes. If the structure has changed perceptibly its properties, the *time-invariant* system assumption is violated and the effects can have serious consequences in the subsequent analysis.

4.7.4. COHERENCE

The ordinary *coherence* function measures the degree of linear dependence between two signals. It indicates the degree of causality in a frequency response function, representing, thus, a level of confidence in the frequency response function estimate. When the *coherence* is equal to unity at any specific frequency, the system is said to have perfect causality at that frequency. Then, the measured response power is caused totally by the measured input power (or by sources which are coherent with the measured input power). A *coherence* value less than unity at any frequency indicates that one or more extraneous noise sources contributed in the measuring of the response power. When the *coherence* is zero, the output is caused entirely by sources other than the measured input.

In general, the *coherence* can be a measure of the degree of noise contamination in a measurement. Thus, with more averaging, the estimate of *coherence* may contain less variance, therefore giving a better estimate of the noise energy in a measured signal. This is not the case if the low *coherence* is due to bias errors such as non-linearities, multiple inputs, or leakage. In all such cases, the estimated *coherence* function may not approach a particular value at each frequency; it will more likely fluctuate in a fashion that is dependent upon the type of noise present in the structure and measurement system.

Low *coherence* values do not necessarily imply poor estimates of the frequency response function. For instance, it may simply mean that more averaging is required for a reliable result. *Coherence* may be low at lightly damped modes without adequate frequency resolution available to define the response peaks. It also tends to be low at repeated roots when the system is not being excited by multiple inputs.

The *coherence* function was calculated and monitored for all the 240 frequency response functions measured. A *coherence* value of 0.9 or greater, at a frequency corresponding to a FRF peak, was deemed adequate to establish the acceptability, and thus good quality, of the measured frequency response functions. In the forthcoming Section 4.9, which reports the modal survey results, a number of measured frequency response functions are illustrated with their respective *coherence* functions.

4.8. MODAL PARAMETER ESTIMATION

Modal parameter estimation is the extraction of natural frequency, damping, and mode shapes from the measured data, which is in a processed form such as frequency response functions. The goal of this data reduction phase is to produce, through mathematical curve fitting procedures, the most accurate possible estimate of the modal parameters for the test article. It is worth noting that the accuracy of the parameters obtained by curve fitting the experimental data is only as good as the data used in the procedure. The quality of the frequency response functions is a crucial factor when judging results of a modal parameter estimation process.

The modal parameter estimation techniques are divided into two categories, *single degree-of-freedom* (SDOF) approximations and *multiple degree-of-freedom* (MDOF) approximations. SDOF estimation techniques operate on one mode at a time. These techniques derive each mode individually, therefore target modes should be relatively uncoupled. If certain modes are contaminated by residual contributions from higher or lower modes, then SDOF estimation techniques may prove inappropriate. MDOF estimation techniques attempt to extract modal parameters for several modes simultaneously. In addition to operating on multiple modes, certain MDOF curve fitters are capable of processing data acquired using multiple inputs. These techniques allow the resolution of closely coupled and heavily damped modes with greater accuracy[11].

A number of SDOF and MDOF estimation techniques have been developed in the past (MDOF techniques can be further categorized by the domain – time or frequency – of the data that they operate on), and an illustration and comparison of all of them is beyond the objective of this study. The method selected, the *polyreference time-domain*

has proven to yield very accurate results and it is described in the next chapter.

4.8.1. POLYREFERENCE TIME-DOMAIN METHOD

The *polyreference time-domain* method for parameter estimation is a MDOF technique that extracts modal parameters from the damped complex exponential response information. The *polyreference time-domain* method is formulated to utilize data corresponding to the free decay of a system generated by the release of an initial condition, but it applies to impulse-response function data as well. Since impulse-response function data are scaled to include the forcing condition, use of this method yields properly scaled modal parameters that can be used to calculate generalized mass and stiffness. As stated in Section 4.2.2, the formulation of the impulse-response function involves the computation of the frequency response function by use of a fast Fourier transform, potentially imposing bias errors, which may degrade the estimation of the modal parameters.

The *polyreference time-domain* method computes the poles, or residues, based upon a specific initial vibration condition of the structure. A number of different initial conditions can be established analogous to the practice of using several exciter positions in ordinary single input modal surveys, until all the important modes have been excited. This is of particular importance when recalling that, in general, all the modes of a structure cannot be characterized from one exciter position, and, likewise, all the modes cannot be determined from one initial condition.

The *polyreference time-domain* method can yield very accurate results since the technique is capable of processing multiple functions from multiple reference locations.

As this algorithm utilizes all measured, damped, complex exponential data, from all references or initial conditions, simultaneously, in the estimation of modal parameters, it can be quite useful for accurately defining closely spaced modes. Another significant advantage of this technique is the ability to detect poles of the system that are identical or nearly identical. It is recalled that poles of the system that are identical are referred to as *repeated roots*; poles of the system that are nearly identical are referred to as *pseudorepeated roots*.

Evaluation of the *polyreference time-domain* method based upon comparisons between experimentally measured and synthesized frequency-response functions is quite impressive when compared to other modal parameter estimation approaches[11]. The major advantage of this technique is its ability to use all the available frequency response functions to come up with a single global estimate for frequency, damping, and mode shapes. It is worth noting that the data acquisition best matches this analysis procedure when all of the data are acquired simultaneously. In addition, by acquiring data simultaneously, undesired *time-invariant* problems are completely avoided. Nevertheless, this estimation method can require a relatively high computational power since, potentially, all the data can be processed for any given estimate.

The *polyreference time-domain* method is a *multiple degree-of-freedom* technique because it uses multiple rows or columns of the frequency response function matrix to obtain global least squares estimates of modal parameters. Resulting values for resonance frequency, damping, and modal vectors reflect the simultaneous influence of multiple modes across multiple reference locations. The use of the *polyreference time-domain* method with only one reference location, as the case of this study, produces

exactly the same results as the *least squares complex exponential* technique. The *least squares complex exponential* analysis, therefore, is really a single-reference case of the polyreference technique. It was, however, decided to refer to the *polyreference time-domain* method as the technique applied, in order to be able to describe its powerful capabilities that may be implemented in a future modal testing application on valve trains.

The modal parameter estimation process was implemented with the help of I-DEAS Test software from MTS. I-DEAS Test is a powerful package that offers not only a wide variety of modal parameter estimation algorithms but also a number of tools to verify the validity of the results for each stage of the process. The data reduction started with the import of the frequency response data into the software. The test article geometry was schematized in the program, consistently with the degrees of freedom of the TAM; each frequency response function was then associated with the proper DOF. The procedure for a *polyreference time-domain* estimation includes the following steps (refer also to Appendix C, which is a more detailed guideline of the procedure implemented):

1. *Generation, plot and analysis of the Mode Indicator Function (MIF)*
2. *Initialization of the correlation matrix*
3. *Construction of the correlation matrix*
4. *Estimation of the frequencies and damping ratios*
5. *Calculation of the poles, or residues, and generation of an analytical function*
6. *Calculation and display of mode shapes*

The first step is to generate the *Mode Indicator Function* (MIF) that serves to simplify the detection of vibration modes in the test data. This is accomplished by manipulating full or partial sets of response measurements, using linear combinations, for the purpose of obtaining a reduced set of functions. The resulting functions indicate the frequencies at which true physical modes occur. Thus, the MIF provides a visual indication of modal density. The next section introduces in detail the MIF and illustrates the MIF calculated for each frequency span studied.

The second step is to initialize the correlation matrix. This is achieved by selecting the response functions, identifying their corresponding reference coordinates, defining the analysis frequency bandwidth, and specifying the maximum number of roots to be calculated. The third step is to accumulate the frequency response functions into the correlation matrix. The correlation matrix can include all of the response functions for a given test or be biased to include only the data for a particular portion of the structure. An additional step can be performed at this point; an error chart from the correlation matrix can be plotted in order to analyze the roots represented in the matrix. The error chart reports the error terms of the correlation matrix. As more roots are included, the error is reduced. By carefully studying the nature of the MIF and error chart, an acceptable number of roots can be determined which includes sufficient modes to describe the data, but without including excessive calculation modes.

The fourth step is to estimate the frequency and damping portions of the roots. The residue portions of each root (amplitude and phase) are set to zero. At this stage, another very useful plot can be prepared, the *stability diagram.* The *stability diagram* aids in determining the number of roots to be used in the analysis; it is a convergence

chart of frequency range by root count range. Section 4.8.3 further explains the use of this chart illustrating one of the plots derived.

The fifth step is to calculate residues for a function with a particular response and reference set. An analytical function is generated based on the root table and compared to the original experimental data. If the comparison is favorable for several functions, the analysis may proceed to the determination of mode shapes. If the comparison indicates deficiencies, the residue calculations can be repeated until satisfactory calculations are obtained. If unsatisfactory results persist, it may be necessary to re-estimate frequencies and damping by selecting a different quantity of roots or starting the whole procedure over with the calculation of a new correlation matrix with new measured response data. The sixth step is to calculate mode shapes for the corresponding estimated parameters. Mode shapes can be then displayed thanks to the geometry schematization prepared at the beginning of the procedure.

4.8.2. NORMAL MODE INDICATOR FUNCTION

As indicated in the previous section, the *Mode Indicator Function* (MIF) serves to simplify the detection of modes in the frequency response data. Using linear combinations, it is possible to manipulate full or partial sets of response measurements in order to obtain a reduced set of functions. The resulting functions, which are called *Mode Indicator Functions,* indicate the frequencies at which vibration modes occur, providing thus a visual hint of modal density. The number of derivable MIF's is equal to the number of *references* used to produce the measured data. The MIF has minima at frequencies where a real normal mode of the structure occurs when excited at the selected *reference* location.

The valleys in the MIF are aligned with major modes of the structure that are present in the frequency response functions. The MIF provides an improved global representation of the modal characteristics of the structure relative to the representation that the frequency response functions are capable of illustrating. For instance, a mode can be absent in a frequency response function because it was not sufficiently excited to be captured at that particular response location. A valley in the MIF graph, however, would reveal the presence of this mode if other frequency response functions were able to capture the mode and they are included in the MIF calculation.

Three types of MIF's can be generated to provide a modal density suggestion, the *normal,* the *power spectra,* and the *multivariate* MIF. The type of MIF selected for this experience is the *normal* MIF. One *normal* MIF was calculated for each frequency span studied, as only one *reference* was used to produce the response data. *Normal* MIF has a

maximum value of unity and a number of local valleys (minima) where modes of the structure exist. The *normal* MIF is a ratio of two sums

$$MIF_{Normal} = \frac{\sum\left(\left|\mathrm{Re}(H)\right| \cdot |H|\right)}{\sum\left(|H|^2\right)}$$

where H represents a frequency response function. The numerator is the sum of the products of the real parts of the functions and their magnitudes. The denominator is the sum of the squares of the function magnitudes. Localized or lower amplitude modes are apparent in this function since the maximum amplitude is normalized to unity. Figure 4.11 illustrates the MIFs calculated for the first two frequency spans analyzed. From the figure, it can be noted that the MIF discloses three valleys in the 0-800 Hz frequency interval, thus three modes exist in this span. Similarly, as in the 800-1600 Hz interval four valleys are detected, four modes exist.

FIGURE 4.11. Normal Mode Indicator Functions (0 – 1600 Hz)

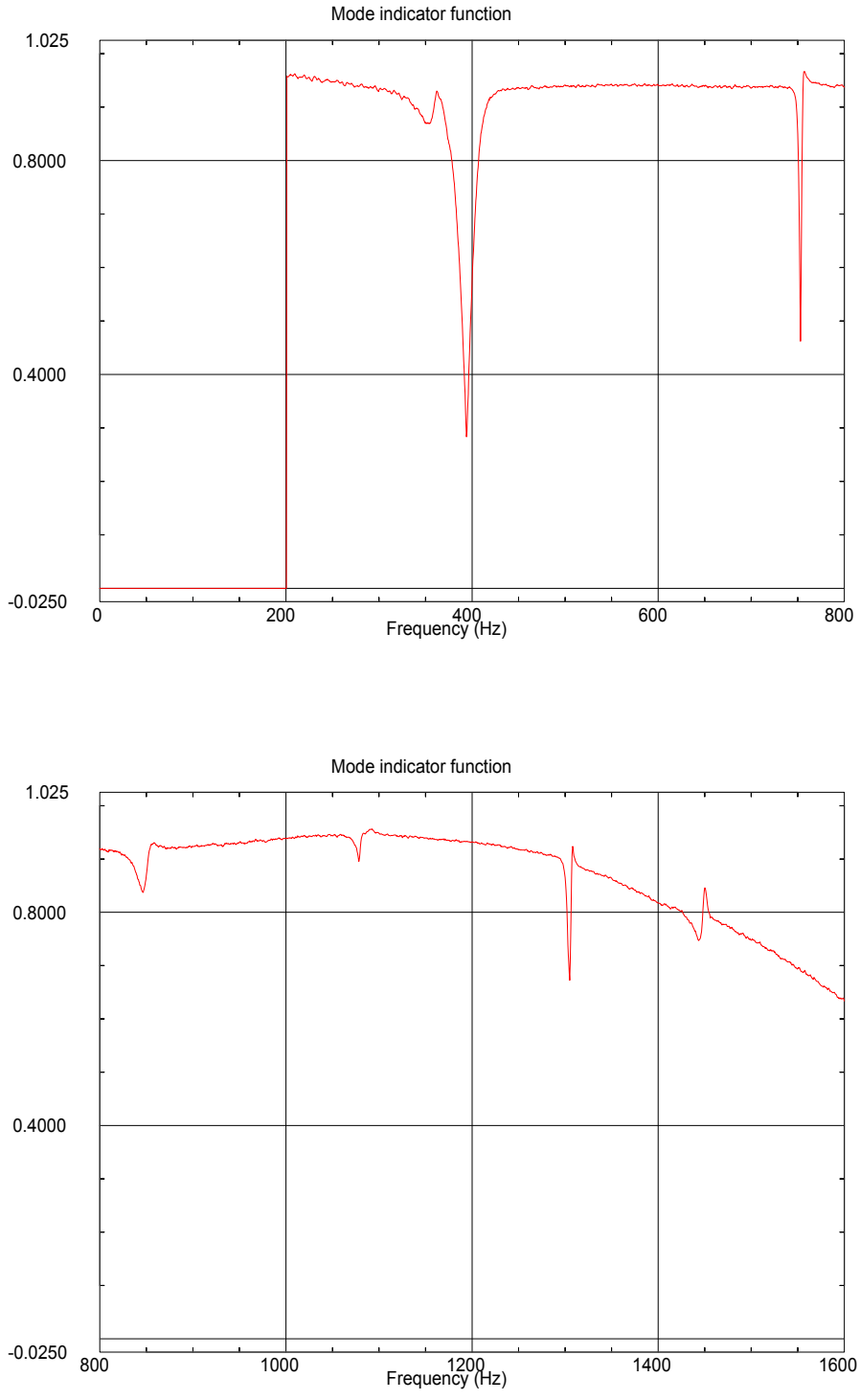

4.8.3. STABILITY DIAGRAM

The *stability diagram* is a graph of frequency range by pole count range that shows the stability of the poles associated with the correlation matrix that was built with the measured response data. The *stability diagram* is a convergence chart that assists in determining the number of roots to be used in the modal parameter estimation. The pole count range and pole count increment are determined from the matrix size and the number of *references* included in the matrix. The stability values are determined by comparing the poles on the *stability diagram* at each pole count to the poles at the previous pole count using the frequency tolerance, damping tolerance, and vector tolerance set in preparing the chart.

The *stability diagram* was prepared for each frequency interval analyzed. Figure 4.12 shows the *stability diagram* used to determine the number of roots employed to estimate the modal parameters in the 0-800 Hz frequency span. It is useful to overlay the *stability diagram* with the MIF, as shown in Figure 4.12, in order to better relate the pole stability with a particular mode. The stability values and the corresponding color definitions are given below:

- *Light blue: new pole*
- *Green: converges for frequency*
- *Red: converges for frequency and damping*
- *Magenta: converges for frequency and force vector*
- *Light pink: stable (converges for frequency, damping and force vector)*

FIGURE 4.12. Stability Diagram for the 0 – 800 Hz Frequency Span

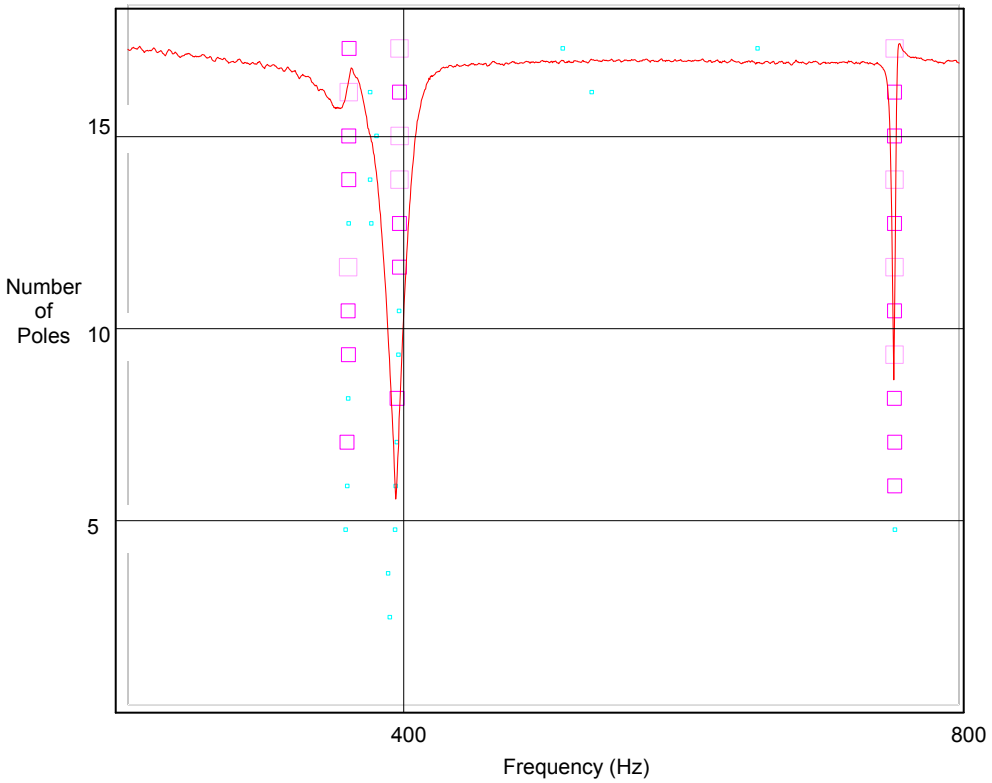

4.8.4. RESIDUES

Once the frequencies and damping portions of the roots have been computed, the residues for a function with a particular response and *reference* set can be calculated. Estimation of residues for a specified response and *reference* means calculating the amplitude and phase of the roots estimated in the previous step. All parameters are included in the calculation of residues. An analytical function is generated based on the root table and compared to the original experimental data. As stated in Section 4.8.1, if this comparison is encouraging for several experimental response functions, the analysis can proceed to the determination of mode shapes. If the comparison indicates deficiencies, the residue calculations must be repeated until satisfactory associations are obtained. In the presence of unacceptable comparison results, it is necessary to re-estimate frequencies and damping by selecting a different quantity of roots. Poor comparisons may also indicate that the current measured data are not adequate or exhaustive to properly construct the analytical function involved in the calculation of residues. In other words, in the case of large dissimilarities, the available experimental response functions may be insufficient to consistently characterize a set of modal parameters for the given structure. Figure 4.13 illustrates two analytical function comparisons with the corresponding experimental response functions. In the figures, the measured responses are plotted in red, whereas and the generated analytical functions are plotted in green.

FIGURE 4.13. Residues (0 – 1600 Hz)

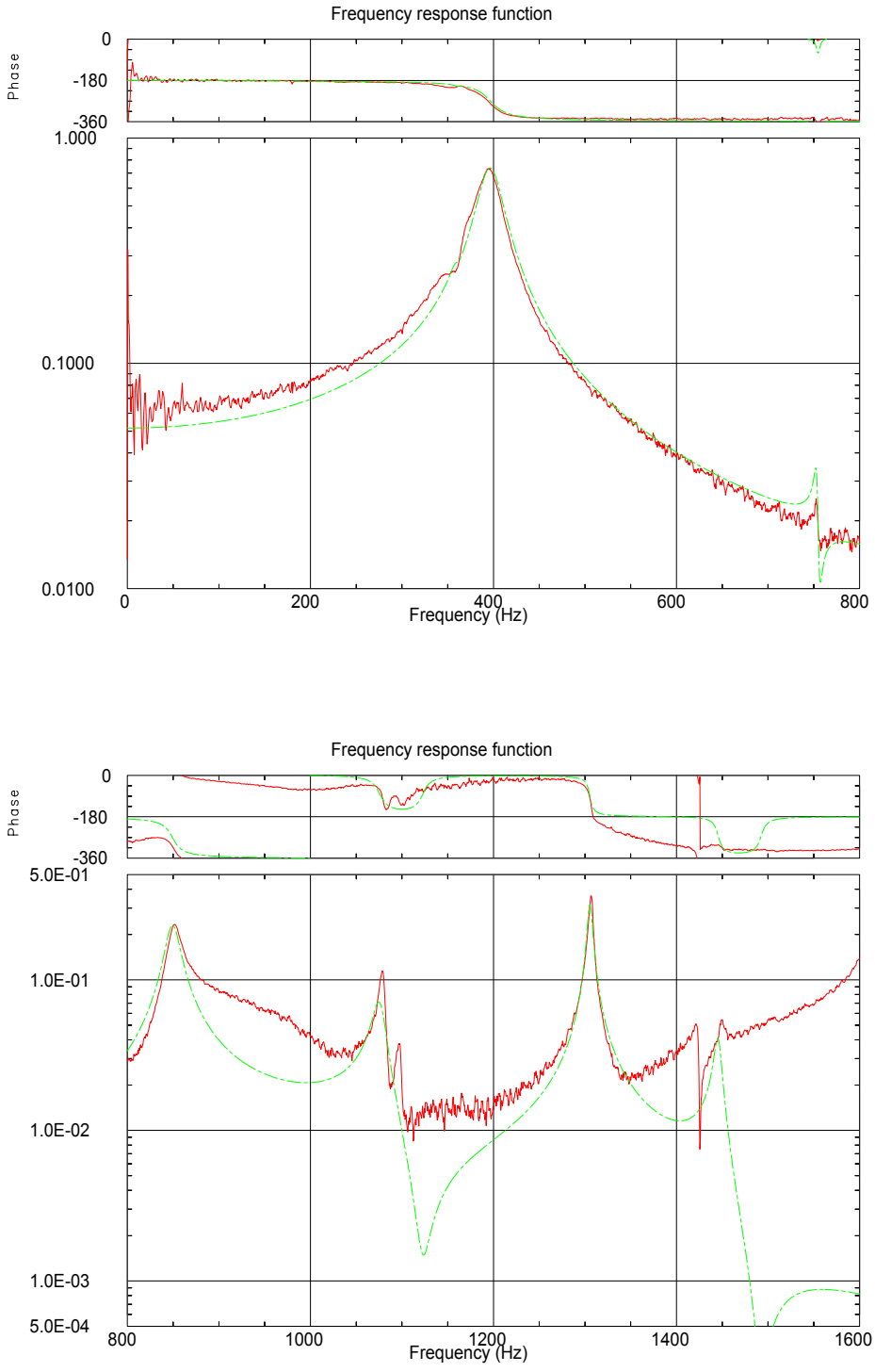

4.8.5. CORRECTION OF DAMPING

In Section 4.7.2, it was stated that while imposing a prescribed profile on the time signal, prior to performing the Fourier transform, minimizes the leakage effect it still distorts the measurement as a result of eliminating some data. It was also acknowledged that, when performing a modal survey, the physical meaning of this distortion is that the modes derived from windowed frequency response functions will appear more damped than what they are in reality. This is the result of the exponential decay imposed on the frequency response functions by the exponential *window* selected for the modal data acquisition. It is now recalled that when the exact form of the applied exponential *window* function is known, it is possible to correct the damping estimated in the modal parameter extraction process.

The function that describes the exponential decay *window* in the Dynamic Signal Analyzer employed (HP 35670A) has the following form:

$$E(t) = e^{-\frac{t}{\tau}}$$

where t – time

τ – *decay time constant*

A *decay time constant* that is guaranteed to decay a signal to less than 5% is:

$$\tau = \frac{T}{4}$$

where T – time record length

This formula was used to establish the *decay time constant* for collecting the data. The time record length (in seconds) is dependent on the following relationship between the frequency span (F, in Hz) and the number of lines of resolution (N):

$$T = \frac{N}{(1.024F)}$$

For instance, referring to the parameters used in this study, for a span of 800 Hz and a resolution of 1600 lines, the time record length is 1.95 seconds (refer also to Table 4.1). This translates into a *decay time constant* of 488 milli-seconds. Figure 4.14 shows the corresponding exponential decay *window* function.

FIGURE 4.14. Exponential Decay Window Function

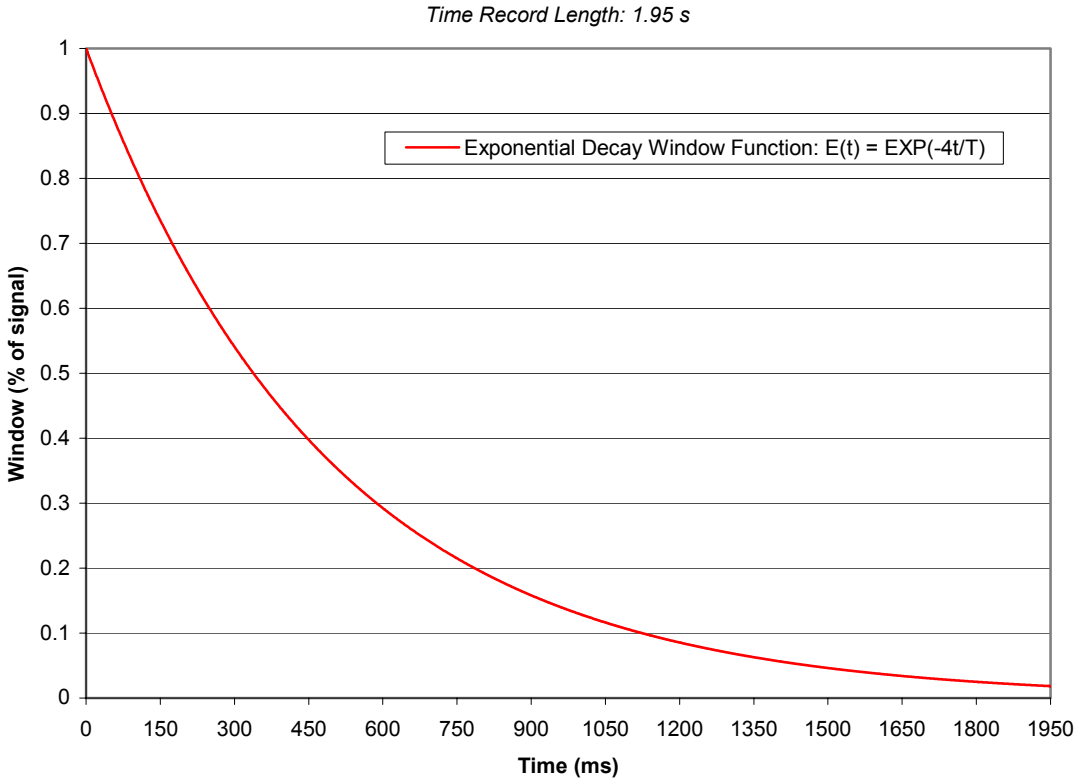

In order to correct the damping estimated in the modal parameter extraction (i.e. to remove the effects of the exponential *window* function on the measured data) the following calculation was performed on the damping of each mode extracted:

$$D_c = D_e - \frac{1}{(\omega_n \tau_a \pi)}$$

where D_c – corrected damping

D_e – uncorrected damping calculated by modal parameter estimation algorithm

ω_n – undamped natural frequency (Hz)

τ_a – τ, *decay time constant* value used in the exponential decay *window* function applied

4.9. EXPERIMENTAL RESULTS

The technique employed for conducting the experimental modal analysis is the frequency response function method. The test article was suspended through very soft elastic cords in order to closely approximate the free condition. The linearity assumption for the test article was confirmed; the structure was also assumed to be *observable* and *time-invariant*. Frequency response function measurements were collected throughout the test article using the *single-point excitation* technique. The type of excitation function selected is the transient impact type and it was applied through a manually operated hammer. Whereas the input pulse force was restricted to one position, at the camshaft, the response was measured at forty different locations, including the input location itself, the *reference*; thus, one *driving point measurement* was also acquired. The forty response measurement locations and directions were dictated by the TAM degrees of freedom derived in the pre-test simulation. The accelerometer distribution can be thus observed in Figures 3.21 A-B; the locations and directions of the measured responses correspond one to one with the TAM DOF. It is recalled that the frequency response functions were acquired one at a time; this approach greatly limited the instrumentation imposition on the structure. Each recorded response for a particular location and direction was the product of an average of ten response measurements for that same location and direction. It is also recalled that, in the data acquisition, the frequency interval of interest (0 – 4800 Hz) was divided into six narrower frequency spans of 800 Hz each in order to capture all the target modes with sufficient resolution; thus, a total of 240 frequency response functions were acquired.

The frequency response functions collected were then used as input to a modal parameter estimation process. In this phase, a curve-fitting procedure, in the time domain, was used to extract the experimental modal parameters from the measured data. Once all the modal parameters were estimated, the corresponding mode shapes were calculated and displayed through simplified test article geometry. Table 4.2 lists the modes derived from the measured frequency response functions; the table also reports the results of the damping correction operation performed for each mode. Figures 4.15 A-L illustrate a number of measured frequency response functions with their respective *coherence* functions. It is recalled that a *coherence* function value of 0.9 or greater, at a frequency corresponding to a frequency response function peak, was deemed adequate to establish the validity of the measured response. In the figures, the frequency response function peaks that correspond to test article modes are labeled accordingly; the corresponding measurement location and direction are also indicated.

The modes for which there was less confidence during the modal parameter estimation process are modes number 7 and 11. However, the results of the *normal modes with differential stiffness* solution for the spring test-vehicle model (illustrated in Section 3.2.4) contributed to the conclusion that these two modes are spring coil local modes. This conclusion was a direct consequence of the fact that the first three experimental spring modes (1st compression Z, 1st lateral bending X, and 1st lateral bending Y; modes' number 3, 4, and 5, respectively) positively matched the spring test-vehicle solution mentioned above. It is worth noting that the accelerometer distribution (or TAM DOF) did not include any measurement located on the spring internal coils;

TABLE 4.2. Experimental Modes

EXPERIMENTAL MODES				
Mode No.	***Exp. Frequency (Hz)***	***Mode Description***	***Uncorrected Damping (%)***	***Corrected Damping (%)***
1	***360***	***Valve - 1st Bending X***	*1.392*	***1.390***
2	***398***	***Valve - 1st Bending Y***	*1.461*	***1.459***
3	***754***	***Spring - 1st Compression Z***	*0.282*	***0.281***
4	***851***	***Spring - 1st Bending X***	*0.928*	***0.927***
5	***1036***	***Spring - 1st Bending Y***	*0.767*	***0.766***
6	***1305***	***Spring - 2nd Compression Z***	*0.818*	***0.818***
7	***1445***	***Spring - Coil Local Mode***	*1.280*	***1.280***
8	***1730***	***Rocker Arm - 1st Torsion***	*4.255*	***4.255***
9	***2087***	***Rocker Arm - 1st Bending Lateral***	*4.170*	***4.170***
10	***2116***	***Spring - 3rd Compression Z***	*1.530*	***1.530***
11	***2296***	***Spring - Coil Local Mode***	*2.734*	***2.734***
12	***2556***	***Head Casting - 1st Torsion X***	*5.039*	***5.039***
13	***2941***	***Head Casting - 1st Torsion Y***	*5.282*	***5.282***
14	***3107***	***Rocker Shaft - 1st Bending Z***	*4.049*	***4.049***
15	***3285***	***Head Casting - 1st Bending X***	*6.166*	***6.166***
16	***4647***	***Head Casting - 1st Bending Z***	*6.676*	***6.676***

FIGURE 4.15.A Frequency Response and Coherence Functions

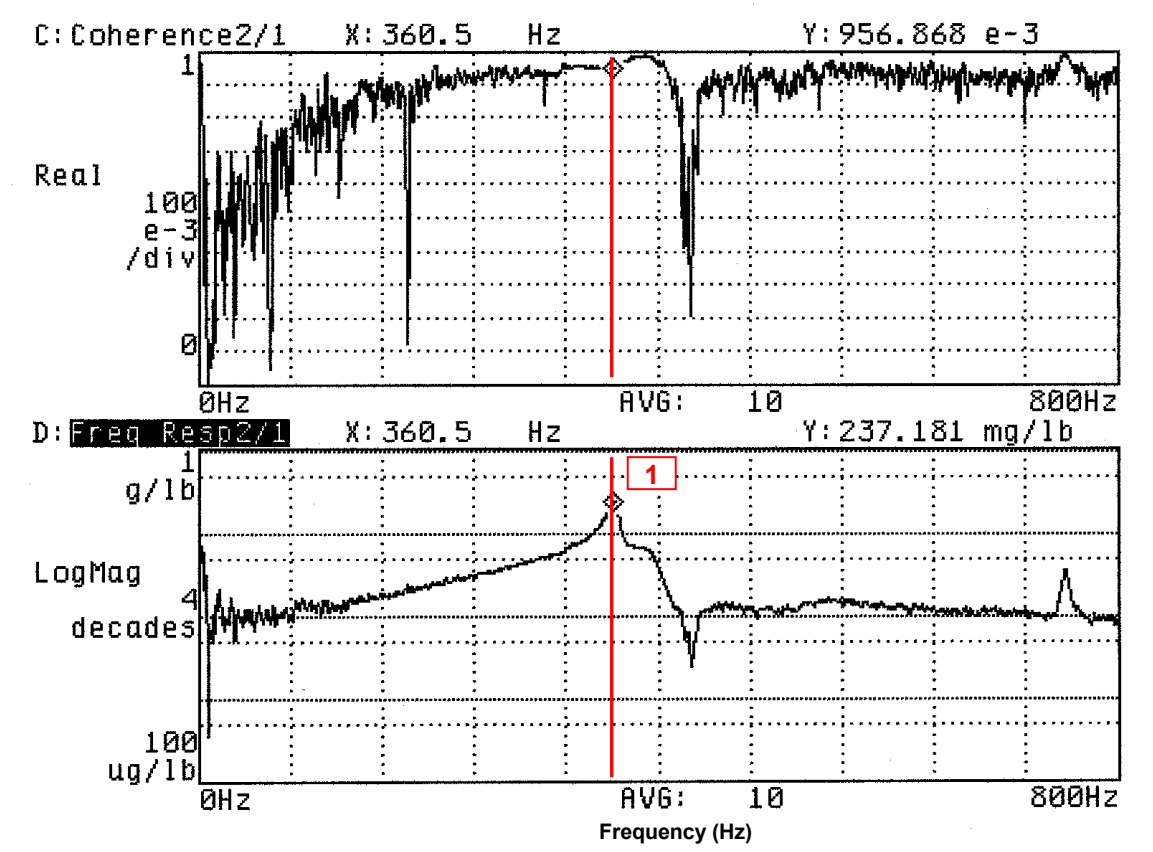

Mode 1: Valve – 1st Bending X (360 Hz)

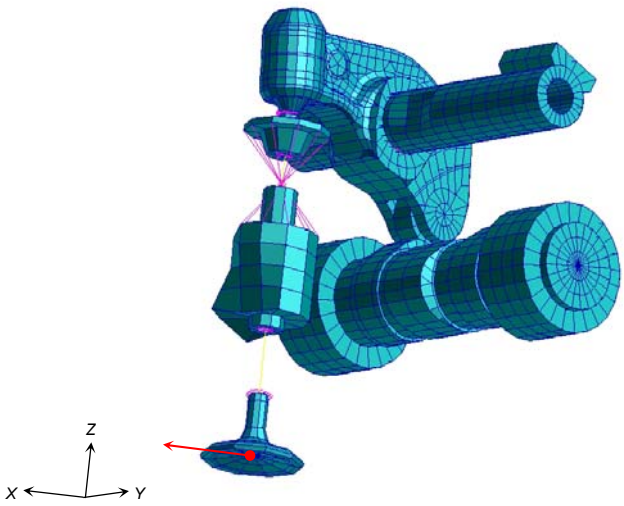

FIGURE 4.15.B Frequency Response and Coherence Functions

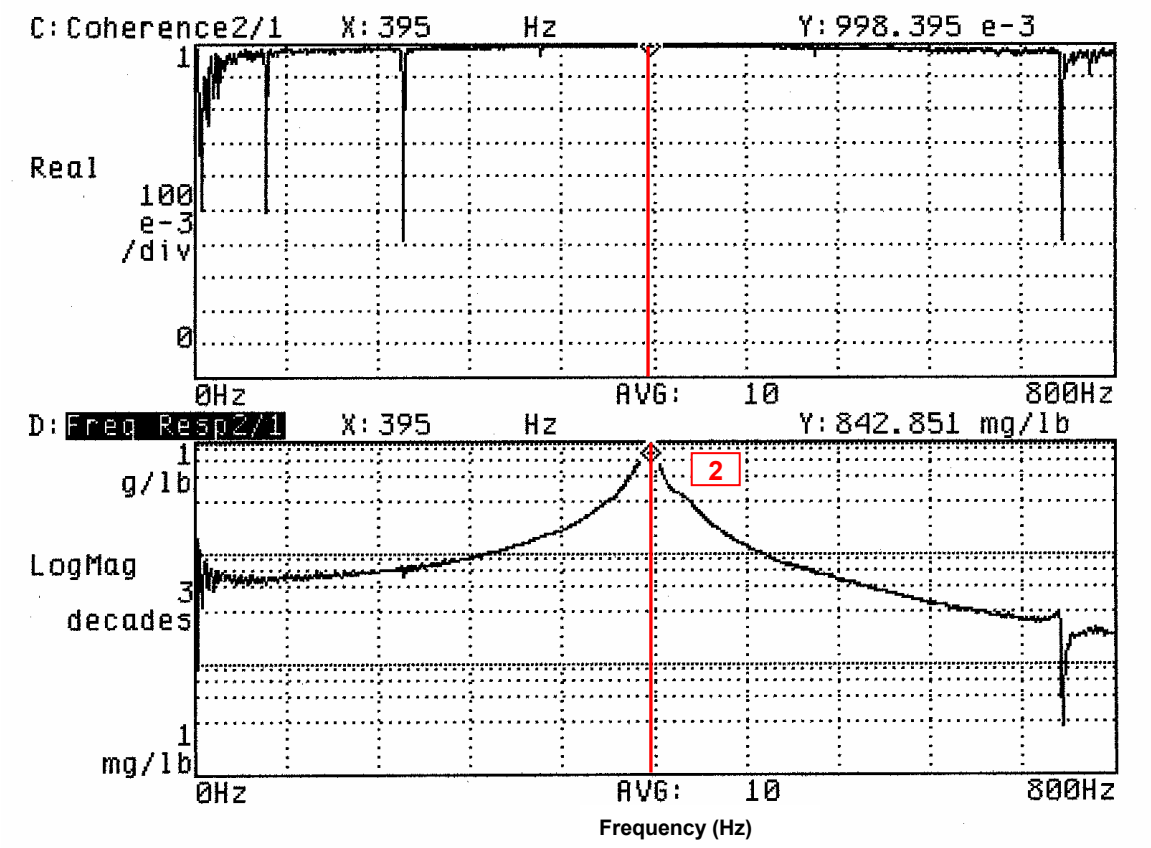

Mode 2: Valve – 1st Bending Y (398 Hz)

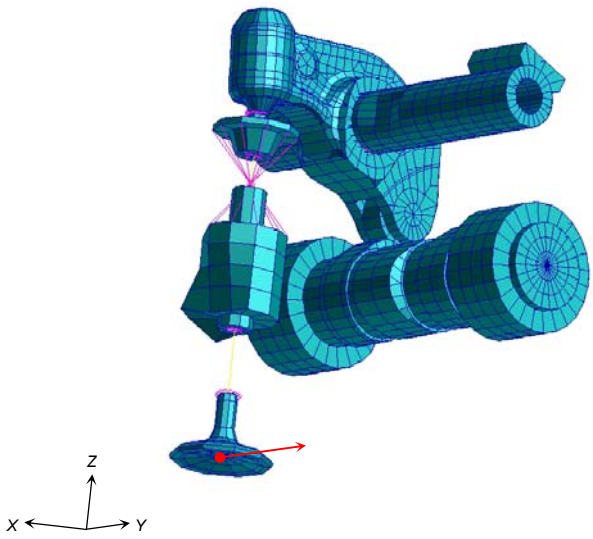

FIGURE 4.15.C Frequency Response and Coherence Functions

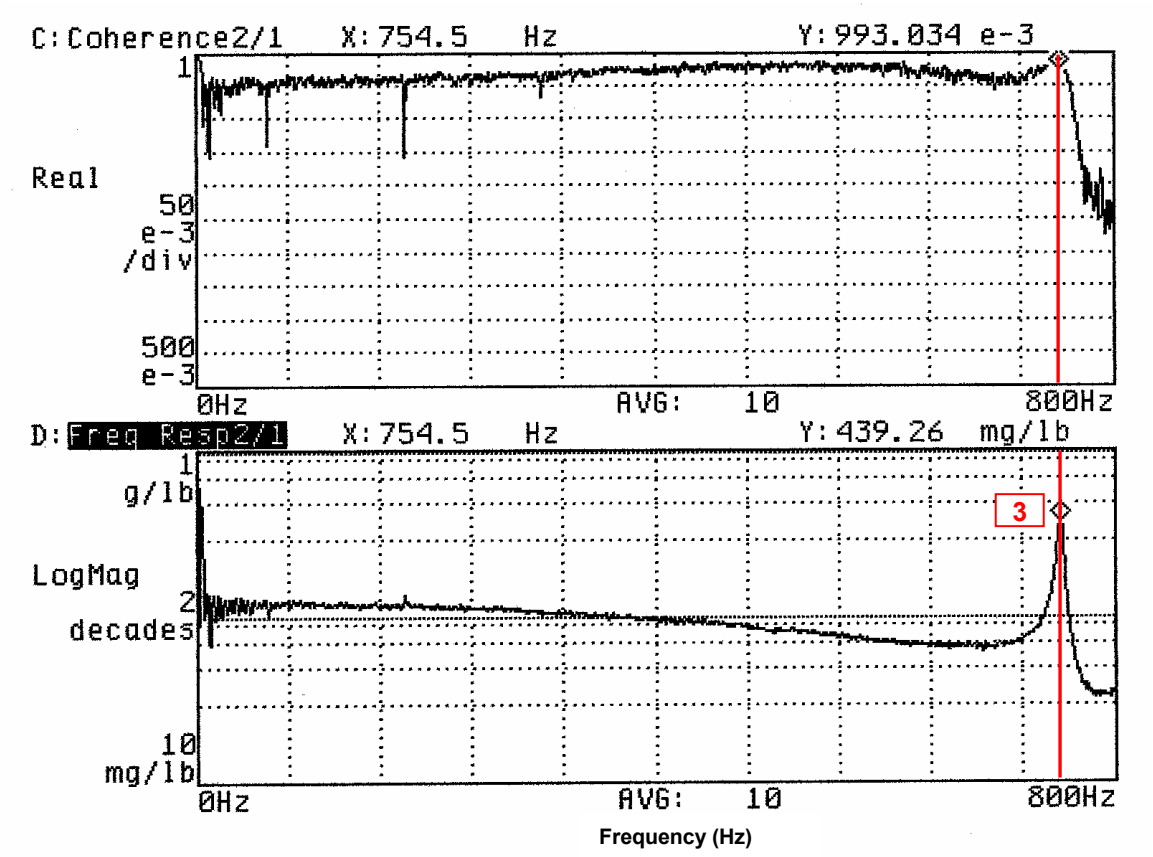

Mode 3: Spring – 1st Compression Z (754 Hz)

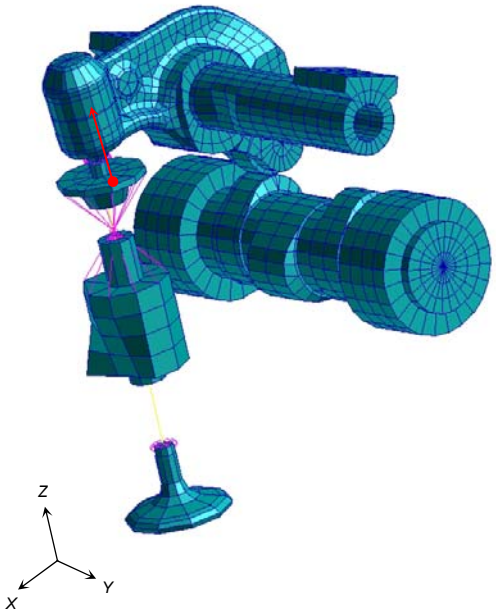

FIGURE 4.15.D Frequency Response and Coherence Functions

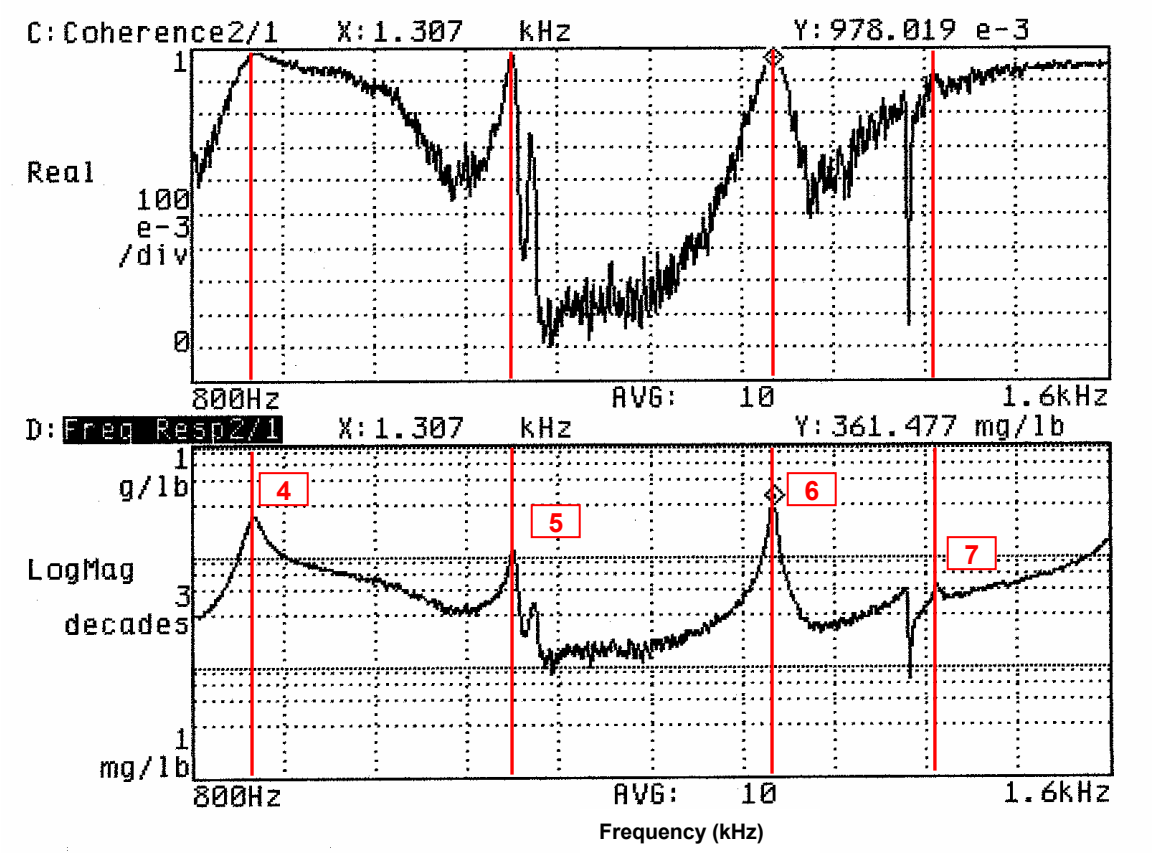

Mode 4: Spring – 1st Bending X (851 Hz)

Mode 5: Spring – 1st Bending Y (1036 Hz)

Mode 6: Spring – 2nd Compression Z (1305 Hz)

Mode 7: Spring – Coil Local Mode (1445 Hz)

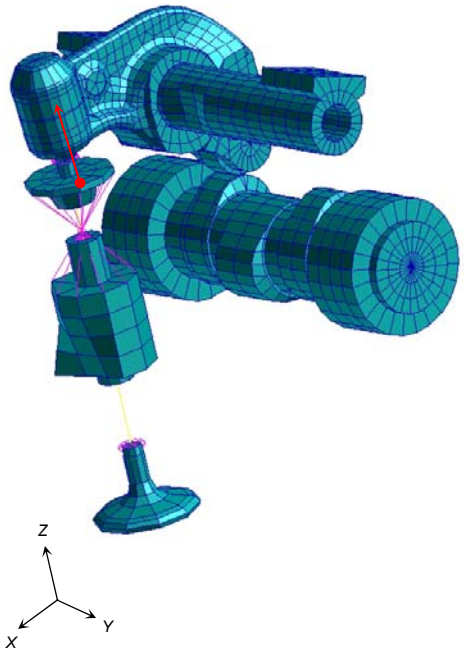

FIGURE 4.15.E Frequency Response and Coherence Functions

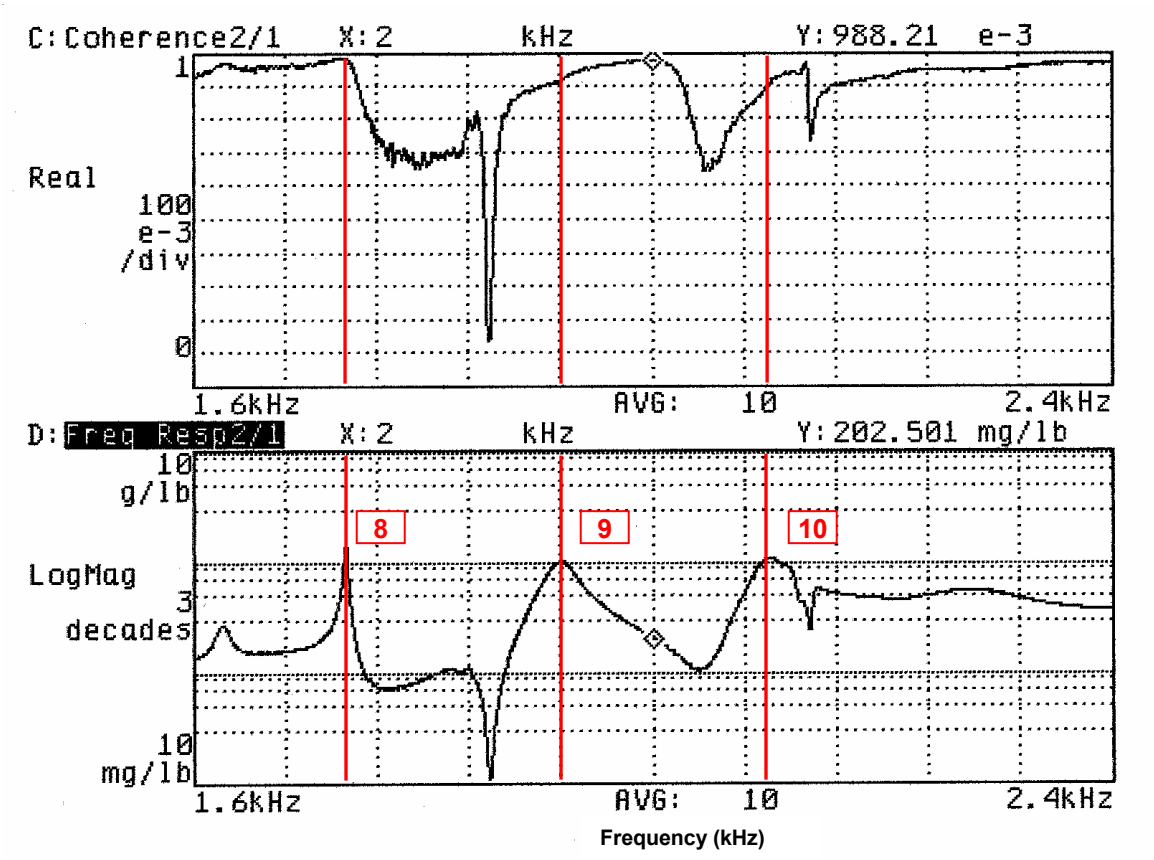

Mode 8: Rocker Arm – 1st Torsion (1730 Hz) ***Mode 9: Rocker Arm – 1st Bending Lateral (2087 Hz)***

Mode 10: Spring – 3rd Compression Z (2116 Hz)

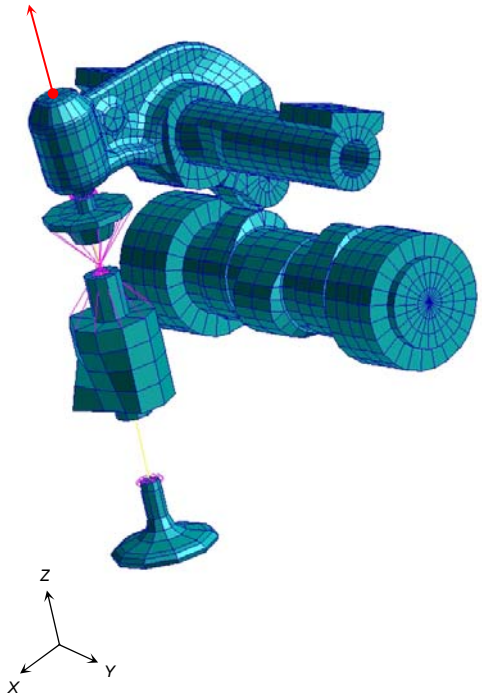

FIGURE 4.15.F Frequency Response and Coherence Functions

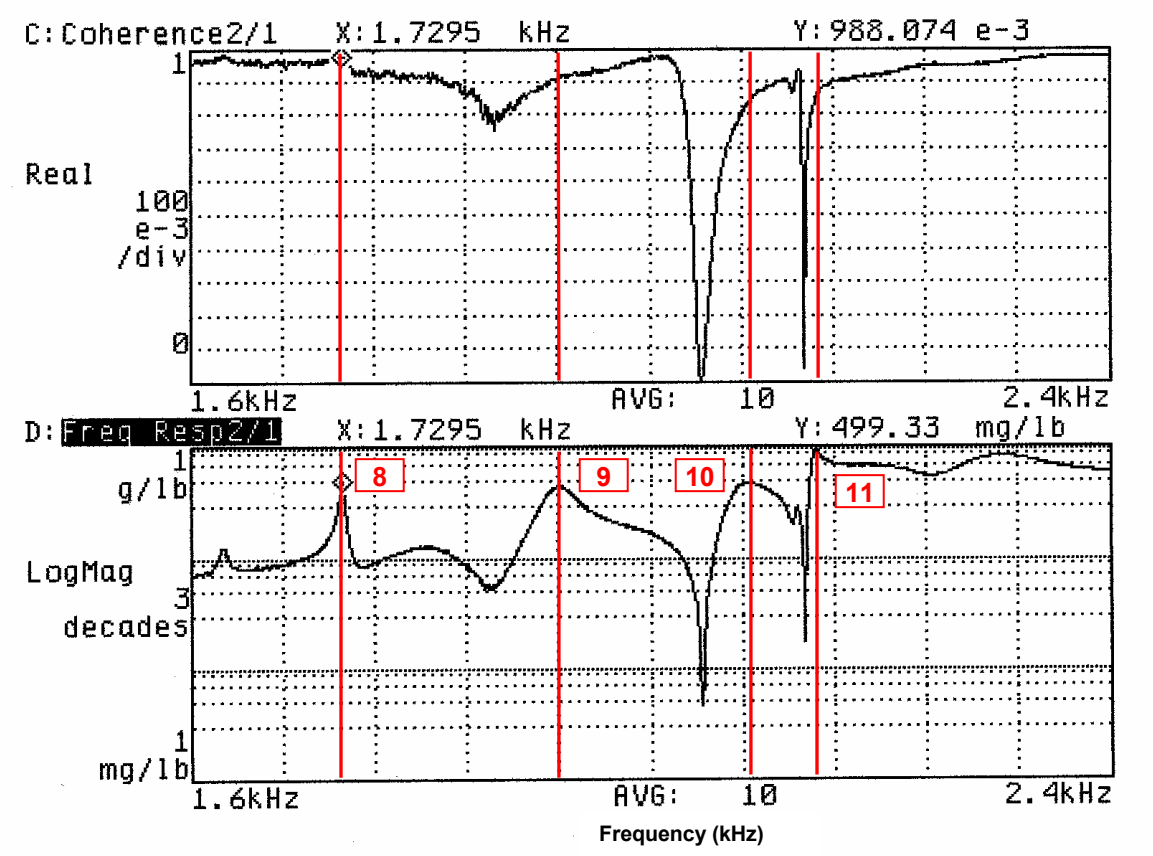

Mode 8: Rocker Arm – 1st Torsion (1730 Hz) ***Mode 9: Rocker Arm – 1st Bending Lateral (2087 Hz)***

Mode 10: Spring – 3rd Compression Z (2116 Hz) ***Mode 11: Spring – Coil Local Mode (2296 Hz)***

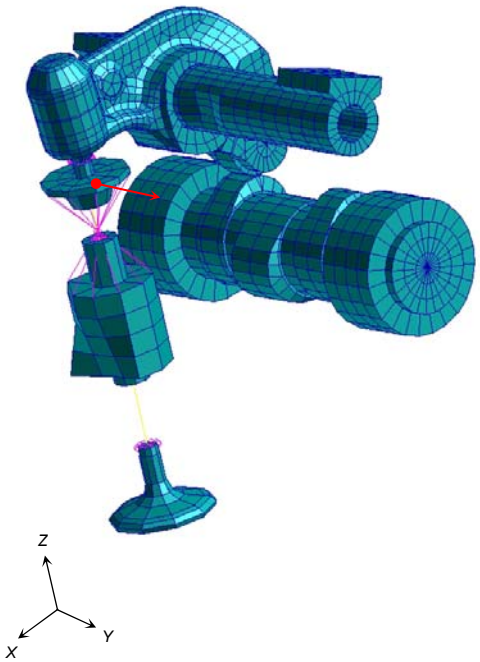

FIGURE 4.15.G Frequency Response and Coherence Functions

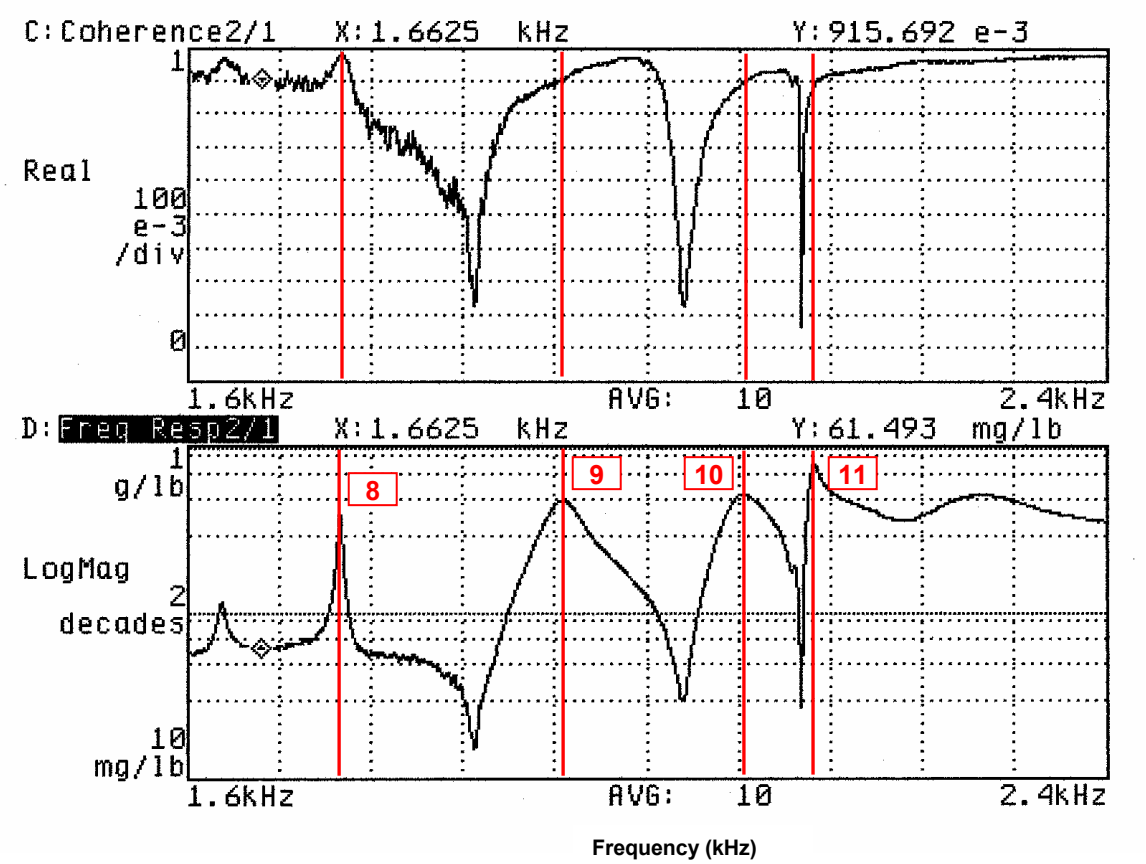

Mode 8: Rocker Arm – 1st Torsion (1730 Hz) ***Mode 9: Rocker Arm – 1st Bending Lateral (2087 Hz)***

Mode 10: Spring – 3rd Compression Z (2116 Hz) ***Mode 11: Spring – Coil Local Mode (2296 Hz)***

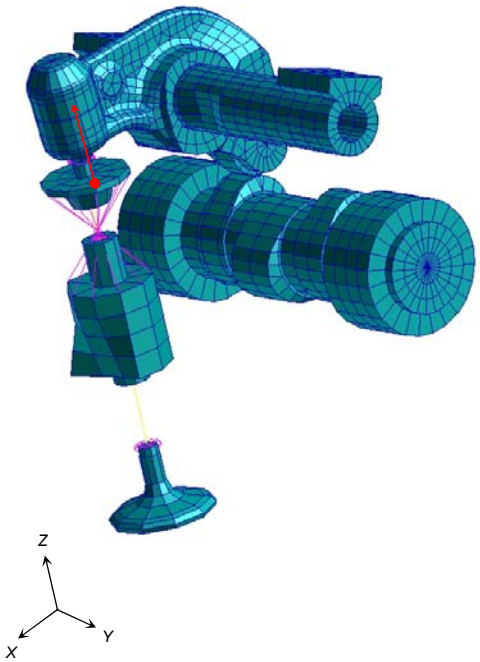

FIGURE 4.15.H Frequency Response and Coherence Functions

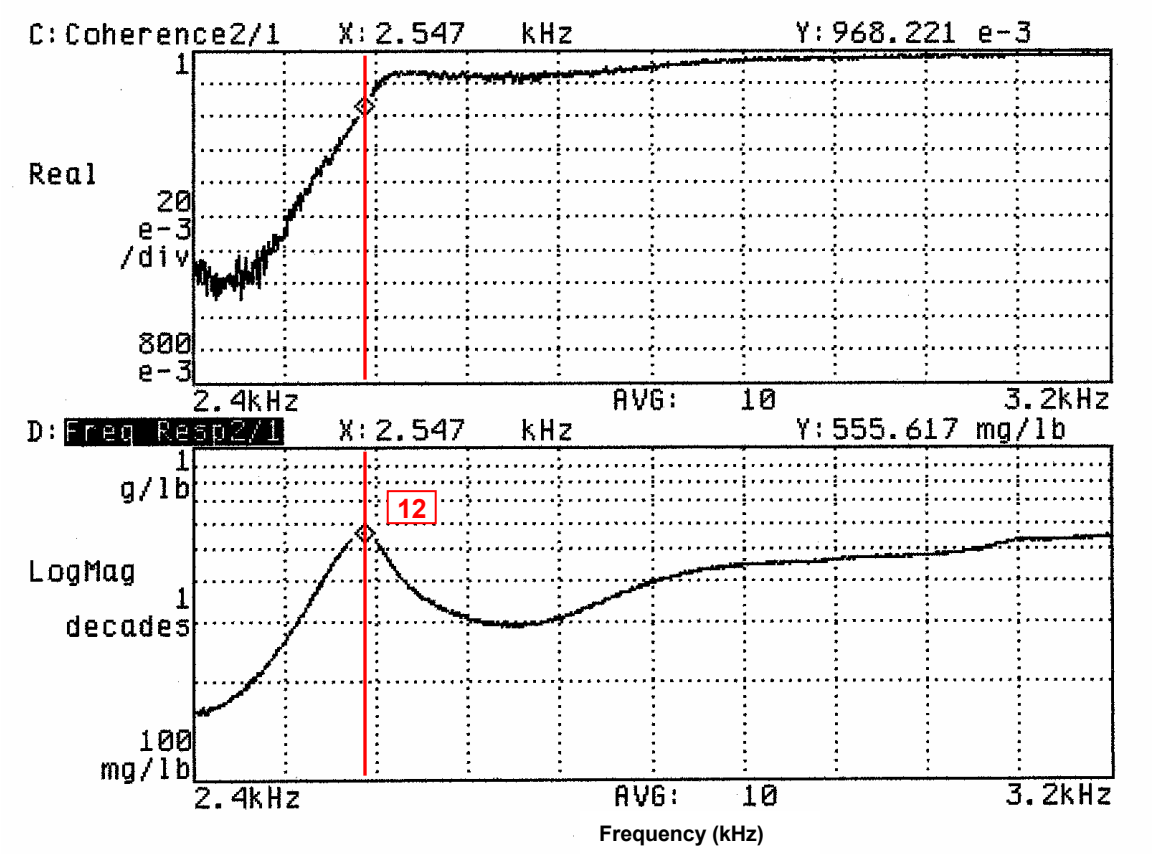

Mode 12: Head Casting – 1st Torsion X (2556 Hz)

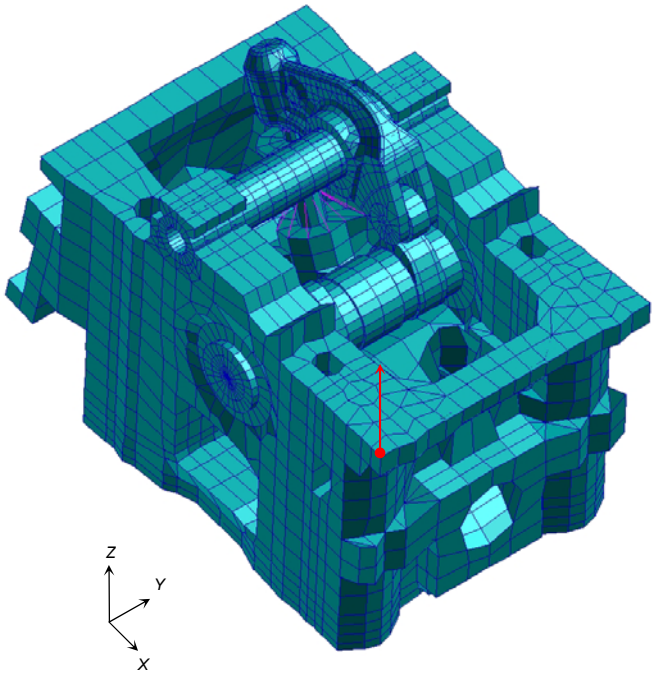

FIGURE 4.15.I Frequency Response and Coherence Functions

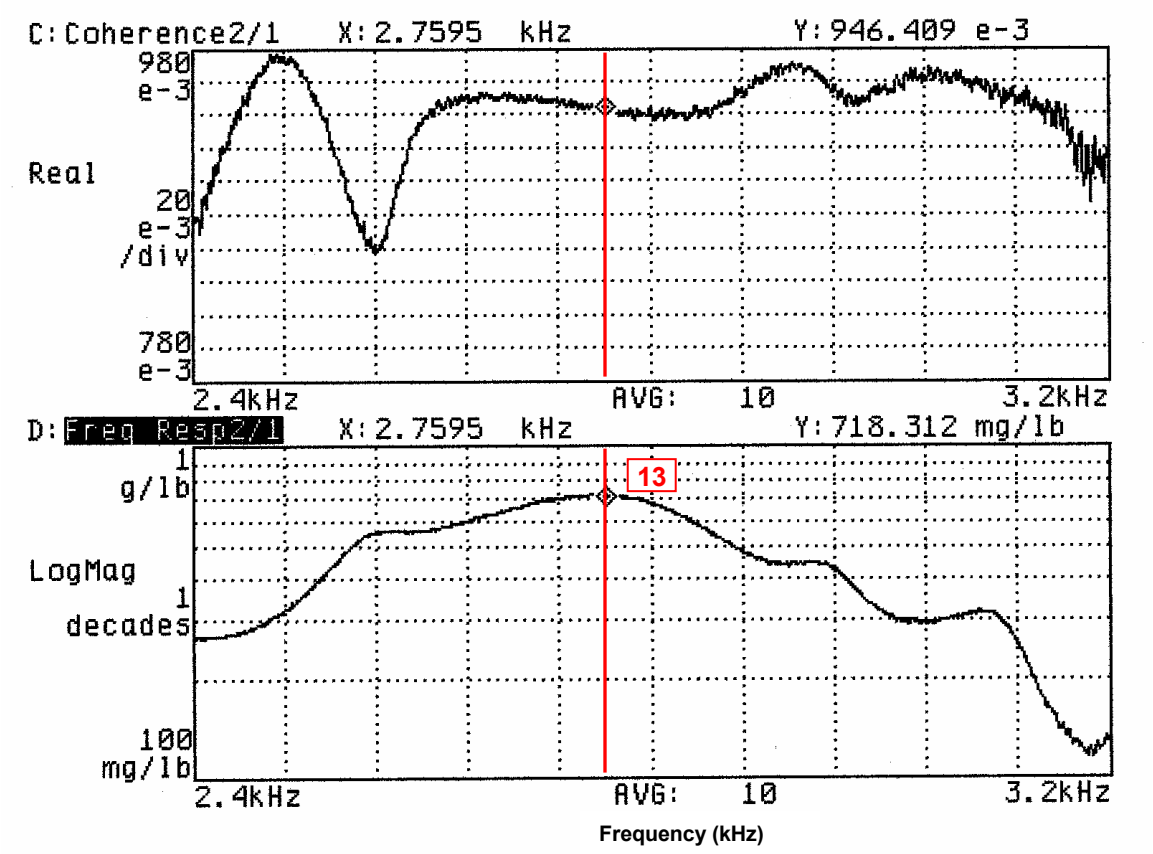

Mode 13: Head Casting – 1st Torsion Y (2941 Hz)

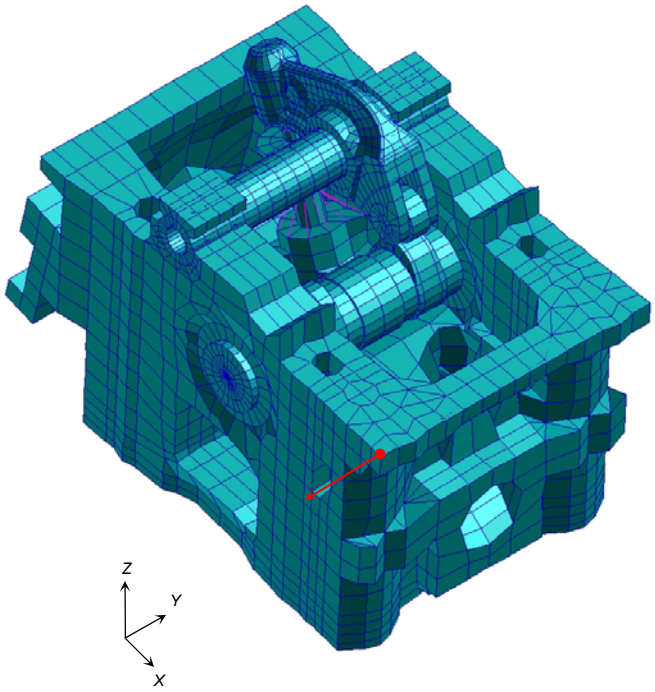

FIGURE 4.15.J Frequency Response and Coherence Functions

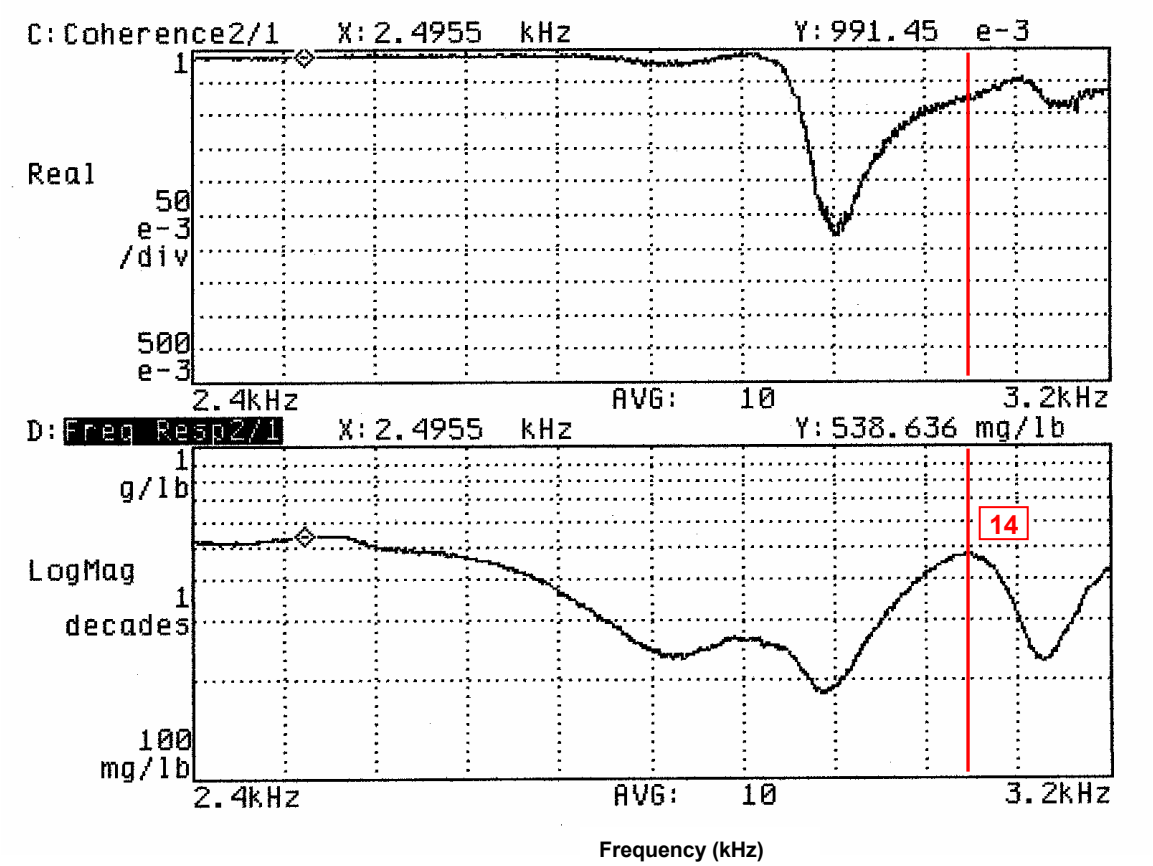

Mode 14: Rocker Shaft – 1st Bending Z (3107 Hz)

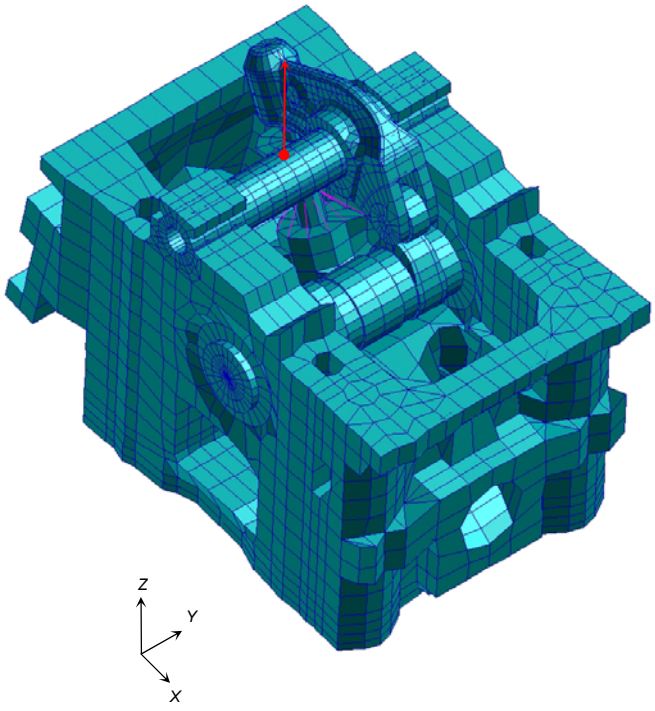

FIGURE 4.15.K Frequency Response and Coherence Functions

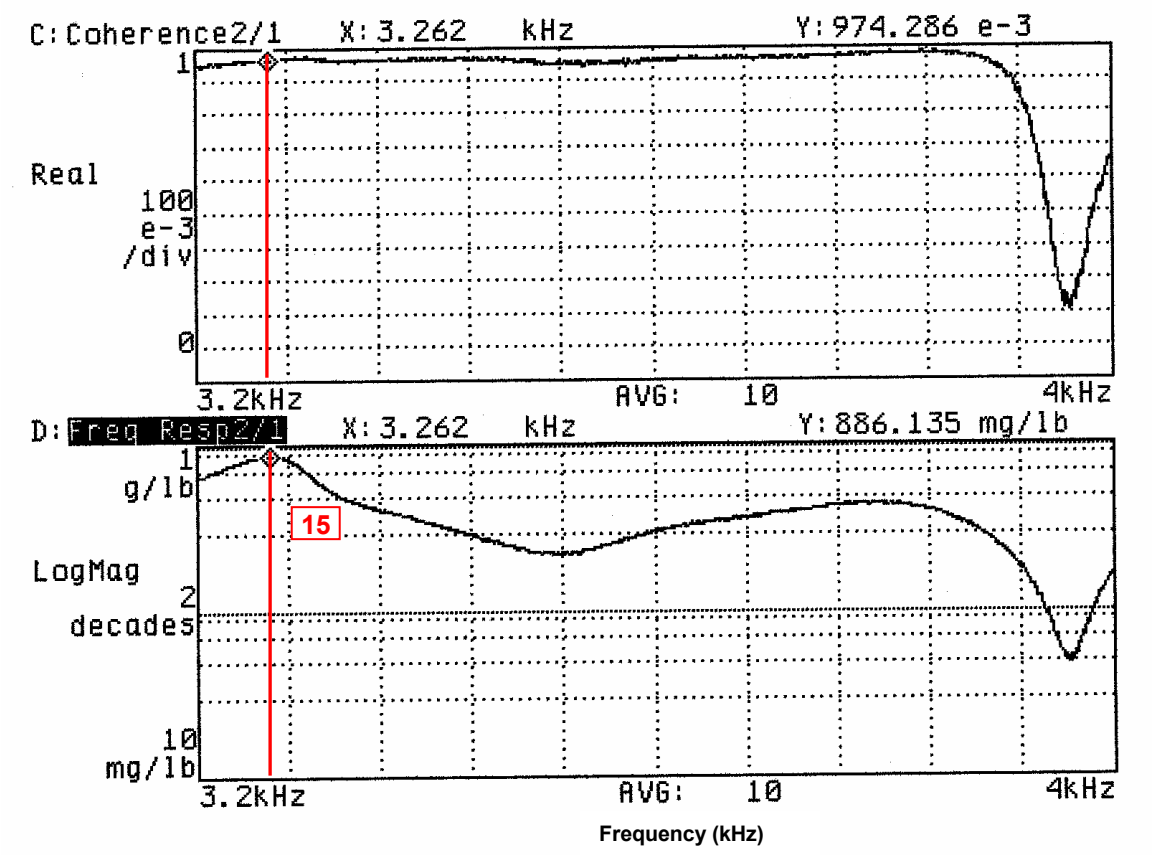

Mode 15: Head Casting – 1st Bending X (3285 Hz)

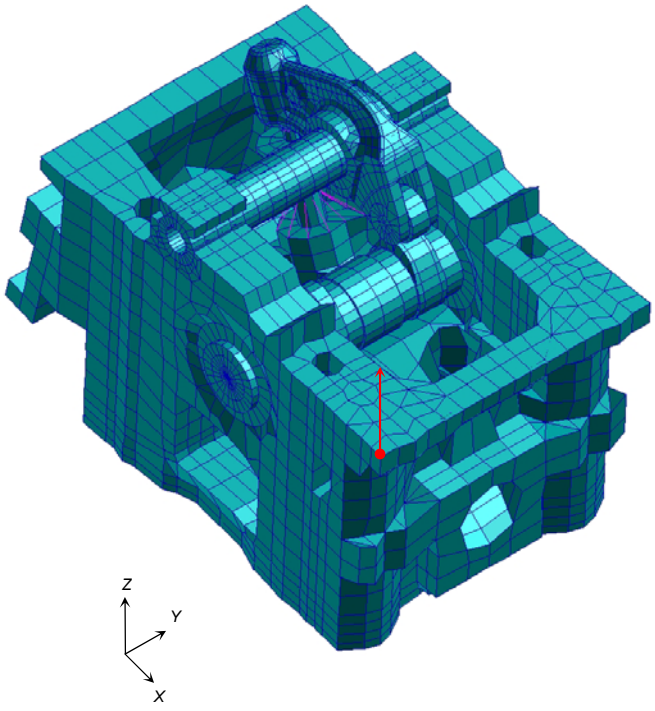

FIGURE 4.15.L Frequency Response and Coherence Functions

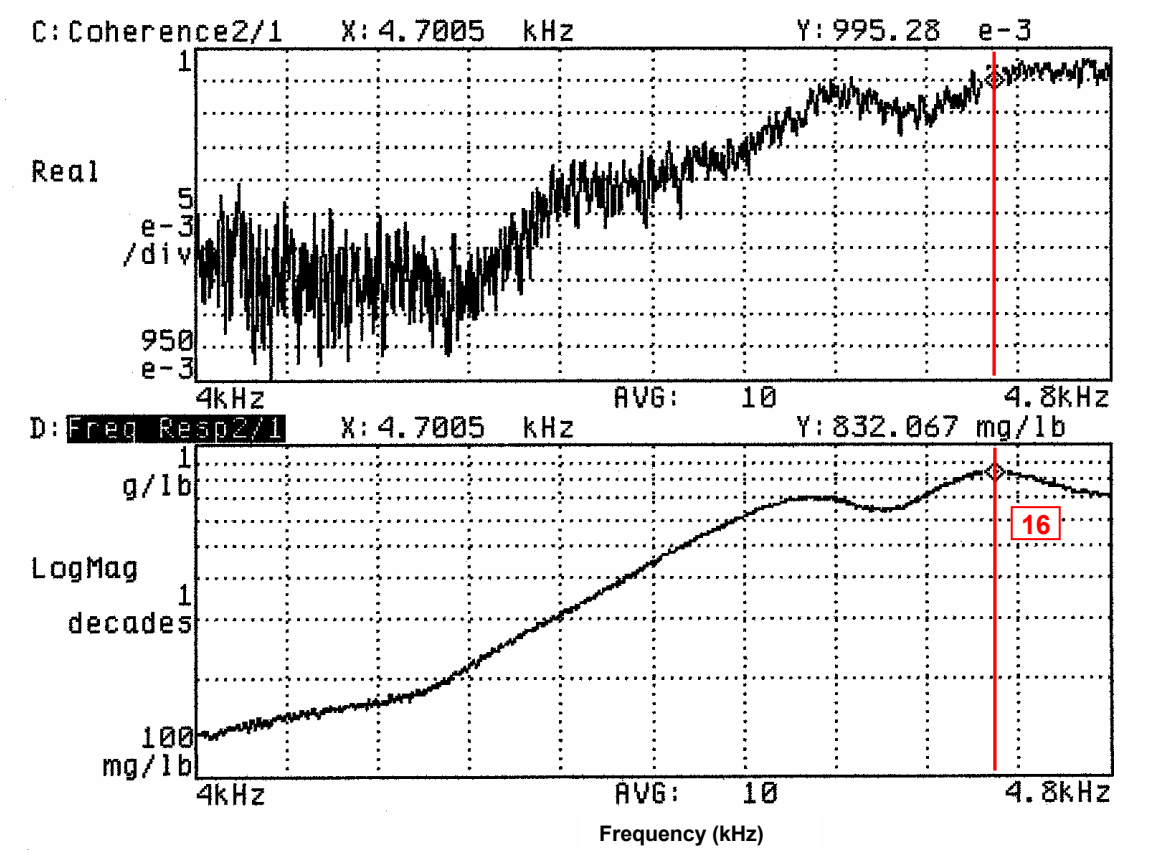

Mode 16: Head Casting – 1st Bending Z (4647 Hz)

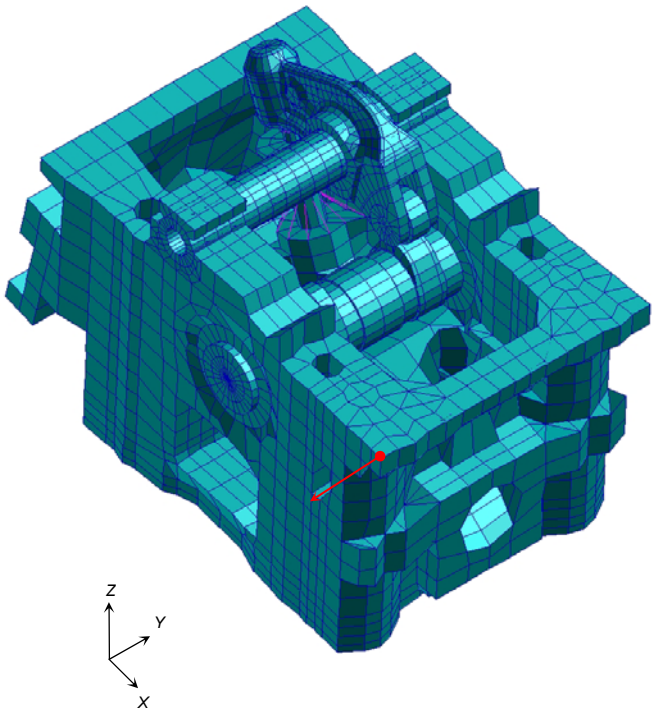

however, three response functions were measured at the top of the spring, as illustrated by Figure 3.21.B. The preliminary comparison of these experimental results to the target modes is presented in the next chapter.

Modes' couples 1-2 and 4-5 should show almost identical natural frequencies, within the couple. Indeed, they are predictable cases of repeated poles, or roots. It is recalled that repeated roots refer to the situation where one complex root or eigenvalue occurs more than once in the characteristic equation. Each root with the same value has an independent modal vector or eigenvector. As stated in Section 4.4, sometimes repeated roots are predictable because of evident geometrical symmetries. However, from Table 4.2, it can be noted that the natural frequencies of these two couples of symmetrical modes are not consistent with the pole repetition effect. In other words, in each mode pair, the natural frequencies of the two coincident modes are not almost identical. An explanation of this discrepancy is offered in Chapter 6.

5. MODEL UPDATING

In the model updating process, the test data is used as the target, and the FEM model parameters are updated to give better agreement between the model and the experimental results. In Section 2.3, it was stated that the various available approaches to address model modifications could be categorized as either modal based or response based. It was also stated that the selected approach is the modal based technique. In this method, the test modal parameters, natural frequencies and mode shapes, are used as targets in the iterative updating process. The model design parameters should represent all parts of the model for which there is less confidence[13].

5.1 PRELIMINARY COMPARISON

The first step in the updating process is to compare the pre-test simulation to the test results in order to identify discrepancies and define model design parameters. Table 5.1 reports a comparison between the target modes and the modes derived experimentally. Table 5.1 clearly suggests that the FEM model did not "capture" experimental modes' number 6, 7, 10, and 11; these modes are either second-order spring modes or local spring coil modes. The model misses these modes because of the spring model nature. To some extent, this discrepancy was expected as the spring model was deliberately prepared with the solution's objective of simplicity. The spring model scheme illustrated in Figure 3.18 is an accurate solution for detecting first-order modes but it cannot be as accurate in representing second-order, and above, modes. In

TABLE 5.1. Target Modes and Experimental Frequencies Comparison

TARGET MODES AND EXPERIMENTAL FREQUENCIES COMPARISON							
Mode No.	**FEM Mode No.**	**FEM Frequency (Hz)**	**Exp. Mode No.**	**Experimental Frequency (Hz)**	**Difference (Hz & %)**		**Mode Description**
1	7	**469**	1	**360**	109	30.3%	**Valve - 1st Bending X**
2	8	**470**	2	**398**	72	18.1%	**Valve - 1st Bending Y**
3	9	**682**	3	**754**	-72	-9.5%	**Spring - 1st Compression Z**
4	10	**844**	4	**851**	-7	-0.8%	**Spring - 1st Bending X**
5	11	**846**	5	**1036**	-190	-18.3%	**Spring - 1st Bending Y**
6		Not Captured	6	**1305**			Spring - 2nd Compression Z
7		Not Captured	7	**1445**			Spring - Coil Local Mode
8	12	**1631**		Not Captured			**Valve - 1st Torsion Z**
9	13	**2102**	8	**1730**	372	21.5%	**Rocker Arm - 1st Torsion**
10	14	**2243**	9	**2087**	156	7.5%	**Rocker Arm - 1st Bending Lateral**
11		Not Captured	10	**2116**			Spring - 3rd Compression Z
12		Not Captured	11	**2296**			Spring - Coil Local Mode
13	15	**2319**	12	**2556**	-237	-9.3%	**Head Casting - 1st Torsion X**
14	16	**3207**	13	**2941**	266	9.0%	**Head Casting - 1st Torsion Y**
15	17	**3412**	14	**3107**	305	9.8%	**Rocker Shaft - 1st Bending Z**
16	18	**3492**	15	**3285**	207	6.3%	**Head Casting - 1st Bending X**
17	19	**4507**		Not Captured			**Valve - 2nd Bending X**
18	20	**4522**		Not Captured			**Valve - 2nd Bending Y**
19	21	**4584**	16	**4647**	-63	-1.4%	**Head Casting - 1st Bending Z**

addition, this spring model cannot predict local coil modes simply because no coils are modeled; in the model, the proper spring stiffness levels are provided by the six spring element stiffness constants, as illustrated in Section 3.2.2. A number of different solutions are available to overcome this spring model limit; however, the development, application and validation of these solutions go beyond the purpose of this correlation

methodology overview. Therefore, the spring model scheme itself is not included in the model design parameter set. Nevertheless, the spring properties of this scheme (i.e. spring elements' stiffness) are still considered design parameters and are then updated to obtain better correlation with the experimental results. Spring mass and inertia are not considered design parameters, either.

On the other hand, Table 5.1 indicates that the experimental approach did not capture FEM mode number 12. The reason of this discrepancy is explained by recalling the considerations made in Section 4.4 regarding the assumption for the test article to be *observable.* It was stated that when this assumption is formulated, the input-output measurements that are made contain enough information to generate an adequate behavioral model of the structure. It was noted, however, that sometimes no response information is available relative to a particular DOF of the structure, converting thus the test article into a partially *observable* structure. One special case that causes this effect was outlined, the case of local rotations. It was concluded that even when the three main response directions (X, Y, and Z) relative to a certain point of the structure are being measured, the three local rotations (RX, RY, and RZ) for the same point might be completely missed. This situation is exactly the case concerning FEM mode number 12. The mode in question is the first torsion of the valve. The accelerometer was located, accordingly with the TAM DOF (refer to Figure 3.21.B), at the valve head along the valve axis, thus it was very difficult for the transducer to "see" valve rotations around its axis. This valve torsion mode can only be characterized by comprising in the modal parameter estimation process measurements that include valve responses taken off the valve axis.

Table 5.1 also indicates that the experimental approach did not capture FEM modes' number 19 and 20, either. This discrepancy is caused by the combination of at least three factors. One factor is the low excitation energy level, as these modes occur at frequencies that are very close to the upper limit of the frequency interval of interest. It is recalled that this upper limit was set through the evaluation of the power spectrum of the input force pulse, as described in Section 4.6.2. The second factor is also related to the excitation; another cause of discrepancy could derive from the fact that the direction of excitation may not be the optimal direction to excite these modes. The third factor, which is possibly the most important, concerns the measurement response locations. The modes in question are second-order bending modes for the valve. As the valve is in fact acting as a cantilever beam and the response measurement locations are all positioned at the valve head (the free end of the cantilever beam; refer to Figure 3.21.B), the valve second bending modes cannot be exhaustively characterized from response data measured merely at this location. In order to better define these modes, response measurements along valve stem are required.

The results of the preliminary comparison can be summarized as follows:

- *The pre-test simulation predicted 15 modes in the frequency interval of interest (0 – 4 800 Hz).*
- *The modal survey measured 16 modes in the same frequency interval*
- *The pre-test simulation did not predict 4 measured modes*
- *The modal survey did not capture 3 predicted modes*
- *Thus, 12 modes were preliminarily correlated*

Explanations for the discrepancies were provided in the previous paragraphs. The twelve correlated modes compare well in terms of natural frequencies and compare very well in terms of modes' sequence. The next section describes how the boundary conditions between the valve train components were updated in order to obtain improved frequency comparison. It is recalled that neither accuracy of geometries nor material properties were considered as model design parameters, as initial values were deemed adequate.

5.2. MODIFIED BOUNDARY CONDITIONS IN THE FEM MODEL

As stated in Section 3.2.1, the boundary conditions employed to attach the valve train components together are critical to the outcome of a valve train modal analysis, as the modal characterization of any structure is extremely sensitive to the applied constraints. After the preliminary comparison between the target modes and the modes derived experimentally, the valve train boundary conditions to be modified reduced to two areas. One area in which the boundary conditions did not prove to accurately represent the constraints in the test article is at the interface of the rocker arm with its shaft. The coupling prepared for the pre-test analysis proved to be excessively rigid. Although in the pre-test solution the rocker arm mode sequence is consistent with the corresponding experimental mode sequence, the predicted rocker arm modes occur at higher frequencies. As explained in Section 3.2.1, RBEs were inserted at the bottom of the coupling interface between these two parts. The number of RBEs employed for this connection was iteratively reduced to obtain better rocker arm natural frequency correlation.

The other boundary conditions that needed adjustment relate to the valve sliding constraints. In model development, RBEs were inserted between the valve guide and the valve stem in order to obtain the proper sliding motion for the valve. It is recalled that valve torsion was not constrained within the valve guide, consistently with the test article. In the model, the sliding motion itself did not present discrepancies with the test article condition (i.e. the valve stem did not execute any "illegal" translation or rotation); however, the number of RBEs employed for creating the sliding clause was excessive, as the predicted modes for the valve occur at higher frequencies than the corresponding frequencies observed in the experimental approach. The number of RBEs employed was then iteratively reduced to obtain better valve natural frequency correlation.

The other boundary conditions created during model development remained untouched, as the assumptions formulated for the involved interfaces proved to be valid (refer to Section 3.2.1). The head casting model also remained untouched, as the predicted modes pertinent to this part of the system showed very good correlation in the preliminary comparison between pre-test and experimental data. The four predicted modes relative to the head casting (FEM modes number 15, 16, 18 and 21; refer to Table 5.1) are in agreement with modal test results not only concerning modal sequence but also frequency values (i.e. the frequency values do not diverge by more than 10% from the corresponding experimental values). As stated in the previous section, the six spring stiffness constants were also updated to obtain better correlation with the experimental results.

5.3. RESULTS

After having introduced the modifications described in the previous section, a new *normal modes* solution was obtained for the updated model. Table 5.2 reports a comparison between the target modes identified in the pre-test simulation and the modes derived through the updated model. The final comparison between the updated model and the experimental results is illustrated and discussed in the next chapter.

TABLE 5.2. Target Modes and Updated FEM Model Frequencies Comparison

TARGET MODES AND UPDATED FEM MODEL FREQUENCIES COMPARISON							
Mode No.	***FEM Mode No.***	***FEM Frequency (Hz)***	***U-FEM Mode No.***	***U-FEM Frequency (Hz)***	***Difference (Hz & %)***		***Mode Description***
1	*7*	***469***	*7*	***371***	*-98*	*-20.9%*	***Valve - 1st Bending X***
2	*8*	***470***	*8*	***372***	*-98*	*-20.9%*	***Valve - 1st Bending Y***
3	*9*	***682***	*9*	***711***	*29*	*4.3%*	***Spring - 1st Compression Z***
4	*10*	***844***	*10*	***913***	*69*	*8.2%*	***Spring - 1st Bending X***
5	*11*	***846***	*11*	***947***	*101*	*11.9%*	***Spring - 1st Bending Y***
6	*12*	***1631***	*12*	***1631***	*0*	*0.0%*	***Valve - 1st Torsion Z***
7	*13*	***2102***	*13*	***1874***	*-228*	*-10.8%*	***Rocker Arm - 1st Torsion***
8	*14*	***2243***	*14*	***2188***	*-55*	*-2.5%*	***Rocker Arm - 1st Bending Lateral***
9	*15*	***2319***	*15*	***2319***	*0*	*0.0%*	***Head Casting - 1st Torsion X***
10	*16*	***3207***	*16*	***3207***	*0*	*0.0%*	***Head Casting - 1st Torsion Y***
11	*17*	***3412***	*17*	***3275***	*-137*	*-4.0%*	***Rocker Shaft - 1st Bending Z***
12	*18*	***3492***	*18*	***3492***	*0*	*0.0%*	***Head Casting - 1st Bending X***
13	*19*	***4507***	*19*	***4308***	*-199*	*-4.4%*	***Valve - 2nd Bending X***
14	*20*	***4522***	*20*	***4312***	*-210*	*-4.6%*	***Valve - 2nd Bending Y***
15	*21*	***4584***	*21*	***4584***	*0*	*0.0%*	***Head Casting - 1st Bending Z***

6. CONCLUSIONS

In the model updating phase, the test modal data was used as the target and the FEM model parameters were updated to obtain better agreement between the model and the experimental results. Prior to initiating the updating process, a preliminary comparison between pre-test simulation and test results was performed in order to identify discrepancies and define model parameters, as illustrated in the previous chapter. Once the model modifications were evaluated and introduced, a new *normal modes* solution was then obtained for the updated model. Table 6.1 reports the final comparison between the modes obtained with the updated FEM model and the modes derived experimentally.

Similarly to the preliminary comparison, the results of this final comparison can be summarized as follows:

- *The updated model predicts 15 modes in the frequency interval of interest (0 – 4 800 Hz).*
- *The modal survey measured 16 modes in the same frequency interval*
- *The updated model does not predict 4 measured modes*
- *The modal survey did not capture 3 predicted modes in the updating model*
- *Thus, 12 modes are correlated in the frequency interval of interest*

Explanations for the discrepancies between the updated model and the results of the modal survey are addressed in the next paragraphs. The twelve correlated modes show improved natural frequency comparison with respect to the preliminary comparison.

TABLE 6.1. Updated FEM Model and Experimental Frequencies Comparison

UPDATED FEM MODEL AND EXPERIMENTAL FREQUENCIES COMPARISON							
Mode No.	***U-FEM Mode No.***	***U-FEM Frequency (Hz)***	***Exp. Mode No.***	***Experimental Frequency (Hz)***	***Difference (Hz & %)***		***Mode Description***
1	*7*	***371***	*1*	***360***	*11*	*3.1%*	***Valve - 1st Bending X***
2	*8*	***372***	*2*	***398***	*-26*	*-6.5%*	***Valve - 1st Bending Y***
3	*9*	***711***	*3*	***754***	*-43*	*-5.7%*	***Spring - 1st Compression Z***
4	*10*	***913***	*4*	***851***	*62*	*7.3%*	***Spring - 1st Bending X***
5	*11*	***947***	*5*	***1036***	*-89*	*-8.6%*	***Spring - 1st Bending Y***
6		*Not Captured*	*6*	***1305***			*Spring - 2nd Compression Z*
7		*Not Captured*	*7*	***1445***			*Spring - Coil Local Mode*
8	*12*	***1631***		*Not Captured*			***Valve - 1st Torsion Z***
9	*13*	***1874***	*8*	***1730***	*144*	*8.3%*	***Rocker Arm - 1st Torsion***
10	*14*	***2188***	*9*	***2087***	*101*	*4.8%*	***Rocker Arm - 1st Bending Lateral***
11		*Not Captured*	*10*	***2116***			*Spring - 3rd Compression Z*
12		*Not Captured*	*11*	***2296***			*Spring - Coil Local Mode*
13	*15*	***2319***	*12*	***2556***	*-237*	*-9.3%*	***Head Casting - 1st Torsion X***
14	*16*	***3207***	*13*	***2941***	*266*	*9.0%*	***Head Casting - 1st Torsion Y***
15	*17*	***3275***	*14*	***3107***	*168*	*5.4%*	***Rocker Shaft - 1st Bending Z***
16	*18*	***3492***	*15*	***3285***	*207*	*6.3%*	***Head Casting - 1st Bending X***
17	*19*	***4308***		*Not Captured*			***Valve - 2nd Bending X***
18	*20*	***4312***		*Not Captured*			***Valve - 2nd Bending Y***
19	*21*	***4584***	*16*	***4647***	*-63*	*-1.4%*	***Head Casting - 1st Bending Z***

This indicates that the selected model parameter values efficiently modified the structural characteristics of the system's model. It is recalled that the selected model parameter set included primarily boundary conditions that interconnect valve train components (refer to Section 5.2). It is also recalled that the mode sequence concerning these twelve modes showed excellent agreement, between pre-test simulation and test data, since the

preliminary comparison. It is finally recalled that neither accuracy of model geometries nor material properties were considered as model parameters in the model updating process, as initial values were deemed adequate.

Figure 6.1 shows a comparison between the pre-test simulation and updated model results relative to the experimental results. This figure is a chart of the error (in frequency) in the numerical approach with respect to the experimental approach. Two sets of data are plotted:

- *Error in frequency of the pre-test modes with respect of the experimental modes*
- *Error in frequency of the modes in the updated model with respect of the experimental modes*

This chart illustrates that, after the model updating process, all the correlated modes in the updated model have natural frequencies whose values do not diverge by more than 10% from the corresponding experimentally derived values. Thus, the objective regarding natural frequency discrepancies set in the Section 2.3 is attained. Figure 6.2 reports the diagonal and off-diagonal term values of the orthogonality check between the correlated modes derived with the updated model and the modes obtained experimentally. The results of this orthogonality check meet the correlation criteria set in Chapter 2.

The discrepancy concerning the second-order spring compression modes and local spring coil modes illustrated extensively in the preliminary comparison (refer to Section 5.1) is still present in this final comparison. It is recalled that the developed FEM spring model is not able to capture these modes because of the simplified spring model

FIGURE 6.1. Frequency Error Comparison Between Pre-Test Simulation and Post-Correlation Models

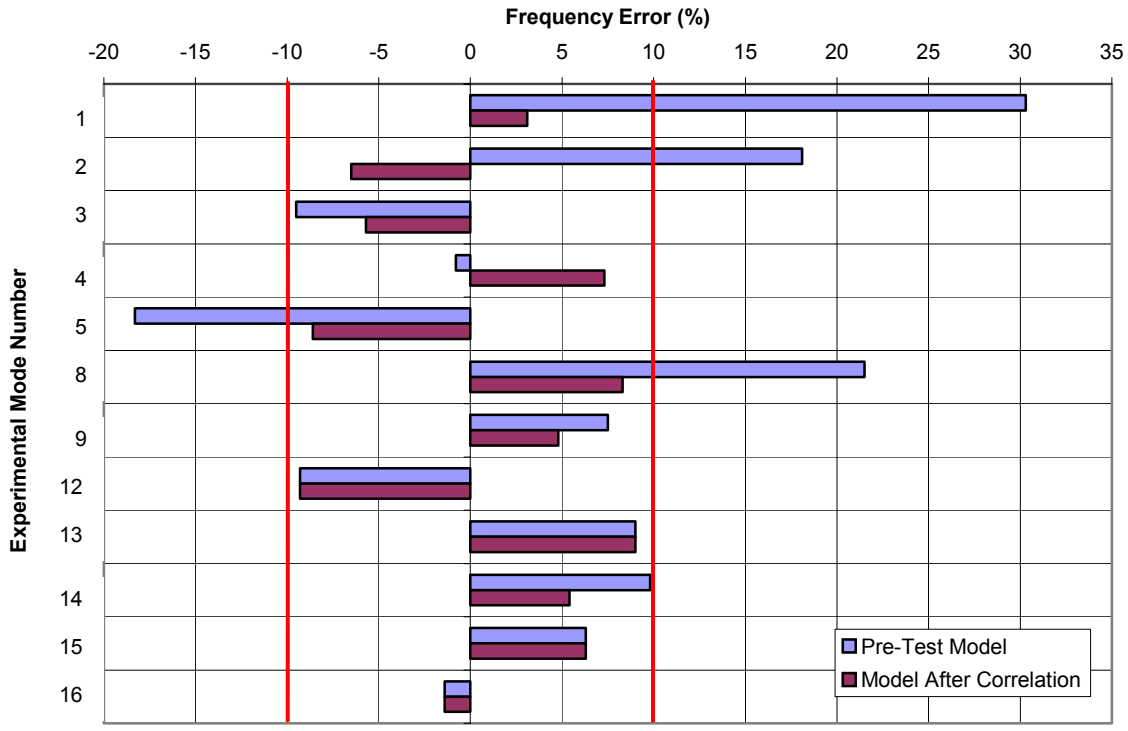

nature. A number of solutions are available to overcome this proven spring model solution limit; some of these are briefly presented in the next chapter. The implementation and evaluation of these solutions go beyond the objectives of this methodology development and application. It is also recalled that even though the spring model scheme itself was not included in the model parameter set, the spring properties of such a solution (i.e. spring elements' stiffness) were considered as model parameters and were updated to obtain better spring frequency correlation, as Figure 6.1 indicates.

FIGURE 6.2. Orthogonality Check between Updated FEM Model Modes and Experimental Modes

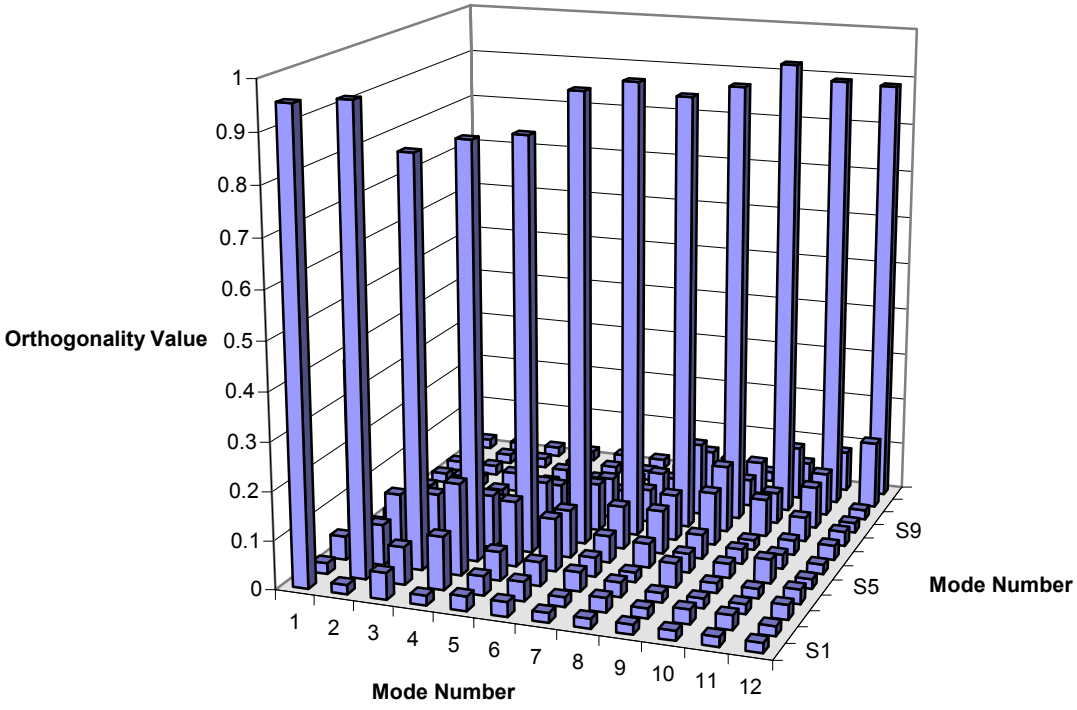

The preliminary comparison also illustrated that the experimental approach did not capture three modes predicted in the pre-test simulation. These modes were deemed as existing modes in the test article and an explanation for each mode discrepancy was presented. One mode concerns the first torsional mode of the valve. This discrepancy was explained by recalling considerations regarding the assumption for the test article to be *observable*. It was noted that in a modal survey sometimes no response information is available relative to a particular DOF of the structure, converting thus the test article into a partially *observable* structure. The particular case of local rotations was introduced. It was illustrated that this torsional mode was not experimentally captured because of lack

of response information regarding local rotations at the valve head. This valve torsion mode can only be characterized by comprising in the modal parameter estimation process measurements that include valve responses taken off the valve axis. Therefore, in this final comparison this discrepancy is still present as no additional experimental responses were acquired and processed.

The other two modes that the experimental approach did not capture relate to second-order bending modes for the valve. In the preliminary comparison, it was noted that this disagreement is caused by the combination of at least three factors. One factor is the low excitation energy level, as these modes occur at frequencies that are very close to the upper limit of the frequency interval of interest. The second factor is related to possibility that the direction of excitation may not be the optimal direction to excite these modes. The third factor, which is possibly the most important, concerns the measurement response locations. As the valve is in fact acting as a cantilever beam and the valve response measurement locations were all positioned at the valve head (the free end of the cantilever beam), the valve second bending modes could not be exhaustively characterized. The discrepancy regarding these two modes is still present in this final comparison, as no further response measurements were acquired and processed. It is recalled that, in order to fully define these second-order bending modes, response measurements acquired along valve stem are required.

In the section in which the experimental results were presented (Section 4.9), a comment regarding repeated roots was formulated. It was stated that modes' couples 1-2 and 4-5 should show almost identical natural frequencies, within the couple. Indeed, they are predictable cases of repeated poles, or roots. It is recalled that repeated roots refer to

the situation where one complex root or eigenvalue occurs more than once in the characteristic equation. It was recalled that sometimes repeated roots are predictable because of evident geometrical symmetries. It was also noted that the experimental natural frequencies of these two couples of symmetrical modes are not consistent with the pole repetition effect. In other words, in each mode pair, the natural frequencies of the two coincident modes are not almost identical. The reason is that, even though the selected modal parameter estimation method (*polyreference time-domain*) is capable of accounting for repeated roots, it properly calculates them only if two or more *references* (input excitations) locations are present in the data. It is recalled that in this study the *reference* was only one, at the camshaft. The use of the *polyreference time-domain* method with only one *reference* location produces exactly the same results as the *least squares complex exponential* technique. The *least squares complex exponential* analysis, therefore, is really a single-reference case of the *polyreference time-domain* technique. However, it was decided to refer to the *polyreference time-domain* method as the technique applied, in order to be able to describe its powerful capabilities that may be implemented in a future study. It is worth noting that the numerical results, obtained both with the pre-test simulation and the updated model, are consistent with the pole repetition prediction (i.e. the natural frequencies of two coincident modes are almost identical).

It can therefore be concluded that this study successfully developed and implemented a methodology to correlate an experimental modal analysis with a FEM modal analysis of a valve train. A proficient pre-test analysis technique was employed to guide the execution of the tests used in the correlation process. This approach not only improved the efficiency of the test process, but the test-analysis model (TAM) that

resulted from the pre-test simulation also provided a means to compare the test and the model both during the experimental approach and during the model updating process.

7. RECOMMENDATIONS

Since the objective of this study was to derive a methodology to correlate an experimental modal analysis with a FEM modal analysis of valve trains in IC-engines, a number of suggestions have been presented throughout all the sections of this report. The following list attempts to summarize four key aspects of the procedure that radically affect the outcome of the correlation:

- System boundary conditions employed both in the experimental and numerical approaches are critical to the modal characterization of not only valve train systems but any structure
- The results of an experimental modal characterization largely depend on the quality of the measured frequency response functions. In order to take advantage of experimental data in the correlation process, the variance and bias errors in the measurements must be reduced to acceptable levels
- In order to ensure that all modal vectors have been found experimentally, a number of excitation points should be utilized, either one at a time or simultaneously. This greatly reduces the possibility of trying to excite the system at a modal vector node. Having multiple input locations significantly enhances the quality of the results obtained in the modal parameter estimation process
- In order to correlate (i.e. to quantify the degree of similarity and dissimilarity) the experimental approach with FEM techniques two concepts must be recalled in the pre-test analysis and test planning: (1) the FEM *normal modes* solution must be *mass-normalized*; (2) at least one *driving-point measurement* must be present in the measured data in order to construct mass-scaled matrices

Suggestions pertinent to the particular application studied in this experience include:

- A spring model capable of predicting second-order spring compression modes and local spring coil modes could be introduced in the updated model. One solution could comprise a full model of the spring (similar to the spring test-vehicle model developed in Section 3.2.2). Another solution could involve a series of the spring model solution employed in this study and illustrated in Figure 3.18. It is worth noting that these options were evaluated during the pre-test model development; however, they were deemed not applicable during the pre-test analysis without considerably complicating the derivation of the TAM
- The updated model could be further developed by including the non-linear properties of the lash-adjuster component.

General recommendations include:

- In some applications (aerospace) tighter correlation criteria are used: 5% for frequency difference, and 0.95 for diagonal orthogonality check values (and 0.5 for off-diagonal values)[4].
- Other methods of comparing modal test data with a FEM model is through the various *model assurance criteria* (MAC). MAC checks are, to some extent, more comprehensive comparisons of mode shapes than pure orthogonality checks.

APPENDIX A. BASIC FOURIER ANALYSIS THEORY

A.1. FOURIER ANALYSIS

The Fourier series and the Fourier integral allow transformation of physically realizable time-domain waveforms to the frequency domain and vice versa. They are mathematical tools for what is referred to as Fourier Analysis. The Fourier series and the Fourier integral were developed by the French mathematician Jean Baptiste Fourier (1768-1830)[3].

A.1.1. THE FOURIER SERIES

If a Fourier series can be written for a waveform, then the components of the series completely describe the frequency content of the waveform. However, there are some conditions that have to be met. One condition for constructing a Fourier series is that the waveform be periodic. In other words, the waveform must repeat itself in time, it must begin at minus infinity and repeat itself out to plus infinity. In mathematical means: if a waveform is represented by the function $x(t)$ and there is a constant time T that exists such that $x(t) = x(t + T)$ holds for all time, t, then $x(t)$ is periodic with time T. A familiar example of qualifying waveforms include sine and cosine waves. But the condition of periodicity is rarely, if ever, met perfectly in the physical world. However, for the purpose of writing a Fourier series, periodicity can be defined over an observable interval.

Beyond periodicity, the remaining conditions for existence of a Fourier series are referred as the Dirichlet conditions. Briefly, they state that:

- If the function *x(t)* that represents the waveform contains discontinuities, their number must be finite in any period.
- The function *x(t)* must contain a finite number of maxima and minima during any period.
- The function *x(t)* must be integrable in any interval.

These conditions, along with that of periodicity, establish the existence of a Fourier series for any given *x(t)*. The general form of the Fourier series is:

$$x(t) = a_0 + \sum_{n=1}^{\infty} (a_n \cos n\omega_0 t + b_n \sin n\omega_0 t)$$

where:

$$f_0 = \frac{1}{T} \qquad \omega_0 = 2\pi f_0 = \frac{2\pi}{T}$$

and the coefficients a_0, a_n and b_n (with n = 1, 2, 3,…) are given by[3]:

$$a_0 = \frac{1}{T}\int_0^T x(t)dt \qquad a_n = \frac{2}{T}\int_0^T x(t)\cos(n\omega_0 t)dt \qquad b_n = \frac{2}{T}\int_0^T x(t)\sin(n\omega_0 t)dt$$

A.1.2. THE FOURIER INTEGRAL

The Fourier series is a useful tool for investigating the spectrum of a periodic waveform, but the world is not made up exclusively of periodic waveforms. The Fourier integral is the mathematical tool used to investigate the time and frequency spectra of non-periodic waveforms.

The Fourier integral is derived from the Fourier series. With proper mathematical

manipulation the Fourier series reduces to:

$$x(t) = \int_{-\infty}^{\infty} X(f) e^{j2\pi ft} df$$

The Fourier coefficients now have become a function of a continuous frequency variable *f,* and are given by:

$$X(f) = \int_{-\infty}^{\infty} x(t) e^{-j2\pi ft} dt$$

These two integrals together are referred to as the Fourier transform pair. The former is generally referred to as the inverse Fourier transform and the latter as the direct Fourier transform.

As implied by its development, the Fourier integral is only applicable to non-periodic waveforms, or, in other words, to waveforms of infinite period. A non-periodic waveform, given by the function *x(t)* and subjected to the Dirichlet conditions, can be transformed from a function in time to a function of frequency by using the direct Fourier transform. When this is done, then *X(f)* is referred to as the Fourier transform of *x(t)*. In the same manner, by using the inverse Fourier transform a frequency-domain function *X(f)* can be inverse transformed to the time-domain function *x(t)*[3].

A.2. THE DISCRETE AND FAST FOURIER TRANSFORMS

The direct and inverse Fourier transforms are frequently difficult to apply directly without some tools. The discrete Fourier transform (DFT) and the fast Fourier transform (FFT) algorithm are the analytical tools to quickly apply Fourier theory.

The task of applying a Fourier transform to a waveform requires the evaluation of a closed-form integral. Since it is of immense utility to compute the Fourier transform digitally, a numerical integration must be performed. There are three distinct difficulties with computing a Fourier transform digitally. First, the desired result is in reality a continuous function; a digital solution will only be able to calculate its value at discrete points. The second problem is the actual evaluation of the integral (equivalent to compute the area under a curve): a numerical solution evaluates it by adding together the areas of narrow rectangles under the curve. The last problem is that even with the summation approximation to the integral, the result cannot be calculated with samples that range from minus to plus infinity. It is clear that the transform must be limited to a finite interval. The result of this numerical computation yields to an approximation of the Fourier transform called discrete Fourier transform (DFT).

The final expression of the DFT is as follows:

$$X_d(k\Delta f) = \Delta t \sum_{n=0}^{N-1} x(n\Delta t) e^{-j2\pi k\Delta f n\Delta t}$$

By some additional manipulations the inverse DFT can be developed:

$$x(n\Delta t) = \Delta f \sum_{n=0}^{N-1} X_d(k\Delta f) e^{j2\pi k\Delta f n\Delta t}$$

Where the variables have the following definitions:

N: number of samples being considered

Δt: the time between samples referred to as *sampling interval;* from this, $N\Delta t$ gives the *window* length, often referred to as the *time record length*

Δf: the sample interval in the frequency domain and is equal to $1/N\Delta t$

n: the time sample index; with values of 0, 1, 2,…, N-1

k: the index for the computed set of discrete frequency components, with values of 0, 1, 2,…, N-1

$x(nN\Delta t)$: the discrete set of time samples that defines the waveform to be transformed

$X(kN\Delta f)$: the set of Fourier coefficients obtained by the DFT of $x(nN\Delta t)$.

From the DFT expression, it can be deduced that the number of operations needed to compute it for N time domain samples is in the order of N^2. It is not difficult then to understand why DFT analysis was generally avoided before the development of modern digital computers. The required number N of samples for defining many real-life waveform functions runs into the hundreds, sometimes a thousand or more.

The fast Fourier transform (FFT) is a particular method of performing the series of calculations to compute a DFT. In other words, it is simply an algorithm that can compute the DFT much more rapidly than other available algorithms. The interpretation of the computational aspect of FFT goes beyond the goals of this basic Fourier analysis review. However, to demonstrate the effectiveness of this algorithm, consider that that the number of operations is reduced from being in the order of N^2 to the order of $N \log_2 N$. The significant savings of $N \log_2 N$ operations versus N^2 operations is apparent in Figure A.1. This is achieved by recognizing certain symmetries and periodicities[3].

The FFT produces significantly faster results for a modal analysis, but more importantly it provides a means for analyzing a system's modal behavior through the computed frequency response function (FRF)

FIGURE A.1. FFT Advantage Over the DFT

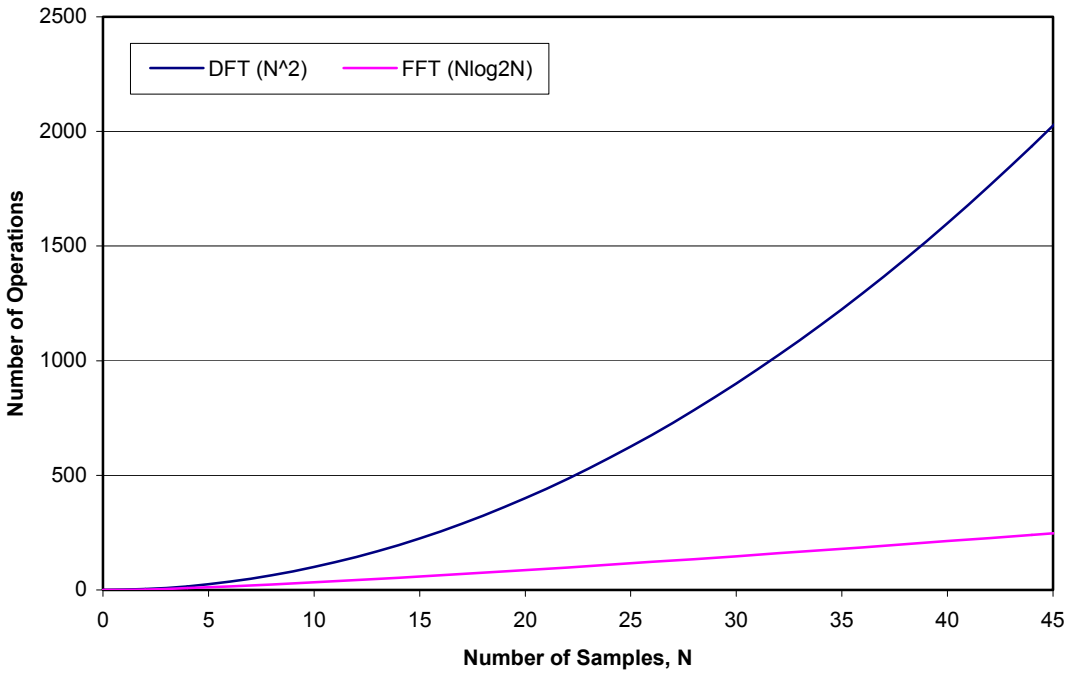

APPENDIX B. TRANSDUCER SPECIFICATIONS

TRANSDUCER SPECIFICATIONS		
Characteristic	***Accelerometer***	***Force Transducer***
Manufacturer	*Endevco*	*Dytran*
Model	*2222C*	*Embedded in Hammer 5850*
Sensitivity	*1.4 pC/g*	*100 mV/lbf*
Resonant Frequency (kHz)	*32*	*75*
Amplitude Linearity (%)	*±1*	*±1*
Amplitude Response (Hz)	*1 to 10,000*	*N/A*
Maximum Input Force (lbf)	*N/A*	*1,000*
Shock Limit (g peak)	*10,000*	*N/A*
Weight (grams)	*0.5*	*275 (Total Hammer Weight)*

FIGURE B.1. Accelerometer Calibration Data (Courtesy of Endevco Corp.)

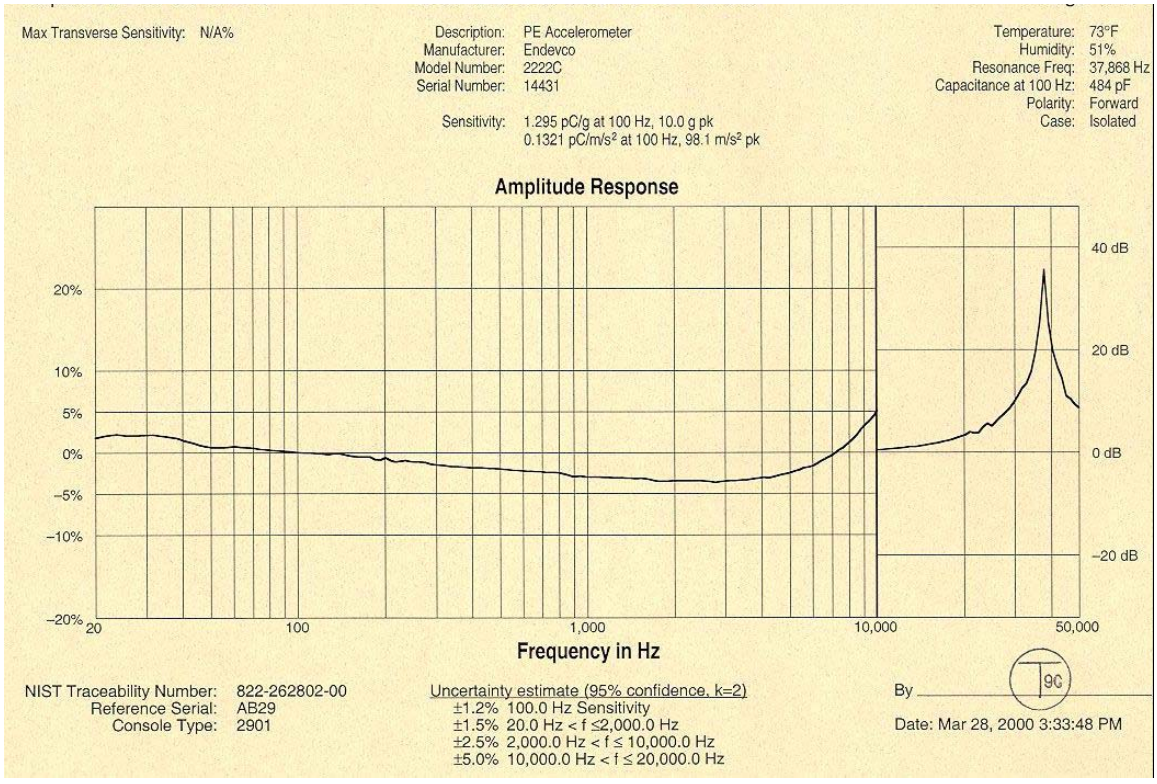

APPENDIX C. CURVE-FITTING WITH I-DEAS TEST GUIDELINE

CURVE FITTING WITH I-DEAS

(Button location code is: Row-Column)

1. **EXPERIMENTAL DATA IMPORT**

a. Convert SDF file to ASCI using SDFTOASC.exe
b. From FILE menu → IMPORT → FUNCTIONS (Spreadsheet Text)
c. Type name of destination file (an .AFU* file)
d. Input full path of ASCI file in I-DEAS prompt window
e. Answer YES for COMPLEX
f. Answer NO for HEADER
g. Answer NO for FIRST ABSCISSA
h. Type COORDINATE (format is: node #, direction, sign)

2. **DATA ADJUSTMENTS NEEDED AFTER THE IMPORT**

a. Select MODAL module (click button 10-1, MANAGE FUNCTIONS)
b. Select one function (one at a time)
c. For DATA ATTRIBUTES IDENTIFIERS modify:
    i. REFERENCE: enter input (i.e. shaker or hammer position) node #, direction, and sign
    ii. FUNCTION TYPE: enter FREQUENCY RESPONSE
d. For DATA ATTRIBUTES ABSCISSA modify:
    i. DATA TYPE: FREQUENCY
    ii. MINIMUM: Start of frequency span in the experimental setup (i.e. zero)
    iii. INCREMENT: Divide frequency span of experimental setup by number of lines of resolution (i.e. 1600)
e. Click APPLY and select next function

3. CURVE FITTING PROCESS

a. Select MODAL module
b. Button 11 – Select POLYREFERENCE (or ORTHOGONAL)
c. Button 21 – Select SELECT REFERENCE → K(key) → Type node # (i.e. 17Z-)
d. Button 12 – Select NORMAL MIF and select all (?) functions
e. Button 82 – TAG peaks (i.e. select peaks with mouse); right button (tag on right) after having narrowed view
f. Button 22 – MCF ON
g. Button 22 – BUILD MATRIX:
    i. Select functions including MIF (?)
    ii. Choose bandwidth and size (peaks X 2)
    iii. Choose name of matrix
h. Button 23 – GRAPH: select OVERLAY XY stab., select the MIF (?)
i. Button 31 – Select PARAMETERS (threshold is 8 by default)
    i. Right click with mouse → MIXED POLE SW → OFF
    ii. Judge POLE # depending on damping stability (in general, start with more POLE # than modes present)
    iii. Right click with mouse → MIXED POLE SW → ON
    iv. Select modes upon damping stability
j. Button 32 – From RESIDUES OPTIONS → set to REAL → ON → FREQUENCY DOMAIN
k. Button 32 – CALCULATE RESIDUES: pick some locations (i.e. type the node #) and check if they look similar to the matrix calculated (experimental data is in red, matrix calculated is in green)
l. Button 33 – Select FREQUENCY POLYREFERENCE SHAPE

i. Choose .APA* and .ASH* filenames and locations
ii. Click OK to continue
iii. Select all the FRF functions for the imported nodes
iv. Select the frequency range

4. POSTPROCESSING

a. Select POSTPROCESSING module
b. Button 11 – Pick MODE SHAPE and place it in DEFORMED SHAPE
c. Button 21 – DISPLAY MODE → Right click with mouse → ALL DONE → TRACELINE → DONE WITH ALL
d. Button 31 – ANIMATED MODE SHAPE → Right click with mouse → ALL DONE → TRACELINE → DONE WITH ALL

* FILE EXTENSIONS: AFU (functions), AMX (correlation matrix) APA (parameters), ASH (mode shapes)

BIBLIOGRAPHY

1. Baker, M. *Review of Test/Analysis Correlation Methods and Criteria for Validation of Finite Element Models for Dynamic Analyses*. IMAC. 1992.
2. Blelloch, P. et al. *Simulation of an On-Orbit Modal Test of Large Space Structures*. IMAC. 1990.
3. Brigham, E. O. *The Fast Fourier Transform and its Applications*. Prentice-Hall. 1988.
4. Brillhart, R. D. et al. *Dynamic Verification of the Space Shuttle T-97 SRM Static Firing Test Stand.* IMAC. 1989.
5. Brillhart, R. D. et al. *Model Improvement and Correlation of the Pegasus XL Launch Vehicle Via Modal Testing.* IMAC. 1995.
6. Brillhart, R. D. et al. *Modal Test and Correlation of the Commercial Titan Dual Payload*. IMAC. 1990.
7. Cheung, Y. K. *Finite Element Methods in Dynamics*. Kluwer. 1991.
8. Conti, P. et al. *Test/Analysis Correlation Using Frequency Response Functions.* IMAC. 1992.
9. Donley, M. et al. *The Use of Pre-Test Analysis Procedures for FE Model/Test Correlation of a Transmission Side Cover.* SAE. 1997.
10. Donley M. et al*. Validation of FE Models for NVH Simulation.* IMAC. 1996.
11. Ewins, D. J. *Modal Testing – Theory, Practice, and Application*. 2nd ed. Research Studies Press. 2000
12. Freed, A. et al. M. *A Comparison of Test-Analysis Models Reduction Methods*. IMAC. 1990.

13. Friswell, M. I. et al. *Finite Element Updating in Structural Dynamics*. Kluwer. 1995.

14. Genta, G. *Vibration of Structures and Machines*. 3rd ed. Springer. 1999.

15. Haubrock, R. et al. *Dynamic Optimization Applied to Test/Analysis Correlation*. IMAC. 1989.

16. Meirovitch, L. *Elements of Vibration Analysis*. 2nd ed. McGraw-Hill. 1986.

17. Norton, R. L. *Machine Design – An Integrated Approach.* 2nd ed. Prentice-Hall. 2000.

18. Norton, R. L. et al. *Analyzing Vibrations in an IC Engine Valve Train*. SAE. 1998.

19. Sergent, P. et al. *A Procedure for the Integrated Development of Test-Analysis Models*. IMAC. 1991.